Die approbierte Originalversion dieser Dissertation ist an der Hauptbibliothek der Technischen Universität Wien aufgestellt (http://www.ub.tuwien.ac.at).

The approved original version of this thesis is available at the main library of the Vienna University of Technology (http://www.ub.tuwien.ac.at/englweb/).

Technische Universität Wien

DISSERTATION

Indoor MIMO Channel Models

ausgeführt zum Zwecke der Erlangung des akademischen Grades
eines Doktors der technischen Wissenschaften

eingereicht an der Technischen Universität Wien
Fakultät für Elektrotechnik und Informationstechnik

von

Dipl.-Ing. Hüseyin Özcelik
Matrikelnummer 9626169
A-1210 Wien, Theodor Körner-Gasse 30/10
geboren in Wien am 15.10.1976

Wien, im Dezember 2004 .....

First Supervisor: Prof. Dipl.-Ing. Dr. Ernst BONEK
Institut für Nachrichtentechnik und Hochfrequenztechnik
Fakultät für Elektrotechnik und Informationstechnik
Technische Universität Wien, Ausria

Second Supervisor: Prof. Dipl.-Ing. Dr. Andreas F. MOLISCH
Department of Electroscience
Lund Technical University, Sweden
and
Mitsubishi Electric Research Laboratory
Cambridge, USA

Zusammenfassung

Im Fokus der Betrachtungen für zukünftige Kommunikationssyteme stehen Mehrantennensysteme bestehend sowohl aus mehreren Sende- als auch mehreren Empfangsantennen (Multiple-Input Multiple-Output, MIMO). MIMO-Systeme ermöglichen durch die Nutzung der räumlichen Dimension des Funkkanals eine deutliche Steigerung der Übertragungskapazität gegenüber konventionellen Kommunikationssystemen (mit je einer Sende- und Empfangsantenne) bei gleicher Sendeleistung und Übertragungsbandbreite. Da das gesamte Potential von MIMO-Systemen von den Eigenschaften des Funkkanals abhängig ist, setzt die Planung, Simulation und Errichtung solcher Systeme eine präzise Modellierung des Funkkanals voraus.

Diese Dissertation befasst sich mit der Modellierung von MIMO-Funkkanälen innerhalb von Gebäuden (Indoor). Zunächst werden die gängigen Kanalmodelle kurz rezensiert. Die Modelle werden dabei in physikalische und analytische Modelle unterteilt. Basierend auf der doppeltrichtungsabhängigen Mehrwegeausbreitung beschreiben physikalische Modelle die elektromagnetische Wellenausbreitung zwischen dem Sender und Empfänger. Im Gegensatz dazu charakterisieren analytische Modelle die Impulsantworten zwischen allen Sende- und Empfangsantennen in einer mathematisch geschlossenen Form. Damit bieten sie eine analytische Basis für den Entwurf von MIMO Übertragungstechniken.

Um zu überprüfen, inwieweit Modelle die Realität nachbilden können, werden diese im Allgemeinen einer experimentellen Validierung unterzogen. So auch MIMO-Kanalmodelle: Im zweiten Teil dieser Dissertation werden bekannte analytische Schmalbandmodelle, nämlich das sogenannte Kronecker Modell, das Weichselberger Modell und die virtuelle Kanalrepräsentation (virtual channel representation) mit Messungen einer umfangreichen Messkampagne bei 5.2GHz in den Büroräumen des Instituts für Nachrichtentechnik und Hochfrequenztechnik der Technischen Universität Wien verglichen. Im Speziellen werden MIMO-Systeme mit linearen Antennengruppen in Betracht gezogen, wobei sowohl die Anzahl der Antennenelemente (von 2×2 über 4×4 bis 8×8) als auch die Elementabstände variiert werden.

MIMO Kanäle weisen unterschiedliche Eigenschaften und Aspekte auf, die - wie sich im Rahmen dieser Arbeit herausgestellt hat - von einer einzigen Metrik alleine nicht erfasst werden können. Folgende vier Metriken werden daher für die Validierung der genannten Modelle verwendet: (i) die *mittlere Transinformation des MIMO Kanals bei gleichförmiger Allokation der Sendeleistung auf die einzelnen Sendeantennen*, als Maß für den Signalgewinn aus dem räumlichen Multiplex-Verfahren; (ii) das *doppelt-richtungsabhängige Leistungsspektrum*, das Einsicht in die räumliche Mehrwegeausbreitung gewährt und das Potential des Kanals für Strahlformung widerspiegelt; (iii) ein *Diversitätsmaß* für die Erfassung der Diversität des Kanals; sowie (iv) eine *Distanz zwischen Korrelationsmatrizen* (CMD), welche Änderungen der Korrelationen des MIMO-Kanals beschreibt.

Die Validierung zeigt, dass die mittlere Transinformation, das Diversitätsmaß und die Kanal-Korrelation am besten vom Weichselberger Modell wiedergegeben werden können. Im Gegensatz zum Weichselberger Modell, das die mittlere Transinformation des gemessenen Kanals (bei einem Signal-Rauschleistungsverhältnis von 20dB) nahezu fehlerfrei nachbildet, zeigt das Kronecker Modell Abweichungen von bis zu mehr als 10%, insbesondere bei 8×8. Hingegen können alle drei Modelle die mittlere Transinformation des gemessenen Kanals für ein 2×2 System mit weitem Elementabstand hinreichend genau modellieren.

Das doppelt-richtungsabhängige Leistungsspektrum wird von keinem der untersuchten Modelle für beliebige Ausbreitungsszenarien und Antennenanzahl genau wiedergegeben. Während das Weichselberger Modell nur Systeme bis zu 4×4 entsprechend präzise modelliert, steigt die Güte der virtuellen Kanalrepräsentation mit zunehmender Anzahl der Antennen (aufgrund der höheren Winkelauflösung). Acht Antennen sind scheinbar trotzdem nicht ausreichend. Da das Kronecker Modell die Unabhängigkeit von Sende- und Empfangsrichtungen erzwingt, sollte es im Allgemeinen nicht für die Modellierung des doppelt-richtungsabhängigen Leistungsspektrums herangezogen werden.

Abstract

Multiple-Input Multiple-Output (MIMO) systems are a promising candidate for future wireless communications systems as they provide high data rates by exploiting the spatial domain under the constraints of limited bandwidth and transmit power. It is the radio propagation channel that determines crucially the characteristics of the entire MIMO system. Therefore, accurate modeling of MIMO channels is an important prerequisite for MIMO system design, simulation, and deployment.

This thesis focuses on MIMO channel models for indoor environments. As a first step, recent work on indoor MIMO channel model is briefly reviewed. The models are classified into physical and analytical models. The result of physical modeling is the characterization of the environment on the basis of double-directional multipath propagation between the location of the transmit and receive array. Analytical models, on the contrary, describe the impulse response between all elements of the antenna arrays at transmitter and receiver. These provide an analytical framework for designing MIMO techniques.

The ultimate test of any model is experimental validation. Consequently, we compare some popular analytical narrowband models, viz. the so-called Kronecker model, the Weichselberger model, and the virtual channel representation with measurements. For these investigations, MIMO systems equipped with uniform linear antenna arrays at both link ends are considered. Both different numbers of antennas, varying from 2×2 to 4×4 and 8×8, and different antenna spacings are studied. As the basis for our comparison we take measurements of an extensive 5.2GHz measurement campaign in the offices of the Institut für Nachrichtentechnik und Hochfrequenztechnik, Technische Universität Wien, Austria.

In the course of this work it turned out that a single metric or performance measure alone is not sufficient to verify the suitability of a MIMO channel model. In order to capture the most important aspects of MIMO channels four different metrics are applied. These metrics are (i) the *average mutual information* (with equal transmit power allocation) describing the spatial multiplexing gain; (ii) the *double-directional angular power spectrum*, giving insight into the multipath structure and potential beamforming gain; (iii) a *Diversity Measure*, describing the degree of diversity of a channel; and (iv) the *Correlation Matrix Distance (CMD)* characterizing the changes in the full channel correlation.

The validation reveals that the Weichselberger model predicts the average mutual information, the Diversity Measure and the full channel correlation best of all three models, independently of the antenna number and antenna separation. Regarding average mutual information it shows an almost perfect match with the measurements at a receive SNR of 20dB, whereas the Kronecker model tends to underestimate the mutual information up to more than 10% especially for large arrays (8×8). When we lower antenna numbers to 2×2 and increase

antenna spacing, all considered models predict mutual information sufficiently well.

Concerning the double-directional angular power spectrum none of the analyzed models can reproduce an arbitrary multipath structure accurately, independently of the array size. While the Weichselberger model can only cope with systems not larger than 4×4 sufficiently, the virtual channel representation improves its performance with increasing antenna numbers due to improved angular resolution. But 8×8 does not seem to be large enough. The Kronecker model forces the double-directional angular power spectrum to be separable and should, in general, not be used for modeling the double-directional angular power spectrum.

Acknowledgment

When I finished my Diplom-Ingenieur degree (MScEE), I did not think about continuing with a Ph.D. research. Instead, I wanted to start working in a company.

Now, three and a half years later, I am very glad that *Prof. Ernst Bonek* has encouraged me for doing a Ph.D. at the *Institut für Nachrichtentechnik und Hochfrequenztechnik* of the *Technische Universität Wien* under his supervision. For the continuous support and guidance throughout the whole period of my research work I am deeply grateful to him.

I also want to thank my colleagues at our Institute and at the *Forschungszentrum Telekommunikation Wien*:

Markus Herdin, with whom I carried out the MIMO measurements, but also did a lot of research together, *Werner Weichselberger* for numerous interesting discussions, *Elmar Trojer*, with whom I shared a room, and *Helmut Hofstetter* for help with the measurements. Moreover, I am grateful to all the other colleagues which I could not name here explicitly. During my stay, I really enjoyed our weekly working group meetings.

Also, I feel obliged to *Prof. Andreas Molisch* for acting as my second supervisor.

Lastly, I want to thank my family, especially my parents, for their tremendous support and confidence.

Contents

1 Introduction 1

1.1 The Historical Context . . . 1
1.2 Wireless Communication Technologies . . . 1
1.3 Outline and Contributions . . . 3
1.4 Notation . . . 4
1.5 Abbreviations . . . 5

2 The Indoor MIMO Channel 6

2.1 Double-directional Radio Propagation . . . 6
2.2 MIMO Channel . . . 8
2.2.1 Relationship to Double-directional Propagation . . . 9
2.3 MIMO Potentials . . . 12
2.3.1 Spatial Multiplexing . . . 12
2.3.2 Beamforming . . . 17
2.3.3 Spatial Diversity . . . 17
2.3.4 Trade-off between Beamforming, Diversity and Multiplexing . . . 17
2.4 Specifics of Indoor Channels . . . 18

3 Review of Existing Indoor Channel Models 20

3.1 Overview . . . 20
3.2 Physical Models . . . 22
3.2.1 The Extension of the Saleh-Valenzuela Model . . . 22
3.2.2 Zwick's Model . . . 23
3.3 Analytical Models . . . 24
3.3.1 Correlation-based Models . . . 24
3.3.2 Propagation-motivated Models . . . 33
3.3.3 Line-of-Sight Channels . . . 36
3.3.4 Broadband Extension to Analytical Narrowband Models . . . 36

3.3.5 Temporal Evolution of Analytical Models . . . 37
3.4 Standardized Models . . . 37
3.4.1 The 802.11n Model . . . 37

4 Measurements **40**
4.1 Setup . . . 40
4.1.1 Channel Sounder . . . 40
4.1.2 Antennas . . . 41
4.2 Scenario . . . 44
4.3 Data Post Processing . . . 44
4.3.1 Averaging over Temporal Snaphots . . . 44
4.3.2 Receive Array Calibration . . . 44
4.3.3 Creation of Spatial Channel Matrix Realizations . . . 47
4.3.4 On the Size of the Statistical Ensemble . . . 47

5 Validation of Analytical Channel Models **49**
5.1 Extraction of Model Parameters . . . 49
5.2 Monte-Carlo Simulations . . . 50
5.3 Metrics for Validation of MIMO Channels . . . 51
5.3.1 A Metric for the Multiplexing Gain . . . 52
5.3.2 A Metric for the Multipath Structure . . . 52
5.3.3 A Metric for the Channel Diversity . . . 53
5.3.4 A Metric for the Change in the Channel Correlation . . . 55
5.4 On the Statistics of the Measured Channels . . . 55
5.5 Variation of Antenna Number . . . 56
5.5.1 Average Mutual Information . . . 56
5.5.2 Joint DoD-DoA Spectrum . . . 60
5.5.3 Diversity Order . . . 64
5.5.4 Correlation Matrix Distance . . . 67
5.6 Variation of Antenna Spacing . . . 69
5.6.1 Average Mutual Information . . . 69
5.6.2 Diversity Order . . . 70
5.6.3 Correlation Matrix Distance . . . 70

6 Summary and Conclusions **77**

A Proof of an Identity **81**

B Sample Eigenvalue Profiles **82**

C Joint DoD-DoA Capon spectra **86**

C.1 Capon spectra for 8×8 MIMO systems 87

C.2 Capon spectra for 4×4 MIMO systems 95

C.3 Capon spectra for 2×2 MIMO systems 103

D Diagonally Correlated Channels **111**

D.1 Diagonally Correlated 2×2 MIMO Channels 111

D.1.1 Derivation and Modeling 111

D.1.2 Capacity 113

D.1.3 Fading Behavior 114

D.2 Diagonally Correlated $n \times n$ MIMO Channels 116

Chapter 1

Introduction

The Historical Context

1.1 The Historical Context

Three major revolutions have changed the human society deeply. In the course of the first revolution, the so-called *neolithic revolution*, human society become sedentary, adopt agriculture and domesticated animals.

The second revolution was the *industrial revolution*. It changed the nature of production fundamentally. Machines replaced tools, steam and other energy sources replaced human or animal power, and skilled workers were replaced with mostly unskilled workers. The industrial revolution transformed agricultural economies into industrial ones.

The third revolution, the ongoing *information revolution*, is symbolized by the coalescence of the worlds of information technology, communications and media. Catchwords are internet, multimedia, and wireless access. The storage, transmission, manipulation and accessability of vast quantities of knowledge or information characterizes this revolution. Thus, information is an essential economic resource.

Communication technologies play a key role, as they make the transmission and accessability of information possible. In particular, the introduction of wireless communication systems has opened new dimensions and new horizons in the field of communications. Communication has been abstracted from the constraints of physical space - people can be reached anytime, anyplace. These advantages have attracted people such that the number of mobile subscribers exceeds the number of fixed-link subscribers in several countries.

1.2 Wireless Communication Technologies

Wireless is evolving, just as the wireline sector evolved from the plain old telephone service to a much wider range of service options, particularly data services. Wireline data traffic volumes increased dramatically from one megabyte (MB) per user and month in 1991 to nearly 200MB per user and month by 1999 [1] due to higher data rates and improved usability. Along with this, penetration increased and, very important, costs decreased.

A similar evolution has been already started and is expected to be continued for wireless. New wireless data technologies such as WLANs (Wireless Local Area Networks), Beyond 3G (3rd Generation) mobile communication systems, home Audio/Visual networks and fixed broadband wireless access will be challenged by fairly high-speed data transmission. Qualcomm forecasts *wireless* data volumes to exceed 200MB per user and month by the year 2006 [1]. WLAN systems providing short range wireless access for home, public environments, and enterprise solutions face the competition of wired LANs. Obviously, currently offered peak data rates of 10Mbit/s are highly inadequate. Beyond 3G mobile communication systems aim to transmit real-time video and multimedia traffic in highest quality. Although not fully specified, future wireless systems will be required to support peak data rates of up to 1Gbits/s [2]. Laptops and PDAs (Personal Digital Assistants) are planned as new devices. All these systems ask for the highest data rates in indoor environments such as hot-spot areas and indoor offices.

One of the most promising candidates for fulfilling the increasing demand for higher data rates with good Quality-of-Service under the constraints of limited bandwidth and restricted transmit power are so-called MIMO systems. MIMO stands for multiple-input multiple-output and denotes systems with multiple antennas at both link ends. In fact, the novelty of MIMO is the exploitation of the spatial domain at both link ends. Communications engineers have previously exploited all other domains. Traditional single-input single-output (SISO) systems allow the exploitation of time, frequency, and code. Smart antenna or adaptive antenna systems, equipped with an antenna array at one link end only [3], allow to exploit space with some restrictions. More specifically, spatial diversity and beamforming gain (array gain) at one link end is achievable. For multi-user systems also interference suppression is possible. An overview of smart antenna techniques can be found in [4, 5, 6, 7, 8]. Aside from polarization, the "full exploitation of space is the final frontier".

MIMO promises more than spatial diversity or beamforming at both link ends separately. As pioneering works by [9, 10, 11] showed, it boosts channel capacity compared to SISO channels by exploiting spatial multiplexing. It enables the transmission of several data streams over parallel non-interfering virtual sub-channels. Dependent on the underlying radio channel, the capacity of a MIMO channel potentially grows linearly with the minimum number of transmit and receive antennas. Capacity limits of various kind of channels are reported in [11, 12, 13, 14, 15]. Several signal processing algorithms were developed to exploit MIMO benefits, particularly the extensive group of space-time codes [16, 17, 18, 19, 20, 21]. Overviews on MIMO in general can be found in [22, 23, 24]. The MIMO radio channel specifies crucially the characteristics of the entire MIMO system. In other words the propagation conditions determine what can be gained by MIMO.

Accurate MIMO channel models are a prerequisite for (i) the site-independent design, simulation, and deployment of MIMO systems, and (ii) the site-specific prediction for MIMO network planning. First comes the physical, electromagnetic wave propagation. 'Conventional' models, which had been developed for SISO and smart antenna systems, are no longer suitable for MIMO systems. Instead, MIMO necessitates the double-directional characterization of the physical wave propagation [25, 26, 27, 28]. Extending conventional models to the MIMO case is not straightforward, since - in addition to the spatial characteristics at both link ends - also their *linkage* has to be considered. The final result of *physical* modeling is the characterization of the environment on the basis of electromagnetic wave propagation. If we now specify antennas at both link ends by setting the number of antenna elements,

their geometrical configuration, and their polarizations, preferably by agreement to reference configurations, we arrive at *analytical* MIMO channel models. These provide an analytical framework for information theory and signal processing people to design transmit and receive techniques like space-time codes and to develop MIMO algorithms in general. An extensive overview of analytical MIMO models that are based on the multivariate complex Gaussian distribution is presented in [29].

Recent work on MIMO modeling focuses its attention on indoor environments, e.g. as [30, 31, 32, 33, 34], since lead-off MIMO systems will be most probably deployed in indoor environments. Although indoor propagation is characterized by the same main propagation mechanisms as outdoor, indoor channels differ significantly from its outdoor counterparts. Specifics of the much more complex indoor propagation has to be taken into account when modeling such channels.

The main goal of this thesis is to give an overview of indoor MIMO channel models. An outline and major contributions follow.

1.3 Outline and Contributions

Chapter 2 introduces the MIMO channel and details its relationship to the double-directional radio propagation. It presents the potentials of MIMO systems, viz. beamforming, spatial diversity and spatial multiplexing. Also, specifics of indoor MIMO channels, as a consequence of the special geometric constellation in such channels, are discussed.

Chapter 3 gives an overview of existing indoor MIMO channel models. The models are categorized in physical and analytical models. The first group treats the double-directional propagation between the location of the transmit and receive array independently of the antenna configuration. The latter describes the impulse response, or equivalently the transfer function, between the elements of the antenna arrays at both link ends, thereby capturing both effects, the physical wave propagation and the influence of specific antenna configurations.

In particular, popular analytical models like the Kronecker model, Weichselberger model, the virtual channel representation and the finite scatterer model will be discussed in detail. The extension of the Saleh-Valenzuela model and Zwick's model, as a representative of physical models, and the recently standardized IEEE 802.11n indoor MIMO channel models are also briefly addressed.

Chapter 4 describes the indoor MIMO measurement campaign at 5.2GHz performed at our Institute, on which the validation of analytical channel models in Chapter 5 is based on. It details the used antennas and equipment, the measurement setup, and the measured scenarios.

A section on data post processing addresses mainly three points. First, it reveals how mutual electromagnetic coupling between the elements of the receive array was combated. Second, it exhibits the creation of different fading realizations of a MIMO channel matrix. Third, considerations on the size of the statistical ensemble when using the measurements for statistical evaluations are presented.

Chapter 5 validates analytical narrowband MIMO models, specifically the Kronecker model, the Weichselberger models and the virtual channel representation. Measurements are compared to Monte-Carlo simulations of these models with parameters extracted from respective measurements.

As measures of quality (metrics), the mutual information with equal transmit power allocation, the double-directional angular power spectrum, a diversity metric, and the Correlation Matrix Distance are used. The models' performances are studied for 2×2, 4×4 and 8×8 systems for fixed antenna inter-element spacings. Also, MIMO systems with different antenna spacings when assuming a fixed antenna number are considered.

Chapter 6 summarizes the major results of this thesis and draws some conclusions.

Appendix D addresses an interesting idea, by which Rayleigh fading MIMO channels are introduced that exhibit higher ergodic capacity than under i.i.d. fading conditions.

1.4 Notation

The following notation will be used throughout the thesis:

$\mathbf{a}$	bold lowercase letters represent vectors
$\mathbf{A}$	bold uppercase letters represent matrices
j	$j = \sqrt{(-1)}$
$(\cdot)^H$	Hermitian transposition (complex conjugate transposition)
$(\cdot)^T$	transposition
$(\cdot)^*$	complex conjugation
$\mathrm{E}\{\cdot\}$	expectation operator
$\mathrm{E}_x\{\cdot\}$	expectation operator with respect to x
$\delta(\cdot)$	Dirac delta
$\mathrm{tr}\{\cdot\}$	trace operator
$\|\| \cdot \|\|_\mathrm{F}$	Frobenius norm
$\mathrm{vec}\{\cdot\}$	vector operator, stacks the columns of a matrix into a column vector
$\mathrm{unvec}\{\cdot\}$	inverse operator to $\mathrm{vec}\{\cdot\}$
$\otimes$	Kronecker product
$\odot$	element-wise (Schur-Hadamard) product
$*$	convolution operator
$\| \cdot \|$	absolute value
$\langle \cdot, \cdot \rangle$	inner vector product
$\det\{\cdot\}$	determinant of a matrix
$\mathrm{rank}\{\cdot\}$	rank of a matrix
$\log_x\{\cdot\}$	logarithm to the base x
$\max_x\{\cdot\}$	maximum with respect to x
$\mathbf{I}$	identity matrix
$\mathbf{I}_n$	identity matrix of size $n \times n$

1.5 Abbreviations

- 3G Third Generation
- APS Angular Power Spectrum
- cdf cumulative density function
- CMD Correlation Matrix Distance
- COST European CO-operation in the fields of Scientific and Technical research
- CSI Channel State Information
- DoA Direction-of-Arrival
- DoD Direction-of-Departure
- GSCM Geometry-based Stochastic Channel Model
- IEEE Institute of Electrical and Electronics Engineers
- i.i.d. independent and identically distributed
- LoS Line-of-Sight
- MIMO Multiple-Input Multiple-Output
- MISO Multiple-Input Single-Output
- MPC Multipath Component
- MVM Minimum Variance Method
- NLoS Non Line-of-Sight
- OFDM Orthogonal Frequency Division Multiplexing
- OLoS Obstructed Line-of-Sight
- pdf probability density function
- Rx Receive, or Receiver
- SIMO Single-Input Multiple-Output
- SNR Signal to Noise Ratio
- Tx Transmit, or Transmitter
- ULA Uniform Linear Array
- WLAN Wireless Local Area Network

Chapter 2

The Indoor MIMO Channel

2.1 Double-directional Radio Propagation

The physical (electromagnetic) wave propagation is the basis for any wireless communication. Especially in a cluttered indoor environment, the transmitted signal propagates to the receiver via a number of different propagation paths (multipaths). Possible interactions of the electromagnetic field with various objects along these multipaths are described by five basic propagation mechanisms. These are free-space propagation, specular reflection, diffuse reflection (or scattering), refraction and diffraction [35]. Figure 2.1 illustrates an exemplary propagation scenario. The LoS (Line-of-Sight) component, propagating directly from the transmitter to the receiver, experiences free-space loss only. Furthermore, specular and diffuse reflections at different scatterers and at a wall are shown. Throughout this thesis we will refer to a scatterer as any object, at which a multipath components (MPC) is either reflected, scattered or diffracted.

In the field of wireless communications, the radio propagation is modeled by the impulse response of the propagation channel between the locations of the transmitter, $\mathbf{r}_{\mathrm{Tx}}$, and receiver, $\mathbf{r}_{\mathrm{Rx}}$, as a sum of contributions of individual MPCs. Disregarding polarization, the dispersion of the channel in delay and angles is described by the *double-directional* channel impulse response [25, 26, 27, 28]

$$h\left(\mathbf{r}_{\mathrm{Tx}}, \mathbf{r}_{\mathrm{Rx}}, \tau, \Omega_{\mathrm{Tx}}, \Omega_{\mathrm{Rx}}\right) = \sum_{l=1}^{L} h_l\left(\mathbf{r}_{\mathrm{Tx}}, \mathbf{r}_{\mathrm{Rx}}, \tau, \Omega_{\mathrm{Tx}}, \Omega_{\mathrm{Rx}}\right). \tag{2.1}$$

where τ is the excess delay, the spatial angle Ω_{Tx} characterizes the direction-of-departure (DoD), and Ω_{Rx} the direction-of-arrival (DoA) [1]. A total number of L MPCs above the noise level contribute to the impulse response.

The contribution of the l-th MPC, denoted by $h_l\left(\mathbf{r}_{\mathrm{Tx}}, \mathbf{r}_{\mathrm{Rx}}, \tau, \Omega_{\mathrm{Tx}}, \Omega_{\mathrm{Rx}}\right)$, reads in case of a planar wave as

$$h_l\left(\mathbf{r}_{\mathrm{Tx}}, \mathbf{r}_{\mathrm{Rx}}, \tau, \Omega_{\mathrm{Rx}}, \Omega_{\mathrm{Tx}}\right) = a_l \delta\left(\tau - \tau_l\right) \delta\left(\Omega_{\mathrm{Tx}} - \Omega_{\mathrm{Tx},l}\right) \delta\left(\Omega_{\mathrm{Rx}} - \Omega_{\mathrm{Rx},l}\right), \tag{2.2}$$

[1] The spatial angle Ω coresponds to a point on the unit sphere. It replaces the spherical azimuth and elevation angles.

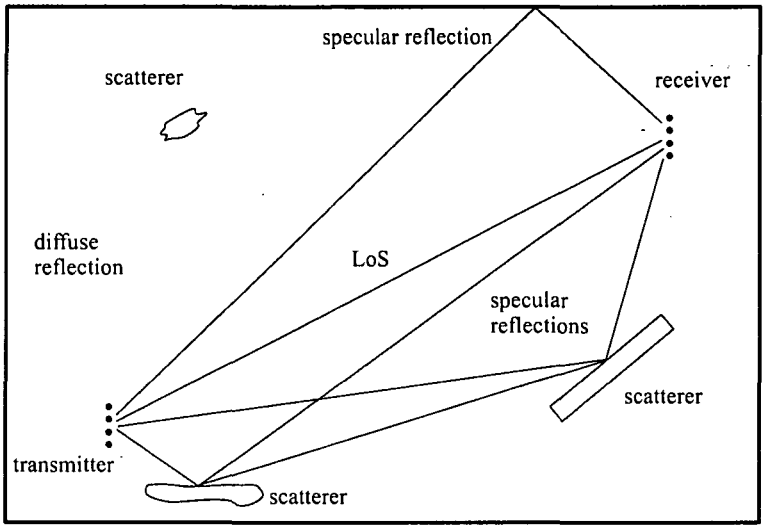

Figure 2.1: Illustration of radio wave propagation between a transmitter and a receiver.

where a_l denotes the complex amplitude, and $\delta(\cdot)$ is the Dirac delta function. The subscript $(\cdot)_l$ indicates the respective wave parameters of the l-th MPC. Arbitrary wave forms can be modeled by appropriate functions for $h_l\left(\mathbf{r}_{\mathrm{Tx}}, \mathbf{r}_{\mathrm{Rx}}, \tau, \Omega_{\mathrm{Rx}}, \Omega_{\mathrm{Tx}}\right)$. Since Maxwell's equations are linear, MPCs with arbitrary wave forms could alternatively also be broken down to a linear superposition of plane waves.

Until now, we only considered a static environment. However, the positions of the transmitter, receiver, and scatterer are in general not fixed but vary. For *time-variant* channels $\mathbf{r}_{\mathrm{Tx}}$, $\mathbf{r}_{\mathrm{Rx}}$, τ, Ω_{Tx}, Ω_{Rx}, and L become a function of (absolute) time t such that we can replace (2.1) by the more general *time-variant* double-directional channel impulse response

$$h\left(t, \tau, \Omega_{\mathrm{Tx}}, \Omega_{\mathrm{Rx}}\right) = \sum_{l=1}^{L} h_l\left(t, \tau, \Omega_{\mathrm{Tx}}, \Omega_{\mathrm{Rx}}\right). \tag{2.3}$$

Polarization can be included by extending the impulse response to a polarimetric (2×2) matrix [36] whose entries link vertical and horizontal transmit polarizations to vertical and horizontal receive polarizations,

$$\begin{bmatrix} h^{VV}\left(t, \tau, \Omega_{\mathrm{Tx}}, \Omega_{\mathrm{Rx}}\right) & h^{VH}\left(t, \tau, \Omega_{\mathrm{Tx}}, \Omega_{\mathrm{Rx}}\right) \\ h^{HV}\left(t, \tau, \Omega_{\mathrm{Tx}}, \Omega_{\mathrm{Rx}}\right) & h^{HH}\left(t, \tau, \Omega_{\mathrm{Tx}}, \Omega_{\mathrm{Rx}}\right) \end{bmatrix}, \tag{2.4}$$

where V and H denote vertical and horizontal polarization[2], which are sufficient for the characterization of the far-field. The contribution of a plane wave MPC reads then as

[2]For instance, $h^{HV}\left(t, \tau, \Omega_{\mathrm{Tx}}, \Omega_{\mathrm{Rx}}\right)$ is the impulse response that couples vertical transmit polarization into horizontal receive polarization.

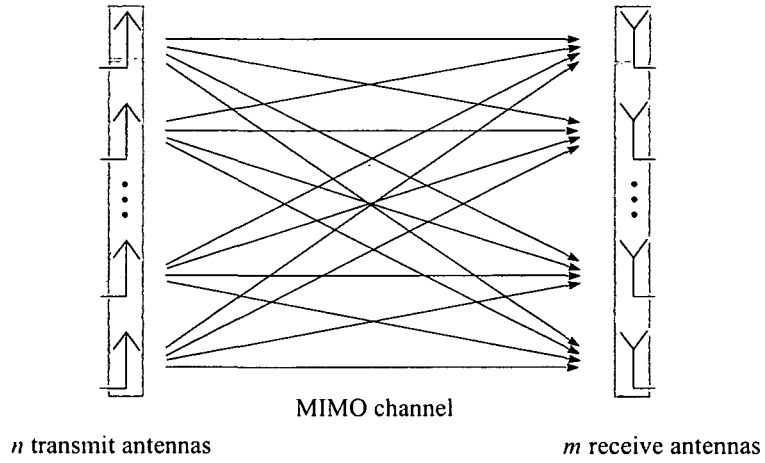

Figure 2.2: Schematic of a MIMO system with n transmit and m receive antennas.

$$\begin{bmatrix} h_l^{VV}(t,\tau,\Omega_{\mathrm{Tx}},\Omega_{\mathrm{Rx}}) & h_l^{VH}(t,\tau,\Omega_{\mathrm{Tx}},\Omega_{\mathrm{Rx}}) \\ h_l^{HV}(t,\tau,\Omega_{\mathrm{Tx}},\Omega_{\mathrm{Rx}}) & h_l^{HH}(t,\tau,\Omega_{\mathrm{Tx}},\Omega_{\mathrm{Rx}}) \end{bmatrix} = \tag{2.5}$$

$$= \begin{bmatrix} a_l^{VV} & a_l^{VH} \\ a_l^{HV} & a_l^{HH} \end{bmatrix} \delta(\tau-\tau_l)\,\delta(\Omega_{\mathrm{Tx}}-\Omega_{\mathrm{Tx},l})\,\delta(\Omega_{\mathrm{Rx}}-\Omega_{\mathrm{Rx},l})\,. \tag{2.6}$$

Herein, the complex amplitude is also a polarimetric matrix, accounting for pathloss and depolarization.

We emphasize that the double-directional impulse response describes the 'pure' propagation channel and is completely independent of antenna elements, antenna configurations, system bandwidth or pulse shaping.

2.2 MIMO Channel

In contrast to conventional communication systems with one transmit and one receive antenna, MIMO (Multiple-Input Multiple-Output) systems are equipped with more than one antenna at both link ends. As a consequence, the MIMO channel has to be described by its response between all transmit and receive antenna pairs.

Let us consider a MIMO system with n transmit and m receive antennas (Fig. 2.2), denoted by $m \times n$. A linear, time-variant MIMO channel is then represented by an $m \times n$ channel matrix $\mathbf{H}(t,\tau)$, with

$$\mathbf{H}(t,\tau) = \begin{bmatrix} h_{11}(t,\tau) & h_{12}(t,\tau) & \cdots & h_{1n}(t,\tau) \\ h_{21}(t,\tau) & h_{22}(t,\tau) & \cdots & h_{2n}(t,\tau) \\ \vdots & \vdots & \ddots & \vdots \\ h_{m1}(t,\tau) & h_{m2}(t,\tau) & \cdots & h_{mn}(t,\tau) \end{bmatrix}, \tag{2.7}$$

where the $h_{ij}(t,\tau)$ denote the time-variant impulse responses between the j-th transmit antenna and i-th receive antenna. Since (2.7) describes the channel response between the antennas at both link ends, obviously, it depends on the actual antenna configuration and bandwidth considered.

Given that the MIMO channel is stimulated by the vector valued transmit signal $\mathbf{s}(t)$, the resulting signal $\mathbf{y}(t)$ at the m receive antennas can be expressed as

$$\mathbf{y}(t) = \int_{\tau} \mathbf{H}(t,\tau)\mathbf{s}(t-\tau)d\tau + \mathbf{n}(t). \tag{2.8}$$

Here, $\mathbf{n}(t)$ is the noise and interference signal vector.

On the other hand, a *time-invariant* MIMO channel is described by a delay-only dependent channel matrix $\mathbf{H}(\tau)$ such that its input-output relation reads as

$$\mathbf{y}(t) = \int_{\tau} \mathbf{H}(\tau)\mathbf{s}(t-\tau)d\tau + \mathbf{n}(t) = \mathbf{H}(\tau) * \mathbf{s}(t) + \mathbf{n}(t), \tag{2.9}$$

where $*$ denotes the convolution operator. If the channel is frequency-flat, i.e. the channel matrix is non-zero only for $\tau = 0$, (2.9) simplifies to

$$\mathbf{y}(t) = \mathbf{H}(t)\mathbf{s}(t) + \mathbf{n}(t), \tag{2.10}$$

or for discrete-time equivalently to

$$\mathbf{y} = \mathbf{H}\mathbf{s} + \mathbf{n}, \tag{2.11}$$

when considering one symbol period.

2.2.1 Relationship to Double-directional Propagation

We have just seen two different views on the MIMO channel: whereas the double-directional impulse response directly characterizes the physical propagation channel, the MIMO channel matrix describes the response between the antennas at both link ends, given a specific antenna configuration and bandwidth. For simplicity we will refer (without loss of generality) to time-invariant channels in the following.

The relationship between both viewpoints, again disregarding polarization, can be written as

$$h_{ij}(\tau) = \int_{\Omega_{\mathrm{Tx}}} \int_{\Omega_{\mathrm{Rx}}} \int_{\tau'} h(\mathbf{r}_{\mathrm{Tx}}^{(j)}, \mathbf{r}_{\mathrm{Rx}}^{(i)}, \tau', \Omega_{\mathrm{Tx}}, \Omega_{\mathrm{Rx}}) g_{\mathrm{Tx}}(\Omega_{\mathrm{Tx}}) g_{\mathrm{Rx}}(\Omega_{\mathrm{Rx}}) f(\tau - \tau') d\tau' d\Omega_{\mathrm{Rx}} d\Omega_{\mathrm{Tx}}. \tag{2.12}$$

Here, $\mathbf{r}_{\mathrm{Tx}}^{(j)}$ denotes the j-th transmit antenna coordinates, while $g_{\mathrm{Tx}}(\Omega_{\mathrm{Tx}})$ represents the transmit antenna pattern. The subscript $(\cdot)_{\mathrm{Rx}}$ denotes the same variables for the receive side. Further, $f(\tau)$ stands for the combined impulse response of both antennas, transmit and receive filters.

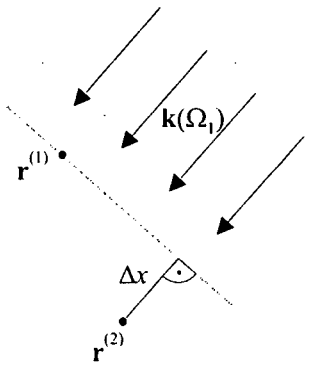

Figure 2.3: Planar wave impinging from direction Ω_1, at two locations $\mathbf{r}^{(1)}$ and $\mathbf{r}^{(2)}$.

Equation (2.12) indicates that, in general, the double-directional impulse response needs to be known between all combinations of transmit and receive antennas.

However, under the *planar wave* and *narrowband array* assumptions this burden can be mitigated. A wave originating from any scatterer to an antenna array can be approximated as planar if the distance between this scatterer and the respective antenna array is large enough compared to the inter-element spacing of that array. For MIMO this must hold true at both link ends.

Now, consider the complex amplitudes of a planar wave at two locations, $\mathbf{r}^{(1)}$ and $\mathbf{r}^{(2)}$, with a certain bandwidth B and an incidence direction Ω_1 (Fig. 2.3). The narrowband array assumption expects the bandwith B to be much smaller than the reciprocal of the transmit time across the antenna array, i.e. the product of array aperture and the bandwidth needs to be much smaller than the velocity of light[3]. If this is fulfilled, the complex wave amplitude at $\mathbf{r}^{(2)}$ is the same as at $\mathbf{r}^{(1)}$, except a phase shift of $\langle \mathbf{k}(\Omega_1), \mathbf{r}^{(2)} - \mathbf{r}^{(1)} \rangle$, where $\langle \cdot, \cdot \rangle$ denotes the inner product and $\mathbf{k}(\Omega_1)$ is the wave vector associated with direction Ω_1. This phase shift is due to the additional propagation distance Δx.

As a consequence, for MIMO it suffices to know the double-directional impulse response between *one* transmit and *one* receive antenna only. The rest follows by introducing appropriate phase shifts. For instance, an MPC given for the antenna coordinates $\mathbf{r}_{\mathrm{Tx}}^{(1)}$ and $\mathbf{r}_{\mathrm{Rx}}^{(1)}$, could be extended to the coordinates $\mathbf{r}_{\mathrm{Tx}}^{(j)}$ and $\mathbf{r}_{\mathrm{Rx}}^{(i)}$ as

$$h_l(\mathbf{r}_{\mathrm{Tx}}^{(l)}, \mathbf{r}_{\mathrm{Rx}}^{(j)}, \tau', \Omega_{\mathrm{Tx}}, \Omega_{\mathrm{Rx}}) = h_l(\mathbf{r}_{\mathrm{Tx}}^{(1)}, \mathbf{r}_{\mathrm{Rx}}^{(1)}, \tau', \Omega_{\mathrm{Tx}}, \Omega_{\mathrm{Rx}}) e^{-j\langle \mathbf{k}(\Omega_{\mathrm{Tx}}), \mathbf{r}_{\mathrm{Tx}}^{(j)} - \mathbf{r}_{\mathrm{Tx}}^{(1)} \rangle} e^{-j\langle \mathbf{k}(\Omega_{\mathrm{Rx}}), \mathbf{r}_{\mathrm{Rx}}^{(i)} - \mathbf{r}_{\mathrm{Rx}}^{(1)} \rangle}. \tag{2.13}$$

To this end, (2.12) can be simplified to

[3] As emphasized in [24], the narrowband *array* assumption does not imply that the *channel* is frequency-flat fading.

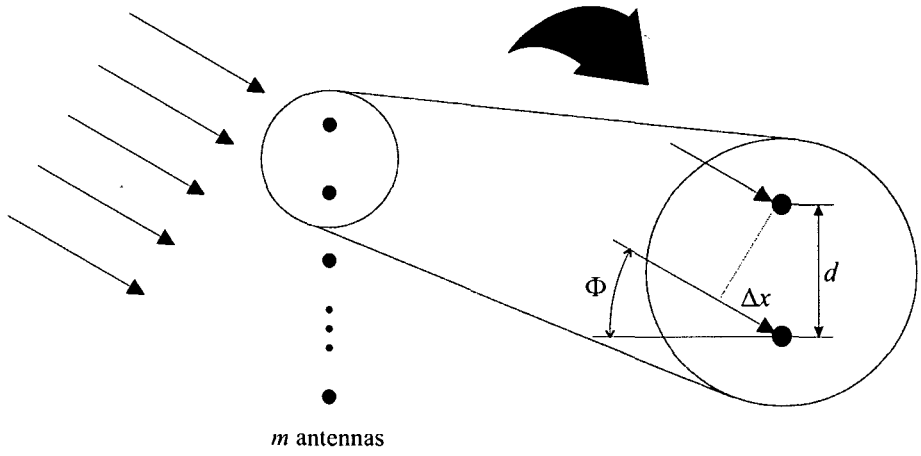

Figure 2.4: Planar wave impinging at the elements of a uniform linear array (ULA).

$$h_{ij}(\tau) = \int_{\Omega_{\mathrm{Tx}}} \int_{\Omega_{\mathrm{Rx}}} \int_{\tau'=0}^{\tau_{\max}} h(\mathbf{r}_{\mathrm{Tx}}^{(1)}, \mathbf{r}_{\mathrm{Rx}}^{(1)}, \tau', \Omega_{\mathrm{Tx}}, \Omega_{\mathrm{Rx}}) e^{-j\langle \mathbf{k}(\Omega_{\mathrm{Tx}}), \mathbf{r}_{\mathrm{Tx}}^{(j)} - \mathbf{r}_{\mathrm{Tx}}^{(1)} \rangle} \cdot e^{-j\langle \mathbf{k}(\Omega_{\mathrm{Rx}}), \mathbf{r}_{\mathrm{Rx}}^{(i)} - \mathbf{r}_{\mathrm{Rx}}^{(1)} \rangle} g_{\mathrm{Tx}}(\Omega_{\mathrm{Tx}}) g_{\mathrm{Rx}}(\Omega_{\mathrm{Rx}}) f(\tau - \tau') d\tau' d\Omega_{\mathrm{Rx}} d\Omega_{\mathrm{Tx}}. \quad (2.14)$$

The above derived relationship could also be written in terms of so-called *steering* and *response* vectors. A response vector is a vector of complex signals over the receive array elements as a response to a specific impinging DoA. Analogously, a steering vector is a vector of antenna weights across the transmit array which are necessary to steer into a specific DoD. Steering and response vectors depend on the DoDs and DoAs of respective waves, the array geometry and, in general, also on the element pattern. Both vectors are fully deterministic, except for a scalar factor.

As an example, when considering *azimuthal* plane wave DoAs only, the response vector of a uniform linear array (ULA) with m identical antennas (c.f. Fig. 2.4) can be expressed as

$$\mathbf{a}_{\mathrm{Rx}}(\Phi) = g_{\mathrm{Rx}}(\Phi) \cdot \begin{pmatrix} 1 \\ e^{-j\cdot\mu} \\ e^{-j\cdot 2\mu} \\ \vdots \\ e^{-j\cdot(m-1)\mu} \end{pmatrix}. \quad (2.15)$$

Here, the regular antenna configuration with separation d causes a constant phase shift of

$$\mu = \frac{2\pi d}{\lambda} \cdot \sin\Phi \quad (2.16)$$

between consecutive antenna elements, where λ is the wavelength and Φ the azimuth DoA. The antenna signals at the array are identical, expect a phase shift dependent on the direction

of the impinging wave. But, if the element patterns would differ, an additional (complex) scaling to each response vector entry due to the different antenna gains for this specific direction has to be considered in (2.15).

Now, the relationship of (2.14) can also be written in terms of steering and response vectors, $\mathbf{a}_{\mathrm{Tx}}$ and $\mathbf{a}_{\mathrm{Rx}}$,

$$\mathbf{H}(\tau) = \int_{\Omega_{\mathrm{Tx}}} \int_{\Omega_{\mathrm{Rx}}} \int_{\tau'} h(\mathbf{r}_{\mathrm{Tx}}^{(1)}, \mathbf{r}_{\mathrm{Rx}}^{(1)}, \tau', \Omega_{\mathrm{Tx}}, \Omega_{\mathrm{Rx}}) \mathbf{a}_{\mathrm{Tx}}(\Omega_{\mathrm{Tx}}) \mathbf{a}_{\mathrm{Rx}}^{T}(\Omega_{\mathrm{Rx}}) f(\tau - \tau') d\tau' d\Omega_{\mathrm{Rx}} d\Omega_{\mathrm{Tx}}. \quad (2.17)$$

When polarization is also considered, (2.17) reads as

$$\begin{aligned}\mathbf{H}(\tau) = \int_{\Omega_{\mathrm{Tx}}} \int_{\Omega_{\mathrm{Rx}}} \int_{\tau'} \big[& h^{VV}(\mathbf{r}_{\mathrm{Tx}}^{(1)}, \mathbf{r}_{\mathrm{Rx}}^{(1)}, \tau', \Omega_{\mathrm{Tx}}, \Omega_{\mathrm{Rx}}) \mathbf{a}_{\mathrm{Tx}}^{(V)}(\Omega_{\mathrm{Tx}}) (\mathbf{a}_{\mathrm{Rx}}^{(V)})^{T}(\Omega_{\mathrm{Rx}}) + \\ & + h^{VH}(\mathbf{r}_{\mathrm{Tx}}^{(1)}, \mathbf{r}_{\mathrm{Rx}}^{(1)}, \tau', \Omega_{\mathrm{Tx}}, \Omega_{\mathrm{Rx}}) \mathbf{a}_{\mathrm{Tx}}^{(H)}(\Omega_{\mathrm{Tx}}) (\mathbf{a}_{\mathrm{Rx}}^{(V)})^{T} \Omega_{\mathrm{Rx}}) + \\ & + h^{HV}(\mathbf{r}_{\mathrm{Tx}}^{(1)}, \mathbf{r}_{\mathrm{Rx}}^{(1)}, \tau', \Omega_{\mathrm{Tx}}, \Omega_{\mathrm{Rx}}) \mathbf{a}_{\mathrm{Tx}}^{(V)}(\Omega_{\mathrm{Tx}}) (\mathbf{a}_{\mathrm{Rx}}^{(H)})^{T} \Omega_{\mathrm{Rx}}) + \\ & + h^{HH}(\mathbf{r}_{\mathrm{Tx}}^{(1)}, \mathbf{r}_{\mathrm{Rx}}^{(1)}, \tau', \Omega_{\mathrm{Tx}}, \Omega_{\mathrm{Rx}}) \mathbf{a}_{\mathrm{Tx}}^{(H)}(\Omega_{\mathrm{Tx}}) (\mathbf{a}_{\mathrm{Rx}}^{(H)})^{T}(\Omega_{\mathrm{Rx}}) \big] \cdot f(\tau - \tau') d\tau' d\Omega_{\mathrm{Rx}} d\Omega_{\mathrm{Tx}},\end{aligned}$$

where $\mathbf{a}_{\mathrm{Tx/Rx}}^{(V)}$ and $\mathbf{a}_{\mathrm{Tx/Rx}}^{(H)}$ denote the steering/response vectors corresponding to the vertical and horizontal polarization.

2.3 MIMO Potentials

By exploiting the spatial channel domain, MIMO systems support *beamforming*, *spatial diversity* and *spatial multiplexing*. The following subsections will discuss these features briefly. In order to avoid unnecessary complexity, we will focus on the spatial domain and therefore refer to frequency-flat channels only. Only one user is considered, i.e. we do not deal with multi-user interference. The only interfering term is the additive noise.

2.3.1 Spatial Multiplexing

The most promising feature of a MIMO channel is its ability to transmit several parallel data streams without requiring more bandwith or transmit power. The number of multiplexed streams depends on the spatial properties of the radio environment. It varies from one, e.g. under Line-of-Sight (LoS) conditions to the minimum of n and m in rich scattering environments. In fact, pioneering works showed in [9, 10, 11] that capacity of MIMO channels can be a multiple of conventional SISO channels.

Strictly following the nomenclature of information theory, we will term the upper limit of data transmission between the channel input and output with arbitrarily small error probability and for a given transmit power allocation as *mutual information*. Note that mutual information refers to an arbitrary, not necessarily optimally chosen transmit power allocation. In contrast, *channel capacity* in Shannon sense will be reserved for maximum mutual information between the link ends.

2.3.1.1 Eigenvalue Decomposition

The singular value decomposition applied to an instantaneous (deterministic) MIMO channel matrix $\mathbf{H}$ reads as

$$\mathbf{H} = \mathbf{U}\mathbf{D}\mathbf{V}^H, \tag{2.18}$$

where the left and right singular vectors of the channel matrix $\mathbf{H}$ constitute the columns of the unitary matrices $\mathbf{U}$ and $\mathbf{V}$, respectively. The diagonal matrix of the corresponding singular values[4] of $\mathbf{H}$, $\sqrt{\lambda_i}$, is denoted by $\mathbf{D}$.

Since $\mathbf{U}$ and $\mathbf{V}$ are unitary matrices, it is obvious that an equivalent representation of the MIMO signal model can be expressed as

$$\tilde{\mathbf{y}} = \mathbf{D}\tilde{\mathbf{s}} + \tilde{\mathbf{n}}, \tag{2.19}$$

Here, $\tilde{\mathbf{y}}$, $\tilde{\mathbf{s}}$ and $\tilde{\mathbf{n}}$ represent transformed receive, transmit and noise vectors, such that $\tilde{\mathbf{y}} = \mathbf{U}^H\mathbf{y}$, $\tilde{\mathbf{s}} = \mathbf{V}^H\mathbf{s}$, and $\tilde{\mathbf{n}} = \mathbf{U}^H\mathbf{n}$.

This orthogonal transformation allows for diagonalizing the channel into a set of uncoupled parallel virtual sub-channels with path gains equal to the elements of $\mathbf{D}$. The number of these virtual sub-channels is determined by the rank of $\mathbf{D}$ which is equal to the rank of the channel matrix[5], $\text{rank}(\mathbf{D}) = \text{rank}(\mathbf{H})$.

2.3.1.2 Mutual Information with Equal Power Allocation

Mutual Information of a Constant (or Deterministic) MIMO Channel

Disregarding the bandwidth, it is well known, that the Shannon capacity of an instantaneous SISO channel with path gain h, in bits/s/Hz, is given by

$$C = \log_2(1 + \frac{P_{\text{Tx}}}{\sigma^2_{noise}}|h|^2) = \log_2(1 + \rho), \tag{2.20}$$

where P_{Tx} denotes the transmit power, σ^2_{noise} is the noise power, and ρ results to the receive SNR, $\rho = \frac{P_{\text{Tx}}}{\sigma^2_{noise}}|h|^2$. For high SNR regions, the channel capacity depends logarithmically on the transmit power.

A generalization of (2.20) to multiple antennas can be derived as follows. Consider a MIMO channel where the total transmit power P_{Tx} is equally spread over the transmit antennas. Then, the mutual information between the channel input and output with equal power allocation can be calculated as the sum of contributions of all virtual sub-channels with corresponding path gains of $\sqrt{\lambda_i}$ and may be written as

[4]The columns of $\mathbf{U}$ are also the eigenvectors of $\mathbf{H}\mathbf{H}^H$, the columns of $\mathbf{V}$ are the eigenvectors of $\mathbf{H}^H\mathbf{H}$, and the elements of $\mathbf{D}$ are the square-roots of the eigenvalues of $\mathbf{H}\mathbf{H}^H$ (which are the same as the ones of its Hermitian $\mathbf{H}^H\mathbf{H}$).

[5]Please note that the rank of a matrix is generally upper limited by the minimum number of its rows and columns. In case of a MIMO matrix, a further limitation comes from the underlying channel: there, the rank is limited by the minimum number of the rows and columns (i.e. the number of receive and transmit antennas), and the number of scatterers.

$$I = \sum_{i=1}^{\text{rank}(\mathbf{D})} \log_2(1 + \frac{P_{\text{Tx}}}{n\sigma^2_{noise}}\lambda_i) = \log_2 \det(\mathbf{I}_m + \frac{P_{\text{Tx}}}{n\sigma^2_{noise}}\mathbf{H}\mathbf{H}^H), \tag{2.21}$$

where $\mathbf{I}_m$ denotes the $m \times m$ identity matrix.

Although its total transmit power stays the same as in case of SISO, the MIMO channels enable much higher mutual information. The more uniform the eigenvalues λ_i are distributed, the higher the mutual information.

In (2.21), the channel matrix $\mathbf{H}$ contains the individual path gains (channel gain). However, a proper normalization of $\mathbf{H}$ allows for representing the mutual information in terms of the average receive SNR ρ, as it is defined by

$$\rho = \frac{P_{\text{Tx}}}{\sigma^2_{noise} mn} \sum_{i=1}^{m}\sum_{j=1}^{n} |h_{ij}|^2 . \tag{2.22}$$

Specifically, if the average pathloss over all transmit-receive antenna pairs (average SISO pathloss) is set to unity, i.e.

$$\frac{1}{mn}\sum_{i=1}^{m}\sum_{j=1}^{n} |h_{ij}|^2 = 1, \tag{2.23}$$

then (2.21) can be alternatively formulated as

$$I = \log_2 \det(\mathbf{I}_m + \frac{\rho}{n}\mathbf{H}\mathbf{H}^H), \tag{2.24}$$

with $\mathbf{H}$, this time, denoting the *normalized* MIMO channel matrix. A step-by-step derivation of the mutual information with equal power allocation can be found in [37].

Mutual Information of a Fading MIMO Channel

Up to now, only a constant, deterministic channel was considered. However, wireless channels are in practice not constant, but fade. The different fading realizations of a channel matrix (channel states) assume values over a continuum. For analytical assessment, channel fading is usually treated stochastically. The fading channel realizations are modeled as random realizations of a stochastic matrix, i.e. a matrix whose elements are random variables.

The mutual information, calculated for each channel state, becomes a random variable described in terms of its statistics. A common way to represent such statistics is the cumulative density function (cdf). Figure 2.5 illustrates the mutual information cdf of an exemplary 4×4 MIMO fading channel with an average receive SNR of 20dB. Useful measures are the *ergodic* (or *average*) and the *outage* mutual information. To be precise, there is a slight difference between the terms ergodic and average. Ergodic refers to the expected value of the mutual information for *stochastically* described channel matrices as it can be expressed by

$$\bar{I} = \mathrm{E}_{\mathbf{H}} \left\{ \log_2 \det(\mathbf{I}_m + \frac{\rho}{n}\mathbf{H}\mathbf{H}^H) \right\}, \tag{2.25}$$

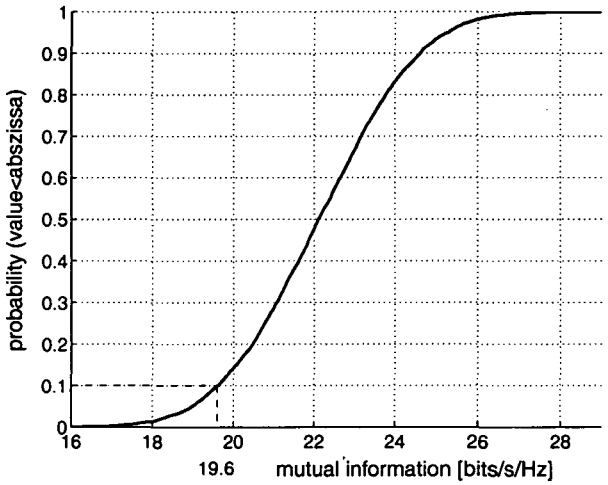

Figure 2.5: The mutual information of a fading channel becomes a random variable that is commonly described by its cumulative density function (cdf): Mutual information cdf of an exemplary 4 × 4 MIMO fading channel with an average receive SNR of 20dB.

where $\mathrm{E}_{\mathbf{H}}\{\cdot\}$ denotes the expectation with respect to $\mathbf{H}$. On the other hand, if different channel matrix *realizations* are considered, we prefer to call the arithmetic mean of the mutual information the average, which is an estimator for the expectation.

The *outage* mutual information is defined as the mutual information achieved, or exceeded, at a given confidence level. For example, if an outage mutual information at a level of 90% is given as 20 bits/s/Hz, then this means that in 90% of all cases, a mutual information of at least 20 bits/s/Hz can be guaranteed. Note that the outage values can be easily obtained from the cdf. Since the cdf plots the probability p for a random variable to be smaller than a certain value x, its complementary probability $(1-p)$ determines the confidence level for the outage value x. For instance, the channel shown in Fig. 2.5 exhibits an outage mutual information of approximately 19.6 bits/s/Hz at a confidence level on 90%.

Normalization of Fading Channels

For fading channels, it is meaningful to normalize all realizations of the MIMO channel with the same factor. This captures the effect of fading. The average receive SNR in (2.25) is then defined by

$$\rho = \frac{P_{\mathrm{Tx}}}{\sigma^2_{noise} mn} \mathrm{E}_{\mathbf{H}} \left\{ \sum_{i=1}^{m} \sum_{j=1}^{n} |h_{ij}|^2 \right\}. \tag{2.26}$$

The normalization factor has to be determined such that the average pathloss of the fading channel over all transmit-receive antenna pairs is set to unity, i.e.

$$\frac{1}{mn} \mathrm{E}_{\mathbf{H}} \left\{ \sum_{i=1}^{m} \sum_{j=1}^{n} |h_{ij}|^2 \right\} = 1. \tag{2.27}$$

Things get more complicated when a comparison of different environments (scenarios) is of interest, e.g. if one wants to compare sets of measured channel matrices taken at different locations. In this case, there are two ways of normalizing the channels at the individual locations [38]. The first applies (2.27) to each location separately, thereby normalizing the different pathlosses out. Since the receive SNR can then be set independently at different locations, this corresponds to a system with power control. Alternatively, a common normalization factor can be applied to all realizations at all locations. This takes the pathloss of different locations into account and therefore corresponds to constant transmit power.

2.3.1.3 MIMO Capacity

The channel capacity of a deterministic (instantaneous) flat-fading MIMO channel equals the maximum mutual information [10],

$$C = \max_{Q:\mathrm{tr}\{\mathbf{Q}\}=P_{\mathrm{Tx}}} \left[\log_2 \det(\mathbf{I}_m + \frac{\rho}{n}\mathbf{H}\mathbf{Q}\mathbf{H}^H)\right], \tag{2.28}$$

where the maximization is performed with respect to the correlation matrix $\mathbf{Q} = \mathrm{E}\{\mathbf{s}\mathbf{s}^{\mathrm{H}}\}$ of the transmit signal, under the power constraint $\mathrm{tr}\{\mathbf{Q}\} = P_{\mathrm{Tx}}$. An optimum power allocation over the sub-channels implies perfect channel state information (CSI) at the transmitter (Tx) and receiver (Rx). Note that perfect CSI assumes the channel matrix $\mathbf{H}$ to be known perfectly and instantaneously at both link ends. As shown in [10], the solution to this maximization problem is to apply Shannon's 'waterpouring' or 'water-filling' principle to the different sub-channels.

For MIMO fading channels capacity has multiple definitions depending on the information about the channel [13]. When assuming perfect CSI at the transmit (Tx) and receive (Rx) side (2.28) can be applied to each channel state such that *ergodic capacity* results simply to

$$\bar{C} = \mathrm{E}_{\mathbf{H}}\left\{\max_{Q:\mathrm{tr}\{\mathbf{Q}\}=P_{\mathrm{Tx}}} \left[\log_2 \det(\mathbf{I}_m + \frac{\rho}{n}\mathbf{H}\mathbf{Q}\mathbf{H}^H)\right]\right\}. \tag{2.29}$$

However, if perfect CSI is available at the receiver but only average information about the channel (channel distribution information) at Tx ergodic capacity reads as

$$C = \max_{Q:\mathrm{tr}\{\mathbf{Q}\}=P_{\mathrm{Tx}}} \left[\mathrm{E}_{\mathbf{H}}\left\{\log_2 \det(\mathbf{I}_m + \frac{\rho}{n}\mathbf{H}\mathbf{Q}\mathbf{H}^H)\right\}\right], \tag{2.30}$$

In this case, a closed form solution for the maximization over $\mathbf{Q}$ does not exist in general. There are solutions only for some idealistic channel distributions. For instance, it is shown in [10] and [11] that uncorrelated transmit signals with uniformly distributed powers, where $\mathbf{Q}$ equals the identity matrix, are optimum for a MIMO matrix with i.i.d. zero-mean complex Gaussian entries.

A tutorial on recent work focused on the capacity of MIMO systems under different assumptions about channel information available at the transmitter and receiver can be found in [13].

2.3.2 Beamforming

Very much like for multiple-input single-output (MISO) or single-input multiple-output (SIMO) systems, where antenna arrays at one link end (adaptive or smart antennas) enable the focusing of transmit/receive power into a certain angular direction [5, 8], MIMO systems also allow for beamforming. By choosing appropriate antenna weights, the directional pattern of the considered array can be modified, i.e. a 'beam' can be formed, such that paths from desired directions may enhanced. For MIMO systems, beamforming can be either applied at the Tx side, the Rx side, or both.

Assuming that no instantaneous CSI is available, the resulting gain (beamforming or array gain) at one link end is limited by the channel properties and the number of antennas at the considered array, i.e. to n at Tx and m at Rx. The more directive the channel is, the higher is its beamforming gain. Thus, the highest beamforming gain is achievable for the most directive MIMO channel with only one DoD and one DoA, e.g. as under LoS conditions. Then, the offered total gain is equal to mn.

Note that high directivity at one link end gives rise to high correlations of the respective antenna signals of a MIMO system (spatial correlations).

2.3.3 Spatial Diversity

Multipath propagation causes the significant problem of fading. An effective method to combat fading is spatial diversity, also known as antenna diversity. It exploits uncorrelated multiple copies (replicas) of the transmitted radio signal which are generally, among others, also spread in the spatial domain. This technique reduces fading and thereby increases the reliability of the radio link.

For MIMO systems, spatial diversity can be again either exploited at the Tx side, the Rx side, or both. If its exploited only at one link end, the degree of diversity is limited to the number of antennas at this link end. In contrast, if diversity is exploited at both link ends, the maximum achievable degree of diversity is equal to mn. Channel correlation reduces diversity. The highest possible degree of diversity is offered by spatially white MIMO channels with its i.i.d. channel coefficients.

2.3.4 Trade-off between Beamforming, Diversity and Multiplexing

As already comprehensively reported in [29, Chapter 6.2], the MIMO channel supports trade-offs between beamforming, diversity and multiplexing. Indeed, the decision which of these potentials should be exploited depends on the spatial structure of the underlying radio channel, see Fig. 2.6. Many scatterers in a broad angular region around the Tx array make the Tx side 'diverse', the antenna signals uncorrelated and allow for diversity. In contrast, a 'directive' channel, i.e. a single strong scatterer or a group of closely-spaced scatterers, may support beamforming. A directive channel gives rise to high antenna correlation. The same holds true for the Rx link end. If both, transmit and receive sides are diverse both features, Tx-Rx-diversity and multiplexing are possible. In this case the optimal trade-off between diversity and multiplexing will be determined by system requirements, e.g. desired data rate and reliability of transmission.

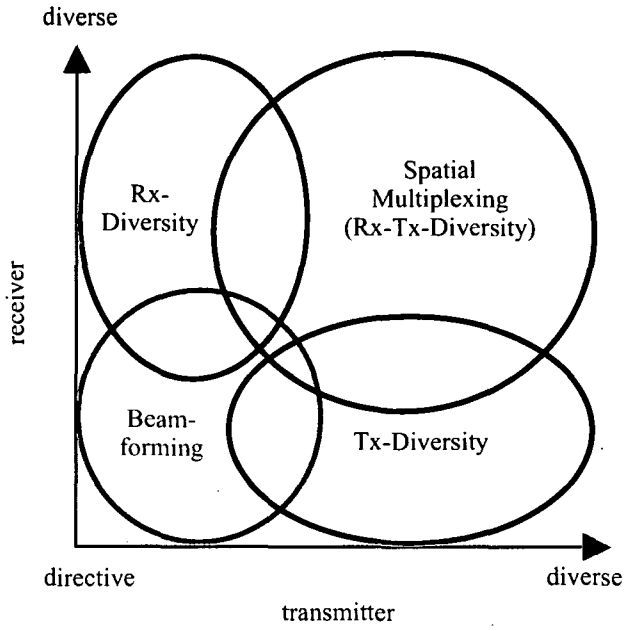

Figure 2.6: The extent to which the channel supports beamforming, diversity or multiplexing depends on the directivity/diversity of both link ends [29, Chapter 6.2].

However, be aware of the fact that the characterization of the MIMO channels at the link ends only, e.g. like the antenna correlations at both link ends, is not sufficient to determine the capability of spatial multiplexing exactly. Even if two MIMO channels show the same complex transmit and receive correlation, the capacity of these channels can differ, depending on the correlation of channel coefficients other than antenna correlations ('diagonal correlations', see Appendix D).

Also note that even in the case of completely uncorrelated antennas at both link ends, the MIMO channel is not guaranteed to support multiplexing ('keyhole' phenomenon). We will discuss this phenomenon in Chapter 3.3.1.5.

In summary, we emphasize that it is the physical wave propagation (radio propagation) that sets the limits for MIMO systems.

2.4 Specifics of Indoor Channels

Indoor radio propagation as it occurs e.g. in office buildings, shopping malls, and airports or railway stations is characterized by the same main propagation mechanisms as outdoor propagation: free-space propagation, specular reflection, diffuse reflection (or scattering), refraction and diffraction.

But the situation is more complex for indoor environments, where numerous objects may act as scatterers. Its main specifics result from

- the smaller distances that are covered, and

- the much larger variability of such environments.

The smaller distances may lead to a smaller delay dispersion, dense multipath propagation with a much higher number of MPCs, non-planar wave fronts, and more diffuse reflections from extended scatterers. Numerous measurements showed that MPCs tend to come in bundles or 'clusters' [39, 40, 41, 42]. The single MPCs within such clusters can rarely be resolved. The authors of [43] observed a diffuse, exponentially decaying tail in the measured power delay profile that could stem from diffuse reflections/scattering of extended objects, or from multiple reflections/scattering of higher order.

Recall that impinging/departing wave fronts may be approximated as planar only if the far-field assumption is met. The distance between the scatterers and antenna arrays has to be large enough compared to the inter-element spacing of the transmit/receive array. Obviously, this condition is not always fulfilled in indoor environments. For instance, a nearby extended scatterer may cause diffuse reflection, showing up in an angular and delay spread of the corresponding MPC. On the other hand, nearby localized ('point') scatterers induce spherical wave fronts.

The reasons for the much larger variability of indoor environments are the following. The propagation within buildings is strongly influenced by the actual scenario, the construction materials, the building type, as well as the number and type of scatterers involved. Walls and scatterers made of different materials affect the radio signal differently. Also, the position and height of the antennas plays an important role. For example, antennas mounted at the center of the ceiling 'see' a different propagation channel than antennas mounted on the wall. Because of the large variability, indoor environments should be further specified as it is done for outdoor environments. It would be meaningful to agree on a set of canonical or reference scenarios.

Another specific of indoor environments is that, compared to outdoor, movements of scatterers and terminals are slower. Consequently, the Doppler shifts are much smaller.

As we will discuss in the next chapter in detail, of course, the specifics of indoor models have to be taken into account when modeling such channels.

Chapter 3

Review of Existing Indoor Channel Models

3.1 Overview

The modeling of MIMO radio channels has attracted much attention since recent studies have demonstrated the impressive channel capacity gain of wireless systems employing multiple antennas on both link ends.

No doubt, lead-off MIMO techniques will be applied particularly in indoor environments. The focus on indoor channels can be argued as follows. MIMO systems will have to be equipped with more than three or four antennas at each link end in order to achieve considerable capacity gains. Devices for such systems will consume much power that is necessary for the parallel receive chains and the advanced MIMO signal processing. This, in turn, will favor devices like laptops, primarily used in indoor environments, which provide sufficient battery power. Furthermore, MIMO channels need to be tracked when aiming high capacity. Since indoor channels are changing slowly they can be tracked easily, which makes them predestined for MIMO applications. As a consequence, recent attempts on MIMO modeling focus its attention on the modeling of indoor channels, pushed by the development of high data rate WLAN systems, Beyond 3G mobile communication systems and other activities.

Due to the specifics of indoor channels, models initially developed for outdoor cannot be applied to indoor one-to-one in general. While some outdoor models need only an appropriate modification of parameter values, others need some adaption of the modeling approach. But there are also models that are based on inherent outdoor channel characteristics and therefore may not be used for indoor purposes at all. An overviews on MIMO channel models, not necessarily for indoor, can be found e.g. in [44].

A variety of indoor MIMO channel models, mostly based on measurements, have been reported in the last years. The proposed models can be classified in various ways. One possible classification is shown in Fig. 3.1.

Herein, we distinguish between *physical models* and *analytical models*[1]. Physical models characterize an environment on the basis of electromagnetic wave propagation by describing the

[1] One would expect the contrary to 'physical' to be 'non-physical'. However, for reasons which will become clear in the sequel, we prefer 'analytical'.

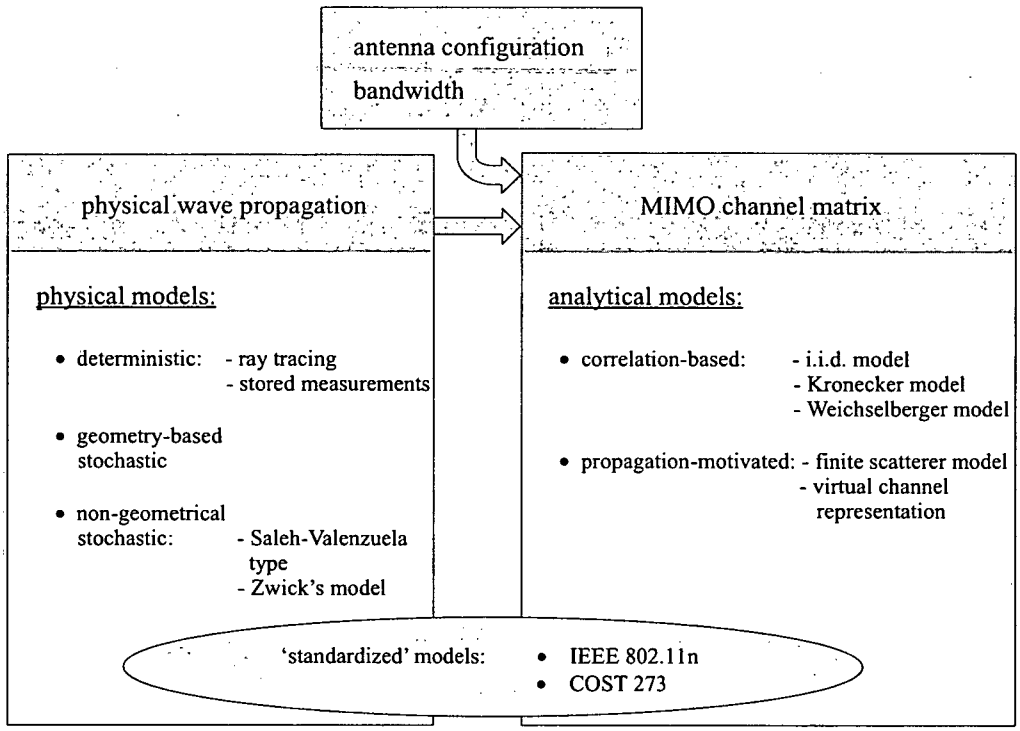

Figure 3.1: Overview of indoor MIMO channel models, with some samples in each category.

double-directional multipath propagation [25, 36] between the location of the transmit array and receive array. They explicitly model wave propagation parameters like complex amplitudes of multipath components, their directions-of-departure, directions-of-arrival, and delays. More sophisticated models also treat polarization and time variations. Depending on the chosen complexity, physical models enable an accurate reproduction of radio propagation. As main drawbacks count the measurement and parameter extraction that is usually very tedious. Obviously, *physical* models are independent of antenna configurations (directional antenna pattern, antenna number, array geometry, polarization, mutual coupling) and system bandwidth. As such they allow to find optimum antenna configurations (including polarization) for each type of scenario.

In contrast, *analytical* models describe the impulse response, or equivalently the transfer function, of the channel between the elements of the antenna arrays at the transmitter and receiver. These impulse responses are combined in a (delay dependent) channel matrix given by analytical mathematical expressions. Analytical models are very popular for developing MIMO algorithms in general, as they allow for reproducing various channel characteristics by changing only a small number of modeling parameters. Of course, different simplifying assumptions on the underlying radio propagation are necessary beforehand. The relationship between physical and analytical models is the same as between wave propagation and the MIMO channel matrix (Chapter 2.2.1). Starting from a physical model we arrive at analytical models, if we specify antenna arrays at both link ends by setting antenna elements (i.e. antenna pattern and bandwidth), their geometrical configuration, and their polarizations, preferably by agreement to reference configurations. Note that a physical model can be easily converted

into an analytical model but not vice versa.

Physical models can be classified as *deterministic*, *geometry-based stochastic* and *non-geometric stochastic models*. The first determine the physical parameters in a fully deterministic way. Examples are ray tracing, e.g. [45], and stored measurement data that can be replayed anytime. The term geometry-based refers to the fact that the modeled impulse response is related to the geometrical location of scatterers and other interacting objects. Their location is chosen stochastically in geometry-based stochastic channel models (GSCM). This class of models was initially introduced independently by [46], [47], [48], [49] and [50] for outdoor environments. A fledgeling version of a GSCM for indoor has recently been developed at our Institute [51]. In contrast, non-geometric stochastic models treat physical parameters completely stochastically by assuming proper distribution functions, e.g. as it is done for the extension of the Saleh-Valenzuela model [52, 30] or the model introduced by Zwick et al. [31].

Analytical models, could be further subdivided into *propagation-motivated models* and *correlation-based models*. The first class treats the channel matrix by modeling propagation parameters. Examples are the finite scatterer model [53] or the virtual channel representation [54]. As it is obvious from the name, correlation-based models treat the MIMO channel by correlations between channel matrix entries. Popular correlation-based analytical channel models are the Kronecker model [55, 56, 57, 58] and the Weichselberger model [59, 29].

For the purpose of comparing different MIMO systems based on the same channel conditions, 'standard' MIMO channel models were established by different organizations. Standardizing a physical model means to agree on a channel model, reference environments, and parameter values for these environments. In principle, also analytical models could be standardized. For indoor MIMO, the only standardized channel model up to now is the IEEE 802.11n model [60]. Apart from this, the European research initiative COST 273 [61] is currently working on standardizing MIMO channel models, including indoor environments. This work is still in progress and will be finalized in June 2004.

An additional classification can be done by distinction between *narrowband* and *broadband* models. While for narrowband (frequency-flat, memoryless) channels, only the spatial channel structure is modeled, the latter introduces frequency-selectivity by modeling both the spatial and temporal channel structure.

Note that the models presented in this chapter are not exclusively indoor models. Particularly analytical channel models can, with appropriately modified parameters, also be applied to outdoor environments.

3.2 Physical Models

3.2.1 The Extension of the Saleh-Valenzuela Model

For SISO channels Saleh and Valenzuela observed that, in indoor environments, MPCs tend to come in bundles or *'clusters'*. They developed a stochastic broadband indoor channel model (the *Saleh-Valenzuela model*) [39] based on the temporal clustering approach with an exponential decay for both power of MPCs within a single cluster as well as for the average cluster power over delay. The cluster arrival process and the MPC arrival process within a cluster are modeled as Poisson processes with different arrival rates. This model was then

extended to the spatial domain by including azimuthal DoAs [41, 40].

For the MIMO case, [52, 30] presented a further extension of the Saleh-Valenzuela model. From experimental data the authors observed clusters as a group of MPCs with similar DoDs, DoAs, and delays. The proposed narrowband channel model expresses the double-directional channel impulse response arising from L clusters and K MPCs per cluster as

$$h\left(\varphi_{\mathrm{Rx}}, \varphi_{\mathrm{Tx}}\right) = \frac{1}{\sqrt{LK}} \sum_{l=0}^{L-1} \sum_{k=0}^{K-1} \beta_{kl} \delta\left(\varphi_{\mathrm{Tx}} - \varphi_{\mathrm{Tx},l} - \Phi_{\mathrm{Tx},kl}\right) \delta\left(\varphi_{\mathrm{Rx}} - \varphi_{\mathrm{Rx},l} - \Phi_{\mathrm{Rx},kl}\right) \tag{3.1}$$

where φ_{Tx} and φ_{Rx} are azimuth DoD and DoA. The mean DoD and mean DoA of the l-th cluster is denoted by $\varphi_{\mathrm{Tx},l}$ and $\varphi_{\mathrm{Rx},l}$. For the l-th cluster, $\Phi_{\mathrm{Tx},kl}$ and $\Phi_{\mathrm{Rx},kl}$ are DoD and DoA of its k-th MPC relative to the respective mean angles, while β_{kl} stands for the complex amplitude.

The directions at both link ends are assumed to be statistically independent of each other, but follow the same distribution. The cluster centers, i.e. the mean DoDs and mean DoAs of clusters, are uniformly distributed over $[0° \ldots 360°)$ while the angular MPC distribution $p(\varphi)$ within each cluster follows a Laplacian distribution with an angular standard deviation of σ,

$$p\left(\varphi\right) = \frac{1}{\sqrt{2}\sigma} e^{|\sqrt{2}\varphi/\sigma|}, \tag{3.2}$$

The complex amplitude of an MPC, β_{kl}, is modeled by a zero-mean complex Gaussian distribution. For reasons of simplicity, it is assumed that MPCs corresponding to a certain cluster have the same power.

Note that a straight-forward extension of (3.1) to a broadband model reads as

$$\begin{aligned} h\left(\varphi_{\mathrm{Rx}}, \varphi_{\mathrm{Tx}}, \tau\right) \;=\; & \frac{1}{\sqrt{LK}} \sum_{l=0}^{L-1} \sum_{k=0}^{K-1} \beta_{kl} \delta\left(\varphi_{\mathrm{Tx}} - \varphi_{\mathrm{Tx},l} - \Phi_{\mathrm{Tx},kl}\right) \cdot \\ & \cdot \delta\left(\varphi_{\mathrm{Rx}} - \varphi_{\mathrm{Rx},l} - \Phi_{\mathrm{Rx},kl}\right) \delta\left(\tau - \tau_l - \tau_{kl}\right). \end{aligned} \tag{3.3}$$

Herein, τ denotes delay, whereas the total delay of each MPC can be decomposed into the delay of the l-th cluster, τ_l, and the delay of the k-th MPC arrival within this cluster,τ_{lk}.

3.2.2 Zwick's Model

In [31], Zwick et al. introduced a stochastic indoor MIMO model that allows a time-variant, polarization-dependent broadband description of the multipath channel. Given the time dependent locations of the Tx and Rx arrays, the frequency response between the center elements of these arrays is expressed as

$$\mathbf{H}\left(t, f, \Omega_{\mathrm{Tx}}, \Omega_{\mathrm{Rx}}\right) = \sum_{l=1}^{N(t)} \Gamma_l(t) e^{-j2\pi f \tau_l(t)} \delta\left(\Omega_{\mathrm{Tx}} - \Omega_{\mathrm{Tx},l}(t)\right) \delta\left(\Omega_{\mathrm{Rx}} - \Omega_{\mathrm{Rx},l}(t)\right). \tag{3.4}$$

Here, each MPC is characterized by its delay $\tau_l(t)$, direction-of-departure $\Omega_{\mathrm{Tx},l}(t)$, direction-of-arrival $\Omega_{\mathrm{Rx},l}(t)$, and the full polarimetric (2×2) transfer matrix $\Gamma_l(t)$. The entries of $\Gamma_l(t)$ include the pathloss and depolarization of all scattering processes of the MPC l. In sum, a number of $N(t)$ MPCs are generated by a birth and death process. More specific, the appearance and disappearance of multipath components over time is modeled based on a marked Poisson process [62, Chapter 16]. After the initialization (birth) of an MPC, its properties are altered until the MPC disappears (death).

Equation (3.4) is then extended under the planar wave assumption to MIMO, where the channel between all transmit and receive antenna elements is of interest, by introducing proper phase shifts of the MPCs. These phase shifts depend on the relative location of the considered antenna elements with respect to the center element and the direction of the MPC, c.f. Fig. 2.3.

The modeling of LoS, NLoS (Non Line-of-Sight) or OLoS (Obstructed Line-of-Sight) scenarios is treated in the same manner, except that the LoS component is added separately in the first scenario. By this, the transition between LoS and OLoS can be simulated very simply. The proposed approach enables the modeling of temporal and spatial correlations. The Doppler behavior of the channel results directly from fluctuating delays. Also, the frequency dependence and small scale fading is caused by coherent superposition of the MPCs and needs no separate treatment.

Deterministic ray tracing results [45, 63] were used to produce the data sets required for the statistical evaluation of the parameters of the proposed model. Based upon these results, the MPC power decay versus relative delay is modeled by a combination of two exponential decaying curves. The variation of the MPC amplitudes around this mean power decay is assumed to be Rayleigh distributed. DoDs and DoAs, as they are referred to the interconnection line between transmitter and receiver, are treated as Laplacian distributed for small delays. For larger delays, a migration to a uniform distribution is assumed. The delays of MPCs are uniformly distributed with the minimum possible delay given by the distance between both arrays and a maximum delay depending on the simulated dynamic range.

Nevertheless, it is questionable how well this ray tracing results reflect reality. For instance the clustering phenomenon, which was observed in several experiments [39, 41, 40, 52], is not explicitly included.

3.3 Analytical Models

3.3.1 Correlation-based Models

3.3.1.1 Definition and Classification

Various narrowband analytical models are based on the *multivariate complex Gaussian distribution* [30]. Their common assumption is that the elements of the channel matrix are strictly correlated Rayleigh-fading. Then, the channel matrix elements follow a joint multivariate zero-mean complex Gaussian distribution given by

$$f(\mathbf{h}) = \frac{1}{\pi^{mn}\det\{\mathbf{R_H}\}}\exp\left\{-\mathbf{h}^H\mathbf{R_H}^{-1}\mathbf{h}\right\} \tag{3.5}$$

with

$$\mathbf{h} = \text{vec}\,\{\mathbf{H}\}, \tag{3.6}$$

where vec$\{\cdot\}$ is the vector operator stacking the columns of an $m \times n$ matrix into one tall, $mn \times 1$ vector. In (3.5), the $mn \times mn$ *full (MIMO) channel correlation matrix*, e.g. in [57, 58],

$$\mathbf{R_H} = \text{E}\left\{\text{vec}\{\mathbf{H}\}\text{vec}\{\mathbf{H}\}^H\right\} \tag{3.7}$$

describes the spatial behavior of the MIMO channel. Hence, it contains the complex correlations between all channel matrix element pairs[2]. Note that the zero-mean multivariate complex Gaussian distribution is *completely* characterized by its second order statistics only. In other words, the spatial properties of a MIMO channel are fully captured by its full correlation matrix $\mathbf{R_H}$ for such a distribution.

MIMO channels following (3.5) can be modeled by

$$\text{vec}\{\mathbf{H}\} = \mathbf{R_H}^{1/2}\text{vec}\{\mathbf{G}\}, \tag{3.8}$$

or equivalently

$$\mathbf{H} = \text{unvec}\left\{\mathbf{R_H}^{1/2}\text{vec}\{\mathbf{G}\}\right\}. \tag{3.9}$$

Here, $(\cdot)^{1/2}$ denotes any matrix square root fulfilling $\mathbf{R_H}^{1/2} \cdot (\mathbf{R_H}^{1/2})^H = \mathbf{R_H}$, unvec$\{\cdot\}$ the inverse operation to vec$\{\cdot\}$, and $\mathbf{G}$ an $m \times n$ random matrix with zero-mean i.i.d. complex circularly symmetric Gaussian entries, respectively. Thereby, the channel exhibits Rayleigh-fading at all antenna elements.

A significant drawback of (3.9) is that it requires the parameters of $\mathbf{R_H}$ to be fully specified, i.e. $(mn)^2$ real valued parameters (for the diagonal entries) and $\frac{1}{2}(mn(mn-1))$ complex valued parameters. This is equal to a total of mn real parameters. Moreover, a direct interpretation of the elements of $\mathbf{R_H}$ with respect to the physical propagation of the radio channel is difficult. As a consequence, several simplifying assumptions on the full MIMO correlation matrix leading to different models were introduced.

Subsequent sections will discuss the narrowband i.i.d. model, the Kronecker model, and the Weichselberger model. A much more detailed framework about models based on the multivariate complex Gaussian distribution can be found in [29, Chapter 5]. There, matrix-valued eigenbases of the MIMO channels are introduced and their simplifications discussed.

3.3.1.2 The i.i.d. Model

The most simple model for MIMO channels is the i.i.d. model. This idealized model assumes a random channel matrix with i.i.d. zero-mean complex circularly symmetric Gaussian elements. Per definition, it describes a spatially white MIMO channel and cannot reproduce any specific spatial channel properties. According to the central limit theorem, such channels only occur in rich multipath environments with independent MPCs arriving and departing

[2]Since we consider zero mean processes only, the correlation and covariance matrices coincide.

from all directions. Nevertheless, it is often used for analytical assessments in information theory, e.g. as in finding closed-form solutions of channel capacity. Note that for the i.i.d. model only one real-valued parameter needs to be specified, i.e. the channel power.

In case of i.i.d. Rayleigh fading, the channel capacity grows asymptotically linearly with the minimum number of Tx and Rx antennas [10, 11]. Furthermore, it is usually believed that ergodic capacity is maximized by such channels. However, Appendix D introduces so-called *diagonally correlated channels* that provide higher ergodic capacity than i.i.d. channels.

3.3.1.3 The Kronecker Model

The so-called Kronecker model, in various forms and notations, was already used by [55, 56, 57] for capacity analysis before being proposed by [58] in the course of the EU (European Union) IST (Information Society Technology) SATURN (Smart Antenna Technology in Universal bRoadband wireless Networks) project [64]. It approximates the full channel correlation matrix by the Kronecker product of the transmitter correlation matrix,

$$\mathbf{R}_{\mathrm{Tx}} = \mathrm{E}\{(\mathbf{H}^H\mathbf{H})^T\}, \tag{3.10}$$

and the receiver correlation matrix (*separability assumption*),

$$\mathbf{R}_{\mathrm{Rx}} = \mathrm{E}\{\mathbf{H}\mathbf{H}^H\}, \tag{3.11}$$

such that it can be expressed as

$$\mathbf{R}_{\mathbf{H}} = \frac{1}{\mathrm{tr}\{\mathbf{R}_{\mathrm{Rx}}\}}\mathbf{R}_{\mathrm{Tx}} \otimes \mathbf{R}_{\mathrm{Rx}}, \tag{3.12}$$

where $\mathrm{tr}\{\cdot\}$ denotes the trace of a matrix and $\otimes$ the Kronecker product. Using the identities $(\mathbf{B}^{\mathbf{T}} \otimes \mathbf{A})\mathrm{vec}\{\mathbf{D}\} = \mathrm{vec}\{\mathbf{ADB}\}$ and $(\mathbf{A} \otimes \mathbf{B})(\mathbf{C} \otimes \mathbf{D}) = (\mathbf{AC}) \otimes (\mathbf{BD})$, (3.9) simplifies to the Kronecker model

$$\mathbf{H}_{\mathrm{kron}} = \frac{1}{\sqrt{\mathrm{tr}\{\mathbf{R}_{\mathrm{Rx}}\}}}\mathbf{R}_{\mathrm{Rx}}^{1/2}\mathbf{G}(\mathbf{R}_{\mathrm{Tx}}^{1/2})^T \tag{3.13}$$

Herein, $\mathbf{G}$ is again a matrix of i.i.d. zero-mean, complex circularly symmetric Gaussian random variables. Beside simplified analytical treatment or simulation of MIMO systems, (3.13) allows for independent array optimization at Tx and Rx. Therefore, and because of the simplicity of this approach, the Kronecker model has become popular. Hence, the model parameters are the receive and transmit correlation matrices only. For an $m \times n$ MIMO channel, it therefore requires the specification of $m^2 + n^2$ real parameters.

Assumptions for a Kronecker Structure

As shown in [65], there is a *pair* of assumptions necessary and sufficient for a Kronecker structure of the full channel correlation matrix :

1. The receive antenna correlation between any pair of receive antennas (i, j) given by

$$\rho_{\mathrm{Rx},ij}(k) = \mathrm{E}\{h_{ik}h_{jk}^*\} \tag{3.14}$$

has to be independent of the transmit antenna k. Here, $(\cdot)^*$ denotes complex conjugation. In matrix notation, we can now define the receive correlation matrix by

$$\mathbf{R}_{\mathrm{Rx}} = \mathrm{E}\{\mathbf{H}\mathbf{H}^H\} = n \cdot (\rho_{\mathrm{Rx},ij}) \,. \tag{3.15}$$

Analogously, the transmit antenna correlation between each transmit antenna pair (k, l) given by

$$\rho_{\mathrm{Tx},kl}(i) = \mathrm{E}\{h_{ik}h_{il}^*\} \tag{3.16}$$

has to be independent of the receive antenna i. In matrix notation, we can now define the transmit correlation matrix by

$$\mathbf{R}_{\mathrm{Tx}} = \mathrm{E}\{\mathbf{H}^T\mathbf{H}^*\} = m \cdot (\rho_{\mathrm{Tx},kl}) \tag{3.17}$$

This leads to equal power $P_h = \mathrm{E}\{|h_{ik}|^2\}$ of all channel matrix elements.

2. The correlation coefficient between any pair of channel matrix elements, as given by the full channel correlation matrix $\mathbf{R}_{\mathbf{H}}$, has to be the product of the corresponding receive and transmit antenna correlation coefficients normalized by the power of one channel matrix element:

$$\rho_{\mathbf{H}_{ik,jl}} = \mathrm{E}\{h_{ik}h_{jl}^*\} = \frac{1}{P_h} \cdot \rho_{\mathrm{Rx},ij} \cdot \rho_{\mathrm{Tx},kl} \tag{3.18}$$

These assumptions can be equivalently formulated in matrix notation with $\mathrm{tr}\{\mathbf{R}_{\mathrm{Rx}}\} = \mathrm{tr}\{\mathbf{R}_{\mathrm{Tx}}\} = m \cdot n \cdot P_h$ and result in the Kronecker factorization of the MIMO correlation matrix:

$$\mathbf{R}_{\mathbf{H}} = \frac{1}{\mathrm{tr}\{\mathbf{R}_{\mathrm{Rx}}\}} \mathbf{R}_{\mathrm{Tx}} \otimes \mathbf{R}_{\mathrm{Rx}}. \tag{3.19}$$

Implications of the Kronecker Model

To consider the effect of the separability assumption on the DoDs and DoAs of the modeled MIMO channel, we have to look at the structure of the receive and transmit correlation matrix for different transmit and receive weights, respectively. Using (3.13), the receive correlation matrix $\mathbf{R}_{\mathrm{Rx},\mathbf{w}}$ for beamforming at Tx side, i.e. using specific transmit weights $\mathbf{w}$, is given by

$$\mathbf{R}_{\mathrm{Rx},\mathbf{w}} = \mathrm{E}\{\mathbf{H}_{\mathrm{kron}}\mathbf{w}\mathbf{w}^H\mathbf{H}_{\mathrm{kron}}^H\} = \frac{1}{\mathrm{tr}\{\mathbf{R}_{\mathrm{Rx}}\}} \cdot \mathrm{E}\left\{ \mathbf{R}_{\mathrm{Rx}}^{1/2}\mathbf{G} \underbrace{\left(\mathbf{R}_{\mathrm{Tx}}^{1/2}\right)^T \mathbf{w}\mathbf{w}^H \left(\mathbf{R}_{\mathrm{Tx}}^{1/2}\right)^*}_{\mathbf{X}} \mathbf{G}^H \left(\mathbf{R}_{\mathrm{Rx}}^{1/2}\right)^H \right\}. \tag{3.20}$$

where we use $\mathbf{X}$ as an abbreviation for the inner part. It is straight-forward to show that $\mathrm{E}\{\mathbf{G}\mathbf{X}\mathbf{G}^H\}$ is always an identity matrix scaled by a complex scalar factor K, if $\mathbf{G}$ is a unit power, independently distributed complex Gaussian random matrix (see Appendix A). Therefore the receive correlation matrix $\mathbf{R}_{\mathrm{Rx,w}}$ for the transmit weights $\mathbf{w}$ is equal to

$$\mathbf{R}_{\mathrm{Rx,w}} = \frac{1}{\mathrm{tr}\{\mathbf{R}_{\mathrm{Rx}}\}} \mathbf{R}_{\mathrm{Rx}}^{1/2} K \mathbf{I} \left(\mathbf{R}_{\mathrm{Rx}}^{1/2}\right)^H = K' \cdot \mathbf{R}_{\mathrm{Rx}}. \tag{3.21}$$

This means that the structure of the receive correlation matrix does not change if we use different transmit weights; the receive correlation matrix is only scaled by a complex constant. Using, for example, a beamforming vector to transmit into an arbitrary but specific direction leads always to (a scaled version of) the same receive correlation matrix and, therefore, to (a scaled version of) the same DoA profile. This holds also true for the transmit correlation matrix and the corresponding DoDs.

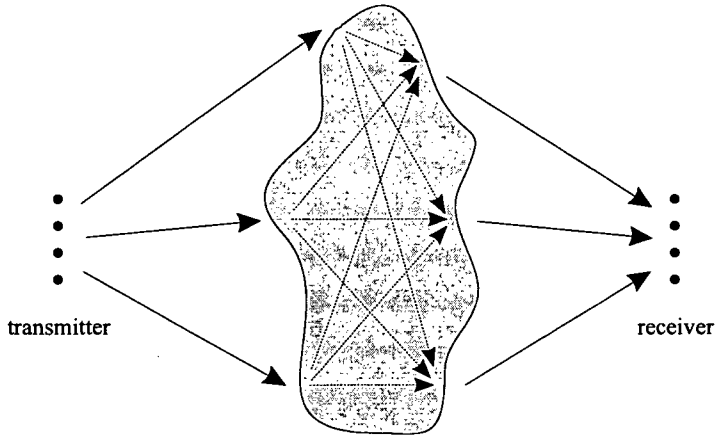

Figure 3.2: The Kronecker model enforces all directions-of-departure to be linked to all directions-of-arrival. The joint DoD-DoA spectrum of a synthesized Kronecker channel is the product of the average DoD and the average DoA spectra.

Considering the joint DoD-DoA spectrum we can therefore say that the Kronecker model enforces it to be the product of the DoD and the DoA spectra. In other words (as illustrated in Fig. 3.2), this means that all directions-of-departure are linked to all directions-of-arrival with the same pattern, only the total power of the DoAs depends on the chosen DoD, analogously only the total power of the DoDs depends on the chosen DoA [66].

A physical interpretation of the Kronecker assumption is this: Irrespective of which transmit weight vector is chosen, the scatterers surrounding the receiver are illuminated by one and the same power distribution. Therefore, the same DoA spectrum is generated. The same DOA spectrum means identical receive correlation. (The total receive power may, of course, vary.) Obviously, this condition is not met in general. Any arbitrary transmit weight vector does include the case of a single antenna transmitting, which is the previously mentioned Assumption 1. Other than stated in [58] and other papers, this condition alone is not sufficient[3].

[3]The problem with [58] is this. In their proof [58, Appendix] the authors presume the relationship they initially intend to prove. Erroneously, they conclude that Assumption 1 is sufficient for Kronecker separability.

Both assumptions (Assumption 1 and Assumption 2) have to be fulfilled. The same holds true for the reverse link.

Deficiencies of the Kronecker Model

As explained before, the main deficiency of the Kronecker model is that it enforces a multipath structure with a separable joint DoD-DoA spectrum. Multi-bounce interactions are necessary (but not sufficient), to comply with this condition. Although it is very likely in indoor channels that single DoDs are linked to single DoAs and vice-versa (single-bounce interactions, c.f. Fig. 3.3), the Kronecker model is not able to reproduce this elementary feature of a MIMO channel.

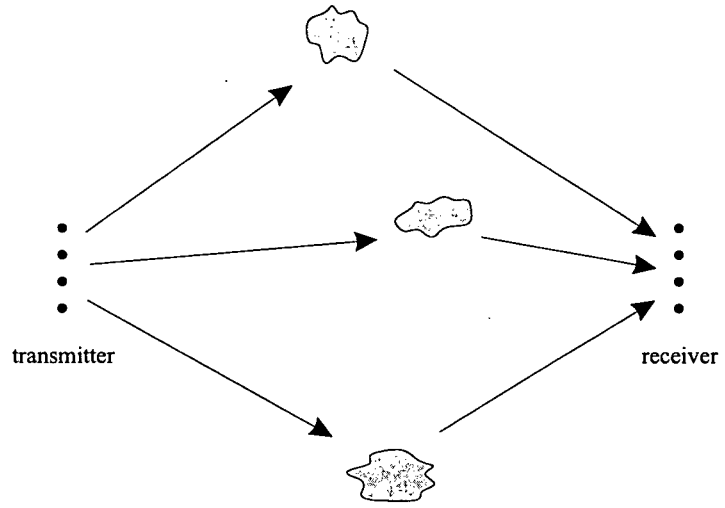

Figure 3.3: Due its separability assumption, the Kronecker model is not able to reproduce MIMO channels with single-bounce interactions.

Obviously, this restriction in the multipath structure also affects the diversity order of a MIMO channel and its capacity. Experimental investigations on the joint DoD-DoA spectrum, mutual information, diversity order and full channel correlation of the Kronecker model will be presented in Chapter 5.

3.3.1.4 The Weichselberger Model

The Weichselberger model [59], [29, Chapter 6.4.3], inspired by the deficiency of the Kronecker model, aims to mitigate the radical simplification of neglecting the spatial structure of the MIMO channel and describing the MIMO channel by separated link ends, as it is done by the Kronecker model. A crucial point in the derivation of this model is to understand the coupling between the transmit and receive eigenmodes for the Kronecker model. Introducing the eigenvalue decomposition of the receive and transmit correlation matrices,

$$\mathbf{R}_{\mathrm{Rx}} = \mathbf{U}_{\mathrm{Rx}}\mathbf{\Lambda}_{\mathrm{Rx}}\mathbf{U}_{\mathrm{Rx}}^{H}, \tag{3.22}$$

$$\mathbf{R}_{\mathrm{Tx}} = \mathbf{U}_{\mathrm{Tx}}\mathbf{\Lambda}_{\mathrm{Rx}}\mathbf{U}_{\mathrm{Tx}}^{H}, \tag{3.23}$$

into (3.13), the Kronecker model can also be written as

$$\mathbf{H}_{\text{kron}} = \frac{1}{\sqrt{\text{tr}\{\mathbf{R}_{\text{Rx}}\}}} \cdot \mathbf{U}_{\text{Rx}} \mathbf{\Lambda}_{\text{Rx}}^{1/2} \underbrace{\mathbf{U}_{\text{Rx}}^{H} \mathbf{G} \mathbf{U}_{\text{Tx}}^{*}}_{\mathbf{G}'} \mathbf{\Lambda}_{\text{Tx}}^{1/2} \mathbf{U}_{\text{Tx}}^{T} \tag{3.24}$$

where the columns of the unitary matrices $\mathbf{U}_{\text{Tx}}$ ($\mathbf{U}_{\text{Rx}}$) denote the eigenvectors at the transmitter (receiver) and $\mathbf{\Lambda}_{\text{Tx}}$ ($\mathbf{\Lambda}_{\text{Rx}}$) the diagonal matrix of the corresponding eigenvalues.

The inner part $\mathbf{G}' = \mathbf{U}_{\text{Rx}}^{H} \mathbf{G} \mathbf{U}_{\text{Tx}}^{*}$ still describes an i.i.d. random matrix with the same properties as $\mathbf{G}$. From (3.24) it can be seen again that, on average, each transmit eigenbasis couples into all receive eigenbases with the same pattern (profile) and vice versa.

The idea of Weichselberger was to relax this restriction and to allow for any arbitrary coupling between the transmit and receive eigenbases, i.e. to model the correlation properties at the transmitter and receiver *jointly*.

Therefore, the proposed Weichselberger model is

$$\mathbf{H}_{\text{weichsel}} = \mathbf{U}_{\text{Rx}} \left(\tilde{\Omega}_{\text{weichsel}} \odot \mathbf{G} \right) \mathbf{U}_{\text{Tx}}^{T}, \tag{3.25}$$

where $\mathbf{G}$, again, is an i.i.d. complex circularly symmetric Gaussian random fading matrix, the operator $\odot$ stands for the element-wise Schur-Hadamard multiplication, and $\tilde{\Omega}_{\text{weichsel}}$ is defined as the element-wise square root of the power coupling matrix Ω_{weichsel}. The positive and real-valued elements $\omega_{\text{weichsel},ij}$ of the power coupling matrix determine the average power-coupling between the i-th and the j-th receive eigenmode.

Following this approach, an alternative representation for (3.25) reads as

$$\mathbf{H}_{\text{weichsel}} = \sum_{l=1}^{m} \sum_{k=1}^{n} g_{lk} \sqrt{\omega_{\text{weichsel},lk}} \mathbf{u}_{\text{Rx},l} \mathbf{u}_{\text{Tx},k}^{T}, \tag{3.26}$$

where g_{lk} denotes the elements of $\mathbf{G}$, and $\mathbf{u}_{\text{Tx},k}$ ($\mathbf{u}_{\text{Rx},l}$) the k-th (l-th) column of $\mathbf{U}_{\text{Tx}}$ ($\mathbf{U}_{\text{Rx}}$), or, in other words, the k-th (l-th) eigenvector of the transmit (receive) correlation matrix.

The full MIMO channel correlation matrix results to

$$\mathbf{R}_{\mathbf{H},\text{weichsel}} = \sum_{l=1}^{m} \sum_{k=1}^{n} \omega_{\text{weichsel},lk} \left(\mathbf{u}_{\text{Tx},l} \otimes \mathbf{u}_{\text{Rx},k} \right) \left(\mathbf{u}_{\text{Tx},l} \otimes \mathbf{u}_{\text{Rx},k} \right)^{H}. \tag{3.27}$$

The Weichselberger model parameters are the eigenbases of the transmit and receive correlation matrices, $\mathbf{U}_{\text{Tx}}$ and $\mathbf{U}_{\text{Rx}}$, and the coupling matrix, Ω_{weichsel}. For modeling an $m \times n$ MIMO channel, $mn + m(m-1) + n(n-1)$ real parameters have to be specified.

However, for studying the MIMO capacity or mutual information, the transmit and receive eigenbases need not to be determined. For such studies only the coupling matrix is necessary. Also, the diversity order is only influenced by the structure of the coupling matrix. In both cases, the specification of mn real parameters is sufficient.

Assumption of the Weichselberger Model

In order to appreciate the effects of the Weichselberger model assumption, we again look at the receive correlation matrix, when transmitting with specific weights $\mathbf{w}$,

$$\begin{aligned}\mathbf{R}_{\mathrm{Rx,w}} &= \mathrm{E}\{\mathbf{H}_{\mathrm{weichsel}}\mathbf{w}\mathbf{w}^H\mathbf{H}_{\mathrm{weichsel}}^H\} = \\ &= \mathrm{E}\{\mathbf{U}_{\mathrm{Rx}}(\mathbf{G}\odot\Omega_{\mathrm{weichsel}})\underbrace{(\mathbf{U}_{\mathrm{Tx}})^T\mathbf{w}\mathbf{w}^H(\mathbf{U}_{\mathrm{Tx}})^*}_{\mathbf{X}}(\mathbf{G}\odot\Omega_{\mathrm{weichsel}})^H(\mathbf{U}_{\mathrm{Rx}})^H\} = \\ &= \mathbf{U}_{\mathrm{Rx}}\Lambda_{\mathbf{w}}\mathbf{U}_{\mathrm{Rx}}^H, \end{aligned} \tag{3.28}$$

where $\Lambda_{\mathbf{w}}$ is a diagonal matrix with its entries depending on $\mathbf{w}$. The proof runs in complete analogy to the one shown in Appendix A.

According to (3.28), the Weichselberger model requires that the *eigenbasis* at the receiver is always *the same* for any spatial transmit weight $\mathbf{w}$. Again, the same requirement holds for the reverse link. However, the eigenvalues of the correlation matrices are not restricted and may vary for different transmit weights. Compared to the Kronecker model the assumption of the Weichselberger model is much less restrictive since the latter does not include identical eigenvalues.

Weichselberger et al. also provide a physical interpretation of their modeling assumption: The receive eigenbasis reflects the spatial structure of the scatterers that are relevant at the receive array. This structure must not depend on the transmit weights. The receive eigenvalues reflect how the scatterers are illuminated by the radio waves propagating from the transmitter. Obviously, this pattern of illumination can change significantly with the transmit weights, since transmitting in certain directions illuminate only certain scatterers and leave others 'dark'. The same interpretation holds for the reverse link.

The question whether the assumption of the Weichselberger model is still too restrictive or not, is studied in Chapter 5. There the performance of the Weichselberger model, with respect to different metrics, is compared to measurements.

Comparison to the Kronecker Model

If the channel is structured such that the coupling matrix reads as

$$\Omega_{\mathrm{weichsel}} = \frac{1}{\sqrt{\mathrm{tr}\{\mathbf{R}_{\mathrm{Rx}}\}}}\begin{bmatrix}\lambda_{\mathrm{Rx},1}\\ \lambda_{\mathrm{Rx},2}\\ \vdots\\ \lambda_{\mathrm{Rx},m}\end{bmatrix}\cdot\begin{bmatrix}\lambda_{\mathrm{Tx},1} & \lambda_{\mathrm{Tx},2} & \cdots & \lambda_{\mathrm{Rx},n}\end{bmatrix}, \tag{3.29}$$

the Kronecker model and the Weichselberger model collapse. Here, $\lambda_{\mathrm{Tx},i}$ ($\lambda_{\mathrm{Rx},i}$) denotes the i-th eigenvalue of the transmit (receive) correlation matrix.

In other words, the coupling matrix can be written as the outer product of the receive and transmit eigenvalue vectors. Hence, the resulting matrix is a rank one matrix.

Structure of Coupling Matrix

In analogy to [54], the structure of $\Omega_{\mathrm{weichsel}}$ influences diversity gain, capacity and beamforming gain experienced on spatially multiplexed channels.

As illustrated in [29, Chapter 6.4.3.4], a diagonally dominated structure of $\Omega_{\mathrm{weichsel}}$ represents a channel where single transmit eigenvectors couple almost into single receive eigenvectors. Such a channel offers high ergodic capacity (since it has full channel rank), but less diversity.

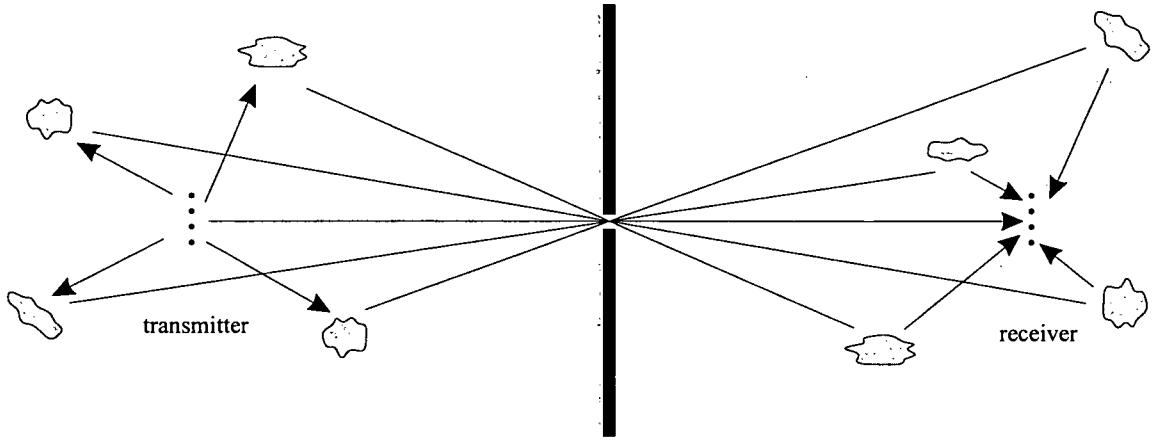

Figure 3.4: Illustration of the 'pinhole' phenomenon: Rich scattering environments around the transmitter and receiver are linked through one 'narrow air pipe' where all multipath components merge.

Indeed, a strictly diagonal coupling matrix models a symmetric Rayleigh-fading channel (a so-called *diagonally correlated channel*) that exhibits *higher* ergodic capacity than under i.i.d. fading conditions. Appendix D demonstrates this surprising result. A uniformly loaded coupling matrix shows lower ergodic capacity but maximum diversity order. If Ω_{weichsel} is dominated by a single element (low rank channel) then a high beamforming gain is possible, but capacity and diversity order are low.

3.3.1.5 The Pinhole Effect

The 'pinhole' phenomenon [67] describes channels where the instantaneous channel matrix realization shows a lower rank than the averaged correlation matrices at the link ends would suggest.

As an extreme case, the instantaneous channel realization is always of rank one while both, transmit and receive correlation matrices show full rank [68] ('keyhole'). Of course, an instantaneous rank reduction is much more likely than a rank-one channel for each single realization.

A physical explanation of the pinhole phenomenon is provided by the concept of a 'narrow air pipe' where all multipath components from the transmitter merge before they, again, split up into received multipath components (Fig. 3.4). Such a narrow air pipe could be formed by a small hole in a metal screen, a waveguide, or cascaded diffractions at edges. Note that the amplitude statistics of pinhole channels is not Rayleigh anymore. Instead, scattering at both 'sides' of the pinhole induce double-Rayleigh fading [69, 70].

Although pinholes have a Kronecker structure on average, the Kronecker MIMO channel model is not capable of reproducing this effect. An extension of the Kronecker model in order to adopt pinholes was proposed by [67, 71]. There, the fading matrix $\mathbf{G}$ in (3.13) is replaced by a rank deficient matrix, $\mathbf{G}_{\text{pinhole}}$, such that

$$\mathbf{G}_{\text{pinhole}} = \mathbf{G}_{\text{Rx}} \mathbf{R}_{\text{S}}^{1/2} \mathbf{G}_{\text{Tx}}. \tag{3.30}$$

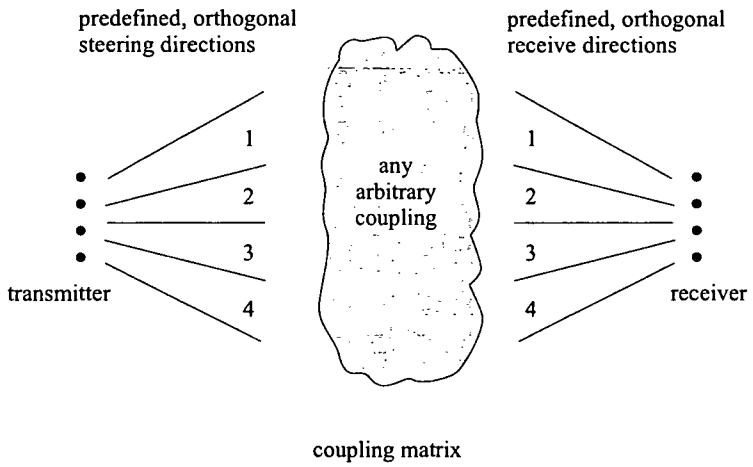

Figure 3.5: Illustration of the virtual channel representation: The spatial structure of the MIMO channel is modeled in the beamspace by using predefined, orthonormal multipath directions that can be coupled arbitrarily. Fading of these components is assumed to be independent.

Here, $\mathbf{G}_{\mathrm{Tx}}$ and $\mathbf{G}_{\mathrm{Rx}}$ represent i.i.d. complex circularly symmetric Gaussian random fading matrices. The rank of the scatterer correlation matrix $\mathbf{R}_{\mathrm{S}}$ limits the instantaneous channel rank without affecting the receive or transmit correlation.

The occurrence of rank-one keyholes seems to be very rare. The authors of [72] could only artificially create keyholes in a controlled laboratory environment by using a piece of rectangular single-mode waveguide.

3.3.2 Propagation-motivated Models

3.3.2.1 Virtual Channel Representation

Initially motivated by the double-directional channel representation [25], the virtual channel representation artificially partitions the angular range at both link ends into fixed, discrete directions ('virtual angles'). These directions are determined by the spatial resolution, i.e. the number of antennas of the considered antenna array. For an n-element array at one link end, n virtual angles are chosen such that the associated steering/response vectors are orthonormal to each other. The *joint* spatial behavior of the MIMO channel is then modeled by specifying the amplitude coupling between those virtual angles at both link ends (c.f. Fig. 3.5).

To this end, the virtual channel representation [54] can be written as

$$\mathbf{H}_{\mathrm{virt}} = \mathbf{A}_{\mathrm{Rx}} \left(\tilde{\Omega}_{\mathrm{virt}} \odot \mathbf{G} \right) \mathbf{A}_{\mathrm{Tx}}^{T}, \tag{3.31}$$

where the columns of the orthonormal matrices $\mathbf{A}_{\mathrm{Tx}}$ and $\mathbf{A}_{\mathrm{Rx}}$ constitute steering and response vectors into the directions of the virtual angles. The elements of the positive and real-valued coupling matrix, $\tilde{\Omega}_{\mathrm{virt}}$, ('virtual channel coefficients') represent the amplitude coupling between the corresponding virtual angles of both link ends. Because it is assumed that the

fading of the different virtual channel coefficients is independent, $\mathbf{G}$ is again modeled by an i.i.d. matrix.

An alternative representation, using the orthonormal steering vectors, $\mathbf{a}_{\mathrm{Tx},l}$, and response vectors, $\mathbf{a}_{\mathrm{Rx},k}$, is given by

$$\mathbf{H}_{\mathrm{virt}} = \sum_{l=1}^{m}\sum_{k=1}^{n} g_{lk}\sqrt{\omega_{\mathrm{virt},lk}}\mathbf{a}_{\mathrm{Rx},l}\mathbf{a}_{\mathrm{Tx},k}^{T}, \tag{3.32}$$

where g_{lk} denotes the elements of $\mathbf{G}$, and $\sqrt{\omega_{\mathrm{virt},lk}}$ the elements of the coupling matrix, respectively. The full channel correlation matrix of the virtual channel representation results to

$$\mathbf{R}_{\mathbf{H},\mathrm{virt}} = \sum_{l=1}^{m}\sum_{k=1}^{n} \omega_{\mathrm{virt},lk}\left(\mathbf{a}_{\mathrm{Tx},l}\otimes\mathbf{a}_{\mathrm{Rx},k}\right)\left(\mathbf{a}_{Tx,l}\otimes\mathbf{a}_{Rx,k}\right)^{H} \tag{3.33}$$

The big advantage of this model is its easy geometrical interpretation. Also, by an appropriate choose of $\tilde{\Omega}_{\mathrm{virt}}$ the level of diversity and multiplexing gain can be specified [54]: The rank of $\tilde{\Omega}_{\mathrm{virt}}$ determines the multiplexing gain, whereas the level of diversity associated with each parallel sub-channel is reflected by the number of virtual receive angles that couple with each virtual transmit angle, and vice versa.

The model is parametrized by the coupling matrix, only. For an $m \times n$ MIMO channel, it therefore requires the specification of mn real parameters.

Please note that there is a degree of freedom for the virtual channel representation in choosing unitary matrices $\mathbf{A}_{\mathrm{Tx}}$ and $\mathbf{A}_{\mathrm{Rx}}$. One steering/response direction can be selected arbitrarily, the remaining directions result from the orthogonality condition.

Comparison to the Weichselberger Model

Evidently, the Weichselberger model and the virtual channel representation only differ in their choice of the domain in which they are modeled. While the former is modeled in eigenspace, the latter is in beamspace (or wavenumber domain). As a consequence, the eigenbasis of the transmit and receive correlation matrices are replaced by unitary steering and transmit matrices. The big advantage of modeling in eigenspace is that fading is independent by definition [59], irrespective of the scatterer distribution. In contrast, fading in beamspace is correlated if modeled with fixed virtual angles, even when uncorrelated scatterers are assumed.

Deficiencies of the Virtual Channel Representation

As just pointed out, the assumption of uncorrelated fading is problematic due to the predefined virtual angles. Regardless of the antenna number, hence angular resolution, scatterers lying between two virtual angles induce correlated fading particularly in the adjacent virtual angles, because of sidelobe effects. Unfortunately, this important effect is not captured by this model. The virtual channel representation does not distinguish between scatterers that are separated by less than the angular resolution.

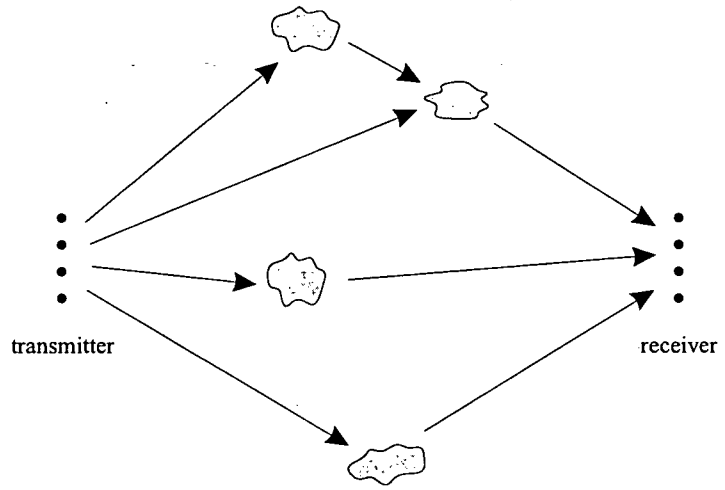

Figure 3.6: Illustration of the finite scatterer model: Propagation paths between transmitter and receiver are modeled by modeling its directions-of-departure, directions-of-arrival and path amplitudes. For broadband, delays can be also included.

3.3.2.2 Finite Scatterer Model

The finite scatterer model [53] treats the double-directional channel by modeling the propagation paths between transmitter and receiver (Fig. 3.6).

In case of narrowband, each multipath is determined by its DoD, DoA and path amplitude. Let us consider a multipath with a complex gain of $s_{lk}e^{\alpha_{lk}}$ departing at the transmitter from the l-th DoD, $\varphi_{\mathrm{Tx},l}$, and arriving at the receiver via the k-th DoA, $\varphi_{\mathrm{Rx},k}$. Further, let $\tilde{\mathbf{a}}_{\mathrm{Tx}}(\Phi_{\mathrm{Rx},l})$ denote the corresponding steering and $\tilde{\mathbf{a}}_{\mathrm{Rx}}(\Phi_{\mathrm{Rx},k})$ the corresponding response vector. Then, the contribution of this single path to the channel matrix can be modeled as $s_{lk}\tilde{\mathbf{a}}_{\mathrm{Rx}}(\Phi_{\mathrm{Rx},k})\tilde{\mathbf{a}}_{\mathrm{Tx}}(\Phi_{\mathrm{Rx},l})^T$.

Summing up the contributions from all paths results in a single channel matrix realization, since the description until now is fully deterministic. If an ensemble of different channel realizations has to be modeled, fading has to be introduced. One possible way is to add random-phase terms to each MPC [73], such that the finite scatterer model can be expressed as

$$\mathbf{H} = \tilde{\mathbf{A}}_{\mathrm{Rx}}(\mathbf{S} \odot \mathbf{G})\tilde{\mathbf{A}}_{\mathrm{Tx}}^T = \sum_{l=1}^{m}\sum_{k=1}^{n} g_{lk}s_{lk}\tilde{\mathbf{a}}_{\mathrm{Rx}}(\Phi_{\mathrm{Rx},k})\tilde{\mathbf{a}}_{\mathrm{Tx}}(\Phi_{\mathrm{Rx},l})^T, \tag{3.34}$$

where $\tilde{\mathbf{A}}_{\mathrm{Rx}}$ denotes a matrix whose columns are the response vectors $\tilde{\mathbf{a}}_{\mathrm{Rx}}(\Phi_{\mathrm{Rx},k})$. Similarly, the steering vectors $\tilde{\mathbf{a}}_{\mathrm{Tx}}(\Phi_{\mathrm{Rx},l})$ constitute the columns of $\tilde{\mathbf{A}}_{\mathrm{Tx}}$. Herein, $\mathbf{S}$ is the matrix of the path amplitudes s_{lk}, while $\mathbf{G}$ is a random fading matrix with g_{lk} denoting its elements. Note that the number of DoDs determines the number of columns of $\mathbf{S}$, whereas the number of DoAs determines the number of rows of $\mathbf{S}$. Correlated fading of components coming from different scatterers has to be regarded by correlations of the respective elements in $\mathbf{G}$. Else, different g_{lk} are modeled as independently distributed.

Note that (3.34) assumes ideal uncoupled omni-directional antennas at both link ends. Deviations from this ideal assumption can be taken into account by multiplying with appropriate transformation matrices [74]. A further assumption is that the distance between scatterers and antenna arrays compared to the inter-element spacing is large enough (far field condition).

In contrast to the virtual channel representation, the finite scatterer model allows for arbitrary numbers of DoDs and DoAs and also their values can be set arbitrarily. The parameters of the finite scatterer model are the DoDs, its corresponding DoAs and path amplitudes.

The authors of [75] determine the number of scatterers of the finite scatterer model at the transmit side and the receive side such that its mutual information complies with measurements ('capacity complying MIMO channel models').

3.3.3 Line-of-Sight Channels

In the previous subsections, only Rayleigh-fading channels were discussed. A straight-forward extension, such that an additional LoS component is considered, enables the modeling of Ricean-fading channels, e.g. as suggested by [76]:

$$\mathbf{H}_{\text{rice}} = \sqrt{\frac{1}{1+K}}\mathbf{H}_{\text{rayleigh}} + \sqrt{\frac{K}{1+K}}\mathbf{H}_{\text{LoS}} \tag{3.35}$$

with the Ricean K-factor $K \geq 0$. The stochastic Rayleigh-fading part is introduced by $\mathbf{H}_{\text{rayleigh}}$. Any analytical model that treats Rayleigh-fading channels can be inserted here. Further, $\mathbf{H}_{\text{LoS}}$ is a deterministic phase-shift-only MIMO matrix accounting for the LoS component. This matrix stimulates the non-zero mean of the channel matrix $\mathbf{H}_{\text{rice}}$.

Finally, a note of caution when trying to extract $\mathbf{H}_{\text{LoS}}$ from MIMO channel measurements. Equation (3.35) could mislead one to think that an ensemble of measured MIMO channel matrices must have non-zero mean. This is not always the case. Indeed, measured Ricean-fading channels may have zero-mean when the considered ensemble contains *spatial* channel realizations. In this case, the phases of the LoS matrix $\mathbf{H}_{\text{LoS}}$ for different spatial realizations vary due to displacement and may result in $\mathbf{H}_{\text{rice}}$ to be zero-mean.

3.3.4 Broadband Extension to Analytical Narrowband Models

One basic idea of extending narrowband MIMO models to broadband is reported in [77]. There, a SISO model introducing the frequency-selectivity is combined with a narrowband MIMO model capturing the spatial properties of the MIMO channel. The resulting broadband model can be expressed as

$$\mathbf{H}(\tau) = \sum_{l=1}^{L} \mathbf{H}_l \delta(\tau - \tau_l), \tag{3.36}$$

where $\mathbf{H}_l$ is the MIMO channel matrix at delay τ_l, accounting for the spatial structure for the corresponding delay tap.

Applying this idea to the narrowband Kronecker model, its broadband extension [33] can be written as

$$\mathbf{H}(\tau) = \sum_{l=1}^{L} \frac{1}{\sqrt{\mathrm{tr}\{\mathbf{R}_{\mathrm{Rx}}^{l}\}}} (\mathbf{R}_{\mathrm{Rx}}^{l})^{1/2} \mathbf{G}_l (\mathbf{R}_{\mathrm{Tx}}^{l})^{T/2} \delta\left[\tau - (l-1)\Delta\tau\right], \tag{3.37}$$

where $\mathbf{R}_{\mathrm{Rx}}^{l}$ and $\mathbf{R}_{\mathrm{Tx}}^{l}$ are the receive and transmit correlation matrices and $\mathbf{G}_l$ the random fading matrix, each for the l-th delay tap. Here, $\Delta\tau$ is the time spacing between two neighboring delay taps. In conformity with the assumption that fading of different delay taps is uncorrelated, the coefficients of the random fading matrices for different delay taps, $\mathbf{G}_l$, are modeled as statistically independent.

If the spatial structure of the frequency-selective MIMO channel stays the same over all delay taps, $\mathbf{H}_l$ will stay constant and only the total channel power will change according to the power delay profile. However, for general indoor scenarios, $\mathbf{H}_l$ will also depend on the delay. Arbitrary power delay spectra can be modeled by setting appropriate channel powers for the different delay taps.

Of course, the proposed broadband extension can be applied to any other analytical narrowband channel model as well.

3.3.5 Temporal Evolution of Analytical Models

Up to now, we only considered random fading matrices $\mathbf{G}$ with zero-mean, i.i.d. complex circularly symmetric Gaussian entries that provide us different channel realizations accounting for small-scale fading. However, such a choice for the random matrix does not allow for treating the temporal evolution of the MIMO channel.

Temporal variation of the channel matrix can be modeled by assigning a Doppler spectrum to each element of the random fading matrix $\mathbf{G}$ [29, Chapter 6.11.1]. This can be done as in the standard SISO case, see e.g. [78], and independently for each element.

3.4 Standardized Models

3.4.1 The 802.11n Model

A standardization group of IEEE proposes a set of 6 channel models for different indoor environments applicable to MIMO WLAN systems, covering both LoS and NLoS conditions [60]. Some of these models are extensions of already existing SISO WLAN channel models [79, 80].

3.4.1.1 Modeling Philosophy

The basic structure is a tapped-delay line model applying the Kronecker (separability) assumption for the joint spatial channel characterization. It is also assumed that the channel's angular and delay domains are separable. In the delay domain, clustering of MPCs is considered. A number of 2 to 6 clusters, depending on the considered environment, is proposed within a power delay profile, which is tapped in delays of 10ns.

The delay as well as the shape of each cluster is predetermined. In the angular domain, only the horizontal plane (azimuth) is treated. Here, each cluster is assigned a mean direction and a cluster angular spread, independently at both link ends. The angular shape of a cluster follows a Laplacian distribution as given by (3.2). In accordance with measurement results, the proposed angular and delay spreads are correlated. The values for the angular spread are taken from MISO measurements and vary in a range of 20° to 40°.

For each delay tap predetermined values for the relative power, DoDs, DoD spreads, DoAs and DoA spreads are listed in a table. In delay a cluster extends over several taps; consequently the description of one tap results from the summation of contributing clusters.

The basic modeling steps can be summarized as follows.

- A pathloss model determines the absolute channel power. Free space loss (power decay coefficient of 2) up to a breakpoint distance and a power decay coefficient of 3.5 after the breakpoint is assumed. The value of the breakpoint distance depends on the actual environment (channel) considered. Additionally log-normal (Gaussian in dB) shadow fading with a standard deviation in the range from 3 to 6dB is also included.

  The individual tap powers have to be determined such that in total the original power delay profile is met.

- For a chosen antenna configuration, the complex correlations between antenna pairs at the transmitter and receiver have to be calculated for each tap, based on the power angular spectrum of the corresponding tap.

- Using these correlations, MIMO channel matrices are synthesized by the Kronecker model (3.13). LoS conditions (Ricean-fading conditions) are modeled as suggested by (3.35). In this case, Ricean K-factors from a specified table are assigned to the first delay tap.

Additionally, Doppler shifts due to slowly moving users, moving vehicles, and/or due to fluorescent lights can be considered.

Furthermore, different antenna polarizations are also treated by assigning cross-polarization discrimination (XPD) values of 10dB to the LoS and 3dB to the Rayleigh part in (3.35) [76].

3.4.1.2 Shortcomings

Although the proposed channel model reflects some important properties of measured indoor channels quite well, it has two main shortcomings:

The first one is the Kronecker assumption. Implications of this assumption were already detailed in Section 3.3.1.3. Please recall that elementary features like single-bounce reflections, as they will occur e.g. from walls, cannot be modeled by the Kronecker model. The choice of the Kronecker assumption is particularly unfortunate for *indoor* MIMO modeling.

As a second point, propagation parameters like the number of clusters or cluster angular spreads have been taken from evaluations in the *angular-delay* domain. This might turn out to be problematic for MIMO modeling as recent investigations [42] showed that the values for these parameters change significantly when evaluating the *joint-angular* (DoD-DoA) domain.

It seems that separability of clusters in the joint-angular power spectrum is better than in the angular-delay power spectrum as the number of detected clusters increase. Specifically, a mean number of about 7 clusters (within a dynamic range of 10dB) was reported in [42] for a rich scattering indoor office environment. It is evident that, along with this, the cluster angular spread becomes smaller. Of course, these parameters strongly depend on the considered environment.

Interestingly enough, only the average mutual information with equal transmit power allocation was used for the validation of the proposed models. This metric reflects only the 'average' multiplexing gain of a MIMO channel. But, as we will detail in Chapter 5.3, it does not capture diversity or beamforming gain sufficiently well.

Chapter 4

Measurements

4.1 Setup

An overview of the measurement setup is shown in Fig. 4.1. We used a vector channel sounder, a two-dimensional x-y positioning table together with the corresponding controller, a receive antenna array and a single transmit antenna, respectively.

With a multiplexer at the receiver, the channel sounder was capable of sounding the channel between a single transmit and eight receive antennas (SIMO) only. Specifically, it measured the complex transfer function between the transmit and all receive array elements by multiplexing each receive element consecutively to a single receiver chain. In order to enable MIMO channel sounding, we mounted the transmit antenna on an x-y positioning table and measured at different transmit antenna locations. The location of the transmit antenna was software controlled by the channel sounder via the positioner.

By this, we sounded the double-directional radio channel between a physical receive antenna array and a *virtual* transmit array. A big advantage of the chosen setup is that it allows for *any desired transmit antenna configuration.* Of course, the channel must be static during one such MIMO measurement. Furthermore, at the transmit side mutual coupling [74, 81, 82, 83, 84, 85] does not influence the results.

4.1.1 Channel Sounder

The measurements were performed with the wideband vector channel sounder RUSK ATM of MEDAV company [86, 87], operating at a center frequency of 5.2GHz.

The measurement principle of the RUSK channel sounder is as follows. Since a sequential operation in the frequency domain would take too much time, the channel sounder excites all frequencies for each transmit/receive antenna pair simultaneously. This is done by taking a OFDM-like signal with identically powered spectral lines. The phases of these spectral lines are optimized such that the crest factor of the transmitted signal is minimized. This method is also known as *frequency domain correlation processing.* The receive and transmit unit of the channel sounder were synchronized via optical fiber.

The channel was probed at 193 equi-spaced frequency bins covering 120MHz of measurement bandwidth within a dynamic range of typically 35dB. This allows for a maximum excess delay

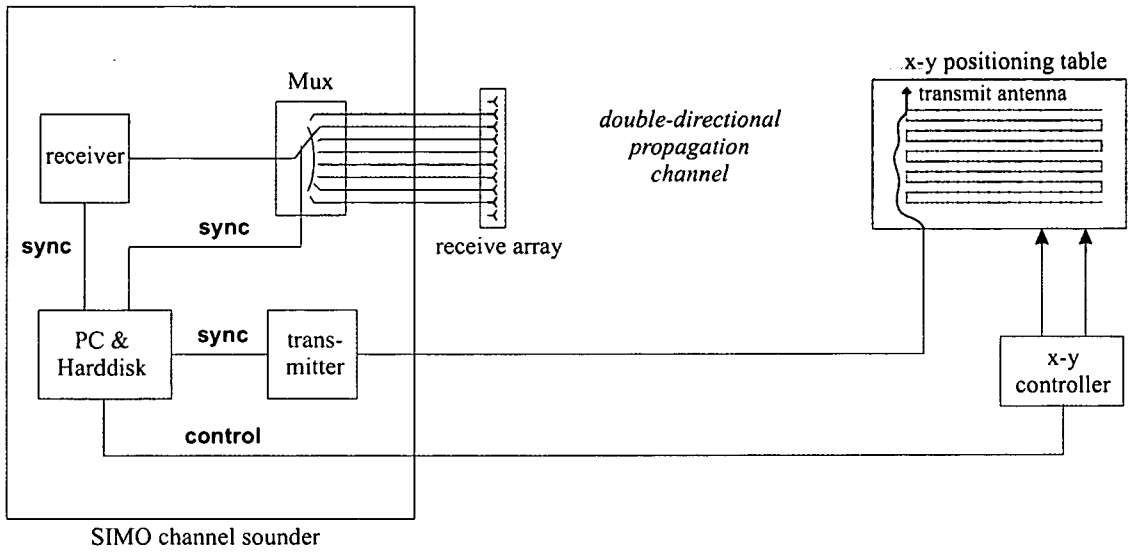

Figure 4.1: Measurement setup.

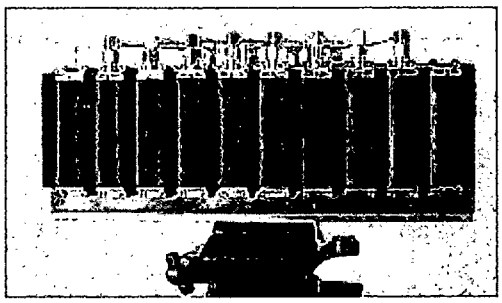

Figure 4.2: 8-element receive array with 2 dummies.

that can be measured of 193/120MHz = 1.6μs and results in a delay resolution in Fourier sense of 8.3ns. The measurement was repeated automatically 128 times (*temporal snaphots*) to facilitate averaging for noise reduction.

Altogether, we got a (128×193×8×200) 4-dimensional complex channel transfer matrix containing the channel coefficients for each temporal snapshot, frequency, receive antenna and transmit antenna position. Since the measurement of the this 4-dimensional matrix took about 10 minutes, we conducted the measurements at night to ensure stationarity.

4.1.2 Antennas

At the Rx side, a uniform linear array (ULA) of eight vertically-polarized printed dipoles with two additional dummy elements was used (see Fig. 4.2). The inter-element spacing between the dipoles was 0.4 wavelength (0.4*lambda*) at 5.2GHz[1].

Each single antenna had a 3dB beamwidth of about 120°. The measured azimuth antenna

[1]Please note that in [88] the interelement spacing of the Rx array was erroneously reported as 0.5λ.

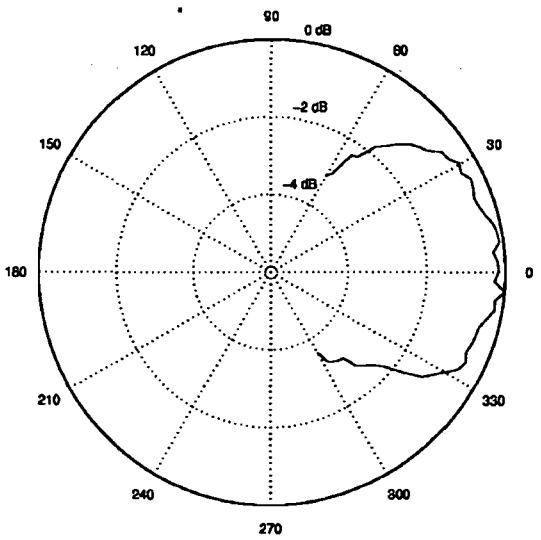

Figure 4.3: Measured azimuth receive antenna pattern in the range from $-60°$ to $+60°$.

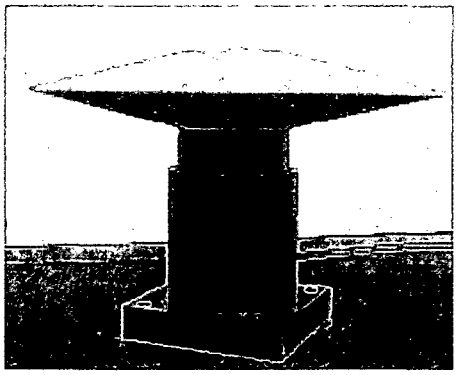

Figure 4.4: Transmit antenna.

pattern for the range of $-60°$ to $+60°$ (Fig. 4.3) was almost identical for each antenna. We fixed the receive array on a wooden tripod at a height of 1.5m.

At the Tx side, a single sleeve antenna, illustrated in Fig. 4.4, was used for the virtual transmit array. The antenna was vertically polarized and omni-directional in the horizontal plane (Fig. 4.5). The height of the antenna was approximately 1m.

The single Tx antenna was moved to 20 possible x- and 10 possible y-positions on a rectangular grid with $\lambda/2$ spacing (again, at 5.2GHz), forming a virtual Tx matrix *without* mutual coupling. A sketch of the virtual transmit array is given in Fig. 4.6. The gray dots indicate the transmit antenna position whereas the dotted line shows the movement path. The direction of the movement is given by the arrow.

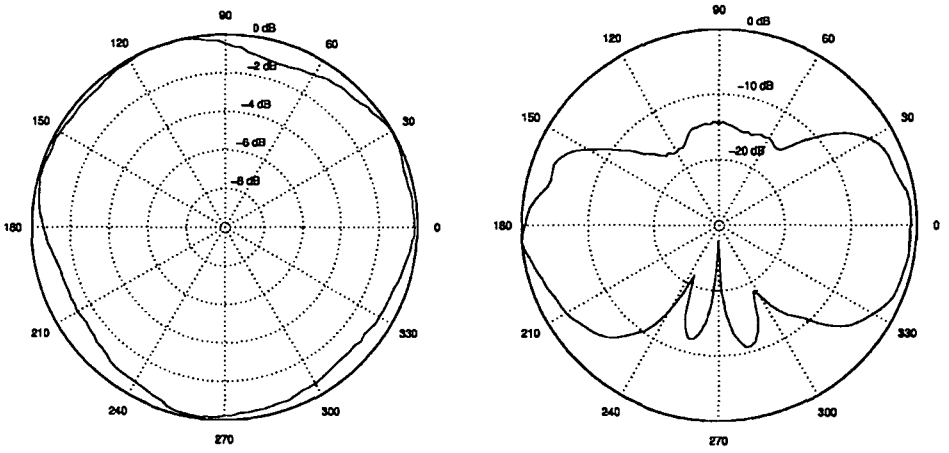

(a) Azimuth pattern.

(b) Elevation pattern.

Figure 4.5: Transmit antenna pattern.

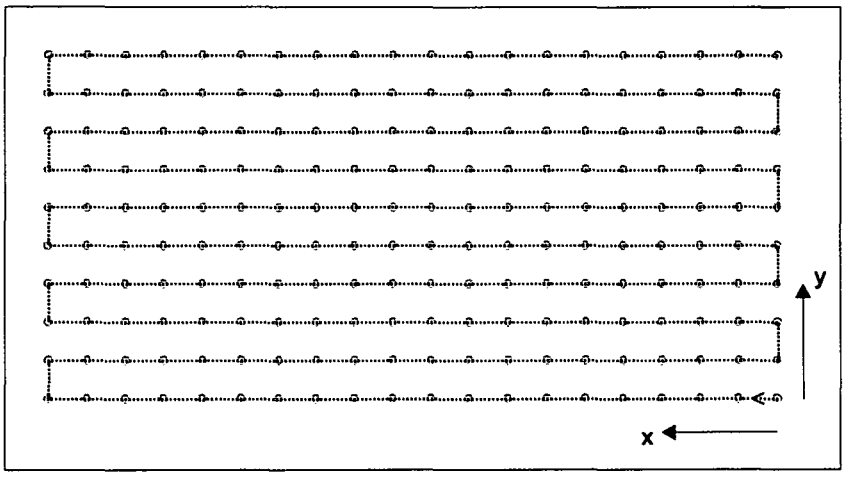

Figure 4.6: Illustration of the virtual transmit array: The transmit antenna was moved along the dotted line on a rectangular grid with $\lambda/2$ spacing (gray dots).

4.2 Scenario

The measurements were conducted in the offices of the *Institut für Nachrichtentechnik und Hochfrequenztechnik*, at the *Technische Universität Wien*. The floor plan of the scenario is plotted in Fig. 4.8. The transmitter assumed a single fixed location in a hallway (indicated by a yellow square). The receive array assumed many different locations in several offices connected to this hallway (red dots). In total, 24 receive positions were measured: 23 of them were in different office rooms, with no direct Line-of-Sight (NLoS) to the transmitter. One was in the hallway with direct LoS to the transmitter. In order to capture the whole azimuth range, we rotated the Rx antenna to three different broadside directions D1, D2 and D3 (c.f. Fig. 4.8) at each position. These directions were angularly spaced by 120°. Thereby, we get 72 different 'scenarios', i.e. combinations of Rx positions and directions.

Some office rooms were amply, others sparsely furnished with wooden and metal furniture and plants. Typical furnitures were computers, monitors, book shelfs, chairs, tables and heaters. The doors between the hallway and the rooms, as well as their frames, were also wooden or glass-filled.

To get a visual impression, Fig. 4.7 shows some exemplary pictures of the measurement environments. It is noteworthy that at the transmitter, absorber foams were used to avoid perturbing reflections from the metallic positioning table.

4.3 Data Post Processing

4.3.1 Averaging over Temporal Snaphots

First, we averaged over all 128 temporal snapshots in order to increase the SNR. This leads to an improved average receive SNR by $10 \cdot \log(128) \approx 21$dB theoretically to values up to $50 - 60$dB, depending on the considered scenario. However, the dynamic range of the channel sounder, which was about 40dB, did not allow for such high improvements. Please note that this averaging neither influences the Signal-to-Interference Ratio (SIR), nor the ratio of the signal to the third-order intermodulation products.

The outcome of this averaging process is (for each scenario) an 8×200 MIMO matrix at each frequency bin.

4.3.2 Receive Array Calibration

At the physical receive array, we face mutual electromagnetic coupling between the antenna elements. Additionally, unequal length and resistance of the feeder and/or multiplexing switch can cause different amplifications of the signals for each antenna. Both effects result in unacceptable errors when DoA estimation is performed [89]. As a consequence, the receive array has to be calibrated [89, 90].

A DoA-independent, time-invariant error model that describes the mutual coupling as well as the different amplifications of the antenna signals is shown in Fig. 4.9. Here, the amplification of the i-th antenna is denoted by c_{ii}, whereas its mutual coupling into the j-th antenna element, $i \neq j$, is denoted by c_{ji}.

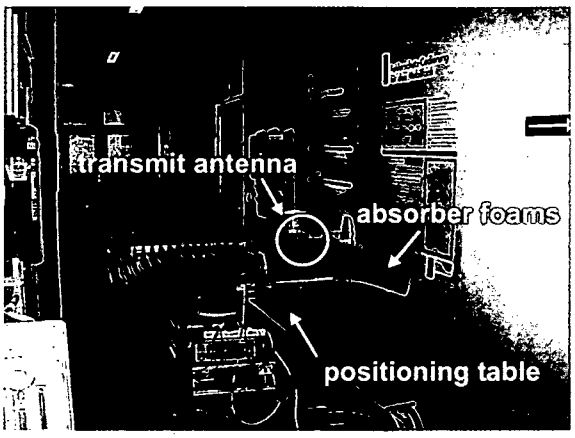

(a) Transmitter.

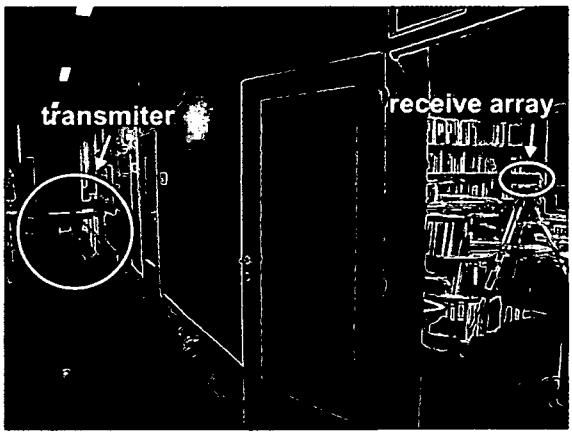

(b) Both link ends at receive position Rx5, direction D3 (Rx5D3).

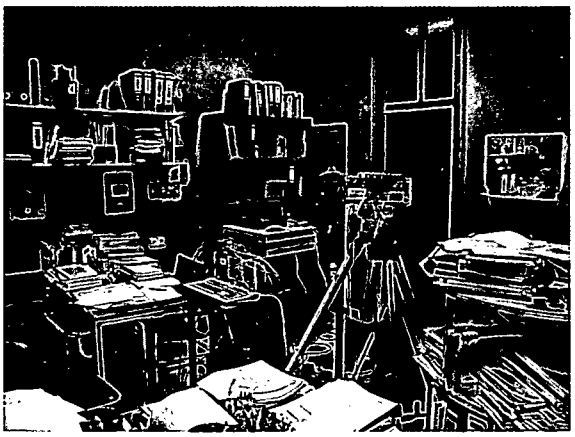

(c) Rx5D3, view into direction D3.

(d) Rx5D3, view opposite to direction D3.

(e) Rx22D1.

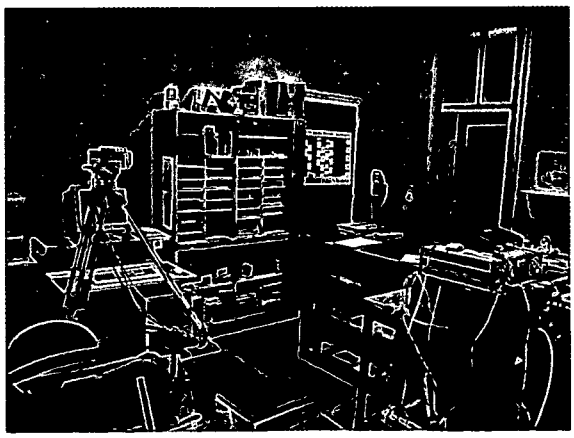

(f) Rx26D3.

Figure 4.7: Pictures of some exemplary scenarios of the 5.2GHz measurement campaign.

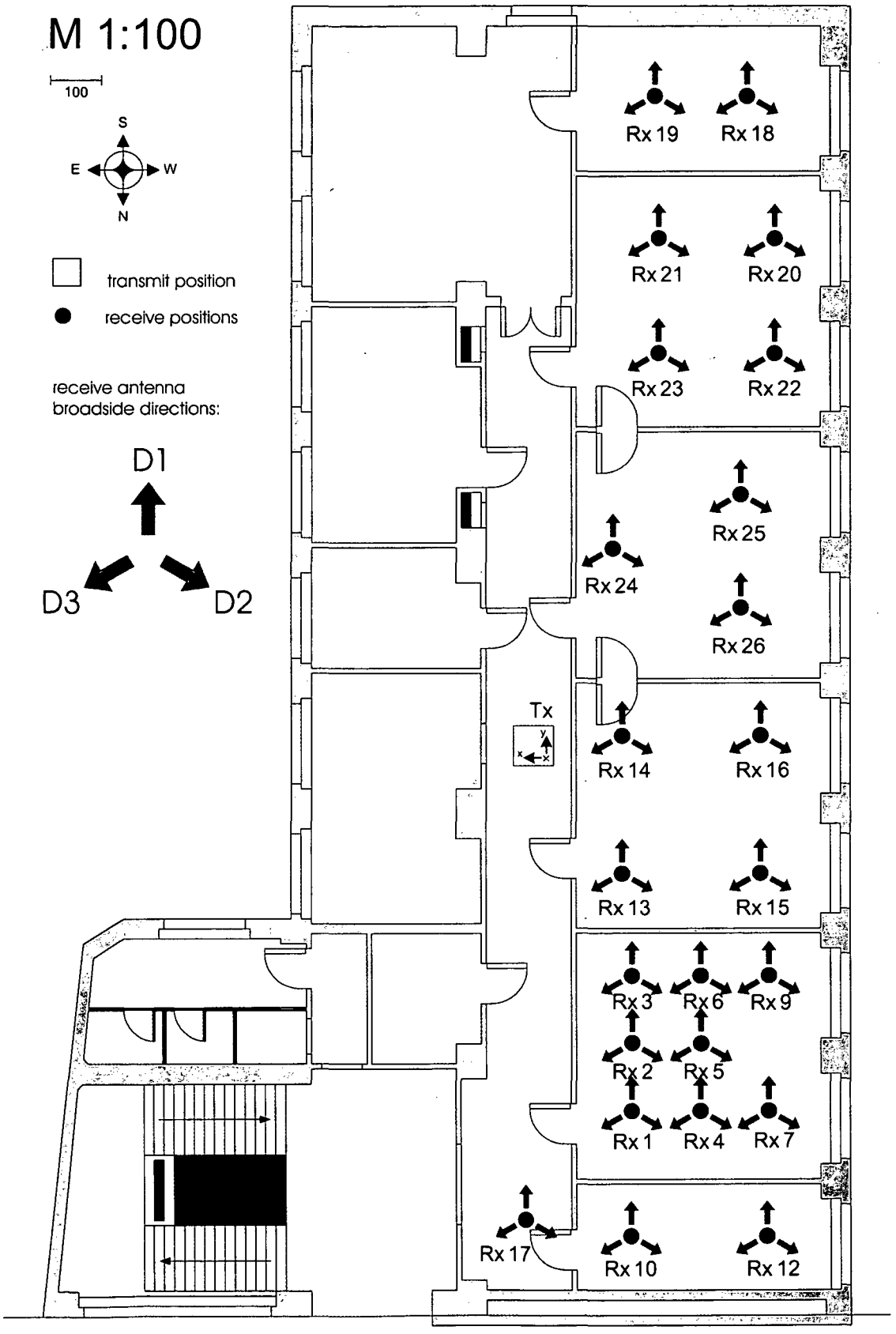

Figure 4.8: Floor plan of the 5.2GHz measurement campaign. In total, 72 different scenarios, i.e. Rx positions and directions, were measured.

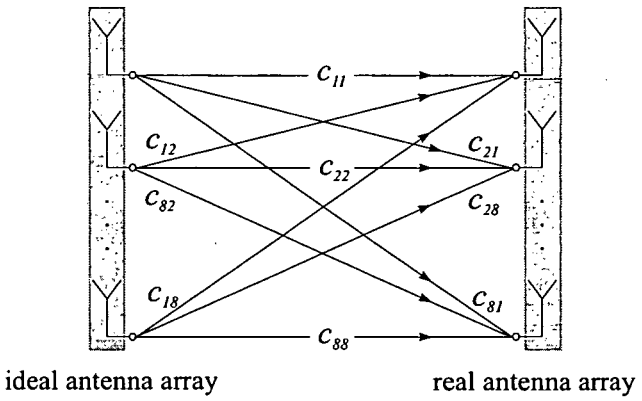

Figure 4.9: Illustration of the mutual coupling error model.

In matrix notation, the erroneous receive vector $\mathbf{r}'$ can be expressed as

$$\mathbf{r}' = \mathbf{C}\mathbf{r} \tag{4.1}$$

where $\mathbf{C} = (c_{ij})_{i,j=1}^{8}$ is the coupling matrix. In order to compensate for the errors, a correction matrix $\mathbf{C}^{-1}$ such that

$$\mathbf{C}^{-1}\mathbf{C} = \mathbf{I}, \tag{4.2}$$

where $\mathbf{I}$ is the identity matrix, has to be multiplied to the distorted array output. The corrected MIMO channel matrix for each frequency $\mathbf{H}(f)$ can be calculated by

$$\mathbf{H}(f) = \mathbf{C}^{-1}\mathbf{H}'(f). \tag{4.3}$$

Here, $\mathbf{H}'(f)$ is the distorted 8×200 MIMO matrix measured at the f-th frequency.

4.3.3 Creation of Spatial Channel Matrix Realizations

The different Tx antenna positions can be used to create different spatial realizations of an $m \times n$ MIMO channel. To give an example: The procedure for an 8×8 MIMO system with a $\lambda/2$ spaced virtual ULA in x direction (Fig. 4.6) is as follows [88]. Using all Rx antennas and selecting 8 adjacent Tx positions in the x direction out of the Tx matrix provides the first spatial realization. Moving this virtual 8-element Tx ULA was over all possible Tx antenna positions results in other spatial realizations. When taking the whole 20×10 transmit array, a maximum number of $13 \cdot 10 = 130$ spatial realizations of the 8×8 MIMO channel matrix can be achieved.

4.3.4 On the Size of the Statistical Ensemble

For the (aggregate) statistical evaluation of each measured scenario (e.g. fading statistics, parameter estimation, estimation of correlation matrices, capacity evaluations), different channel

realizations describing the same statistics are needed. An important aspect in this respect is the size of the statistical ensemble.

For narrowband analysis, besides spatial realizations, also the 193 different frequencies can be used. This is possible because it can be assumed that the wave propagation and therefore the statistics do not change significantly within a relative bandwidth of about 2.3%. In contrast to this, only spatial realizations can be used for broadband analysis.

But, which is the correct ensemble size? On the one hand, the chosen realizations should be sufficient to describe a complete ensemble for each considered scenario. We stress that the quality of statistical estimates depends on the number of measured statistical realizations - the more the better. Since the different frequencies are not independent but correlated, it is advantageous to take as many transmit positions as possible, even for narrowband analysis. The coherence bandwidth of the different scenarios according to [91] was estimated to be larger than 5.8MHz [92, page 42]. Therefore, depending on the considered scenario, within the measurement bandwidth of 120MHz about 20 independent frequency samples can be expected. Regarding the number of spatial channel realizations, of course, taking all 200 transmit antenna positions would be ideal.

On the other hand, the absence of *large-scale* fading across the chosen transmit array must be ensured. The chosen realizations must only contain *small-scale* fading variations. In other words, the statistical samples must not span a region which exceeds the stationarity region of the statistics under consideration. This was checked in two different ways. First, the mean channel power for each transmit antenna position, averaged over the frequencies and Rx antennas, was calculated [93]. It turned out that there are scenarios where the average power was not constant over the area of the transmit array but varied significantly, indicating large-scale variations. Second, the DoDs (together with their powers) departing from different sections of the transmit area were plotted by calculating the Capon's spectrum (see Chapter 5.3.2) for shifted versions a virtual ULA at the transmit array [88]. In absence of large-fading, they should stay the same. Again, it turned out that for some scenarios the DoD spectrum varied significantly.

As a consequence of both analyses, only a subset of 12×6 transmit antenna positions may be used. The evaluations in the following chapters always refer to this subset unless differently stated.

Chapter 5

Validation of Analytical Channel Models

The ultimate test of any model is experimental validation. In terms of MIMO channels this means comparing channel models with channel measurements. In this chapter, some analytical narrowband channel models reviewed in Chapter 3.3 will be evaluated and compared with the measurements at our Institute. Specifically, the Kronecker model, the Weichselberger model and the virtual channel representation will be investigated each for different MIMO systems. In the first part, given a fixed antenna inter-element spacing, the number of antennas will be varied from 2×2 to 4×4 and 8×8. In the second part, the performance of these models will be also studied for different antenna spacings, this time with number of antennas fixed.

The following approach will be used to validate the models: For each scenario we will (i) extract model parameters from measurement; (ii) generate synthesized channel matrices with these parameters by Monte-Carlo simulations of the three models; (iii) compare different metrics calculated from the synthesized channels with those extracted directly from the respective measurement.

5.1 Extraction of Model Parameters

In order to extract model parameters from the measurements, different realizations of the MIMO channel matrix are necessary for each scenario. Recall that besides spatial channel realizations also frequency realizations can be used for the analysis of narrowband channel models. The procedure for generating different spatial realizations of a channel matrix was already described in Chapter 4.3.

The model parameters of the Kronecker model, i.e. the single-sided receive ($\mathbf{R}_{\mathrm{Rx}}$) and transmit correlation matrix ($\mathbf{R}_{\mathrm{Tx}}$) are estimated by

$$\hat{\mathbf{R}}_{\mathrm{Rx}} = \frac{1}{N} \sum_{r=1}^{N} \mathbf{H}(r) \grave{\mathbf{H}}(r)^H, \tag{5.1}$$

$$\begin{aligned}\hat{\mathbf{R}}_{\mathrm{Tx}} &= \frac{1}{N}\sum_{r=1}^{N}\left[\mathbf{H}(r)^H\mathbf{H}(r)\right]^T \\ &= \frac{1}{N}\sum_{r=1}^{N}\mathbf{H}(r)^T\mathbf{H}(r)^*, \end{aligned} \tag{5.2}$$

where N is the number of channel realizations, while $\mathbf{H}(r)$ denotes the r-th channel realization. It is noteworthy that these estimators are, because of the noise, in principle biased [94]. However, since the measurement SNR was in a range of 30 to 40dB, this bias can be neglected.

Applying the eigenvalue decomposition to the estimated correlation matrices,

$$\hat{\mathbf{R}}_{\mathrm{Rx}} = \hat{\mathbf{U}}_{\mathrm{Rx}}\hat{\mathbf{\Lambda}}_{\mathrm{Rx}}\hat{\mathbf{U}}_{\mathrm{Rx}}^H, \text{ and} \tag{5.3}$$

$$\hat{\mathbf{R}}_{\mathrm{Tx}} = \hat{\mathbf{U}}_{\mathrm{Tx}}\hat{\mathbf{\Lambda}}_{\mathrm{Rx}}\hat{\mathbf{U}}_{\mathrm{Tx}}^H, \tag{5.4}$$

the estimated power coupling matrix $\hat{\mathbf{\Omega}}_{\mathrm{weichsel}}$ of the Weichselberger model can be obtained by

$$\hat{\mathbf{\Omega}}_{\mathrm{weichsel}} = \frac{1}{N}\sum_{i=1}^{N}\left(\hat{\mathbf{U}}_{\mathrm{Rx}}^H\mathbf{H}(i)\hat{\mathbf{U}}_{\mathrm{Tx}}^*\right)\odot\left(\hat{\mathbf{U}}_{\mathrm{Rx}}^T\mathbf{H}(i)\hat{\mathbf{U}}_{\mathrm{Tx}}\right). \tag{5.5}$$

Analogously, by taking unitary steering/response matrices $\mathbf{A}_{\mathrm{Tx}}$ and $\mathbf{A}_{\mathrm{Rx}}$ instead of the eigenbasis estimates $\hat{\mathbf{U}}_{\mathrm{Tx}}$ and $\hat{\mathbf{U}}_{\mathrm{Rx}}$, the estimated coupling matrix of the virtual channel representation $\hat{\mathbf{\Omega}}_{\mathrm{virt}}$ can be calculated by

$$\hat{\mathbf{\Omega}}_{\mathrm{virt}} = \frac{1}{N}\sum_{i=1}^{N}\left(\mathbf{A}_{\mathrm{Rx}}^H\mathbf{H}(i)\mathbf{A}_{\mathrm{Tx}}^*\right)\odot\left(\mathbf{A}_{\mathrm{Rx}}^T\mathbf{H}(i)\mathbf{A}_{\mathrm{Tx}}\right) \tag{5.6}$$

For $\mathbf{A}_{\mathrm{Tx}}$ and $\mathbf{A}_{\mathrm{Rx}}$ one steering/response direction was selected towards the broadside direction of the antenna array.

Table 5.1 summarizes the number of real-valued parameters that have to be specified for modeling an $m \times n$ channel. However, mind the following exception: When only mutual information is of interest, the number of necessary parameters of the Kronecker model and the Weichselberger model reduce to $m + n$ and mn, respectively.

5.2 Monte-Carlo Simulations

Using the extracted model parameters from the measurements, channel matrix realizations according to the Kronecker model

$$\hat{\mathbf{H}}_{\mathrm{kron}} = \frac{1}{\sqrt{\mathrm{tr}\{\hat{\mathbf{R}}_{\mathrm{Rx}}\}}}\hat{\mathbf{R}}_{\mathrm{Rx}}^{1/2}\mathbf{G}(\hat{\mathbf{R}}_{\mathrm{Tx}}^{1/2})^T, \tag{5.7}$$

	number of real-valued parameters
i.i.d.	1
Kronecker	$m^2 + n^2$
Weichselberger	$mn + m(m-1) + n(n-1)$
virtual channel representation	mn
full R_H-model	$(mn)^2$

Table 5.1: Number of model parameters of various analytical channel models.

the Weichselberger model

$$\hat{\mathbf{H}}_{\text{weichsel}} = \hat{\mathbf{U}}_{\text{Rx}} \left(\tilde{\hat{\Omega}}_{\text{weichsel}} \odot \mathbf{G} \right) \hat{\mathbf{U}}_{\text{Tx}}^T, \tag{5.8}$$

and the virtual channel representation

$$\hat{\mathbf{H}}_{\text{virt}} = \mathbf{A}_{\text{Rx}} \left(\tilde{\hat{\Omega}}_{\text{virt}} \odot \mathbf{G} \right) \mathbf{A}_{\text{Tx}}^T \tag{5.9}$$

are synthesized by introducing different fading realizations of the i.i.d. complex circularly symmetric Gaussian, unity-variance random fading matrix $\mathbf{G}$. For the different MIMO systems, the number of realizations was chosen to be equal to the respective number of measured realizations.

5.3 Metrics for Validation of MIMO Channels

If we want to judge the goodness of a MIMO channel model, we first have to specify 'good' in which sense. The quality of a model has to be defined with a view toward a specific channel property or aspect which we are interested in. Then we need metrics or performance figures that cover the desired channel aspects. Then, the application of these metrics to measured and synthesized channels enable a comparison or ranking of the models investigated.

Of course, it would be very helpful and highly advantageous to have a single metric that is capable of capturing all properties of a MIMO channel. However, this is not possible since the application of a specific metric implies a reduction of reality to some selected aspects, as modeling always does.

In the literature a multitude of metrics or performance figures have been proposed in the past. Among these were ergodic mutual information, outage mutual information, ergodic capacity, outage capacity, cdfs of the mutual information, capacity cdfs, eigenvalue statistics, correlation figures, and angular power spectra. The complexity of the proposed metrics range from single-number metrics to complex performance measures. Obviously, the more complex a metric is, the more information it provides. But on the other hand a direct comparison of two channels based on a complex metric becomes more difficult.

To illustrate this, let us consider metrics covering the offered multiplexing gain of a channel. No doubt that single-number metrics, e.g. the ergodic mutual information, allow for an easy comparison of different models. But what about using much more complex metrics e.g. as the eigenvalue statistics? The eigenvalue statistics plots distributions of the instantaneous

eigenvalues of the Gramian $\mathbf{H}\mathbf{H}^H$. In order to compare the eigenvalue statistics of two channels in a quantitative manner we would need a further, separate measure of distance. So we are back at 'single numbers'.

To summarize, there exists not one metric alone, but several metrics to verify the suitability of models for different aspects of MIMO systems. Consequently, we will use in the following four different metrics:

- the *mutual information with equal transmit power allocation*, since the most promising aspect of MIMO systems is the capacity increase due to the multiplexing gain offered by the virtual parallel sub-channels in the spatial domain [10, 11];
- the *joint DoD-DoA spectrum*, giving insight to the multipath structure and therefore the potential beamforming gain of a MIMO channel [13];
- a specific *Diversity Measure* introduced by Ivrlac and Nossek [95] describing the degree of diversity of a channel [29, Chapter 5.3.8]; and
- the *Correlation Matrix Distance* (CMD) that characterizes the changes in full spatial channel correlation matrices, as it was initially proposed by Herdin and Bonek [96] for a different purpose.

Mind that different metrics can yield different quality rankings of channel models as both, models and metrics, cover different channel aspects. The suitability of a metric strongly depends on the relevance of this metric to the MIMO system to be deployed.

5.3.1 A Metric for the Multiplexing Gain

As a metric for the potential multiplexing gain, the average mutual information with equal transmit power allocation is utilized. This value is calculated for each scenario by using (2.24) and averaging over all realizations of the respective scenario.

The normalization is done such that for each scenario the average power of the channel matrix elements h_{ij} is set to unity [38], i.e.

$$\frac{1}{N}\frac{1}{n}\frac{1}{m}\sum_{r=1}^{N}\sum_{i=1}^{m}\sum_{j=1}^{n}|h_{ij}(r)|^2 = 1. \tag{5.10}$$

Here, $h_{ij}(r)$ is the r-th realization of the corresponding channel matrix element h_{ij}. In fact, such a normalization characterizes the channel for the case of given or fixed receive SNR.

In the subsequent evaluations, the average receive SNR for each scenario is always set to 20dB.

5.3.2 A Metric for the Multipath Structure

For studying the double-directional multipath structure of a MIMO channel, the joint DoD-DoA Angular-Power-Spectrum (APS) is calculated using the *Capon's beamformer*, also known as *Minimum Variance Method (MVM)* [97, 98],

$$\mathbf{P}_{Capon}(\varphi_{\mathrm{Rx}}, \varphi_{\mathrm{Tx}}) = \frac{1}{\left(\mathbf{a}_{\mathrm{Tx}}(\varphi_{\mathrm{Tx}}) \otimes \mathbf{a}_{\mathrm{Rx}}(\varphi_{\mathrm{Rx}})\right)^H \mathbf{R}_{\mathbf{H}}^{-1} \left(\mathbf{a}_{\mathrm{Tx}}(\varphi_{\mathrm{Tx}}) \otimes \mathbf{a}_{\mathrm{Rx}}(\varphi_{\mathrm{Rx}})\right)}, \tag{5.11}$$

with the normalized steering vector $\mathbf{a}_{\mathrm{Tx}}(\varphi_{\mathrm{Tx}})$ into direction φ_{Tx} and response vector $\mathbf{a}_{\mathrm{Rx}}(\varphi_{\mathrm{Rx}})$ from direction φ_{Rx}.

Capon's beamformer was preferred over the simpler Bartlett beamformer [99, Chapter 9] because it provides better angular resolution. On the other hand, it is much more robust and easier to implement than super-resolutional parametric estimation methods like ESPRIT [100, 101, 102] or SAGE [103, 104]. Also, we want to avoid discussions about the model order and the reliability of estimations of directions by these methods. The single-sided marginal spectra (DoD and DoA) are calculated by the one-dimensional Capon's beamformer expressed by

$$\mathbf{P}_{\mathrm{DoD,Capon}}(\varphi_{\mathrm{Tx}}) = \frac{1}{\mathbf{a}_{\mathrm{Tx}}^H(\varphi_{\mathrm{Tx}}) \mathbf{R}_{\mathrm{Tx}}^{-1} \mathbf{a}_{\mathrm{Tx}}(\varphi_{\mathrm{Tx}})}, \text{ and} \tag{5.12}$$

$$\mathbf{P}_{\mathrm{DoA,Capon}}(\varphi_{\mathrm{Rx}}) = \frac{1}{\mathbf{a}_{\mathrm{Rx}}^H(\varphi_{\mathrm{Rx}}) \mathbf{R}_{\mathrm{Rx}}^{-1} \mathbf{a}_{\mathrm{Rx}}(\varphi_{\mathrm{Rx}})}. \tag{5.13}$$

5.3.3 A Metric for the Channel Diversity

As reported in [29, Chapter 5.3.8], the eigenvalues λ_i of the MIMO channel correlation matrix $\mathbf{R}_{\mathbf{H}}$ describe the average powers of the independently fading matrix-valued eigenmodes of a MIMO channel that is sufficiently described by its second order moments. Its offered degree of diversity is determined only by the *complete* eigenvalue profile. As an example, the eigenvalue profiles of the measured and synthesized 8×8 channels at the representative receive position Rx20 into direction D1 (Rx20D1) is plotted in Fig. 5.1. Other sample eigenvalue profiles are shown in Appendix B.

Even if it can not reflect the whole information of the complete eigenvalue profile, a useful single-number metric for Rayleigh fading MIMO systems, the so-called *Diversity Measure* $\Psi(\mathbf{R}_{\mathbf{H}})$,

$$\Psi(\mathbf{R}_{\mathbf{H}}) = \left(\frac{\mathrm{tr}\{\mathbf{R}_{\mathbf{H}}\}}{||\mathbf{R}_{\mathbf{H}}||_{\mathrm{F}}}\right)^2, \tag{5.14}$$

was recently introduced by [95]. Here, $\mathrm{tr}\{\cdot\}$ denotes the trace of a matrix, while $||\cdot||_{\mathrm{F}}$ stands for the Frobenius norm. It is noteworthy that, since the following matrix identities hold,

$$\mathrm{tr}\{\mathbf{R}_{\mathbf{H}}\} = \sum_{i=1}^{K} \lambda_i \quad \text{and} \quad ||\mathbf{R}_{\mathbf{H}}||_{\mathrm{F}} = \sqrt{\sum_{i=1}^{K} \lambda_i^2}, \tag{5.15}$$

(5.14) can be equivalently written in terms of the eigenvalues

$$\Psi(\mathbf{R}_{\mathbf{H}}) = \frac{\left(\sum_{i=1}^{K} \lambda_i\right)^2}{\sum_{i=1}^{K} \lambda_i^2}. \tag{5.16}$$

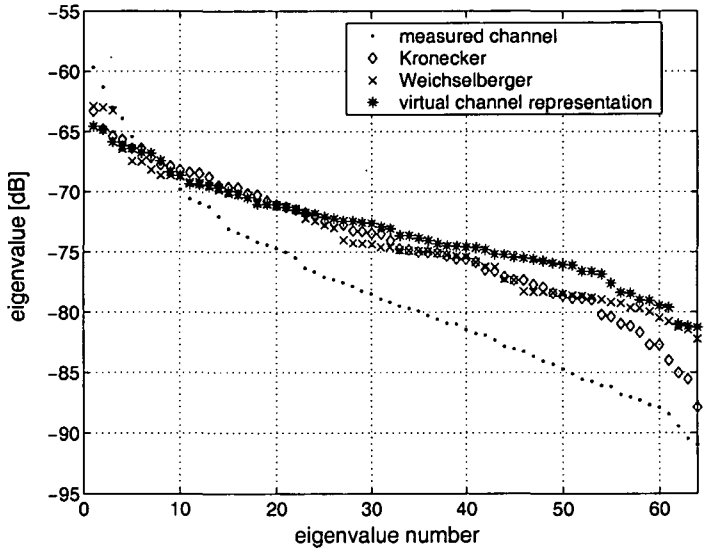

Figure 5.1: Eigenvalue profiles of 8 × 8 MIMO channels at the example scenario Rx20D1. Note that vertical axis includes channel power.

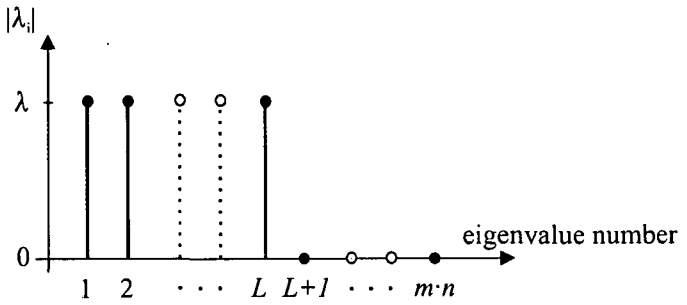

Figure 5.2: A beneficial property of the *Diversity Measure* $\Psi(\mathbf{R_H})$: If $\lambda = \lambda_1 = \lambda_2 = \ldots = \lambda_L > \lambda_{L+1} = \ldots = 0$ then the Diversity Measure becomes $\Psi(\mathbf{R_H}) = L$, the number of significant eigenvalues.

Nice properties of the presented metric are that

- $1 \leq \Psi(\mathbf{R_H}) \leq (n \cdot m)$: it is bounded between 1 and the dimension of $\mathbf{R_H}$.
- If $\lambda = \lambda_1 = \lambda_2 = \ldots = \lambda_L > \lambda_{L+1} = \ldots = 0$ then the Diversity Measure becomes $\Psi(\mathbf{R_H}) = L$, the number of significant eigenvalues (see Fig. 5.2).

For the example scenario referred in Fig. 5.1, the Diversity Measure of the measured channel is approximately 10. The respective value for the Weichselberger model, the Kronecker model, and the virtual channel representation can be calculated as 21, 26 and 31. Evidently, the more uniform the eigenvalues are distributed the higher the Diversity Measure, as desired.

5.3.4 A Metric for the Change in the Channel Correlation

In order to characterize the changes in the channel correlation, [96], [92, Chapter 4.4.1] introduced the *Correlation Matrix Distance* (CMD),

$$d_{CMD} = 1 - \frac{\mathrm{tr}\{\mathbf{R_H}\mathbf{R}_{\hat{\mathbf{H}}}\}}{||\mathbf{R_H}||_{\mathrm{F}}||\mathbf{R}_{\hat{\mathbf{H}}}||_{\mathrm{F}}}, \tag{5.17}$$

based on the inner product of two full MIMO correlation matrices $||\mathbf{R_H}||_{\mathrm{F}}$ and $||\mathbf{R}_{\hat{\mathbf{H}}}||_{\mathrm{F}}$. Initially, the CMD was proposed for analyzing spatial stationarity, as the two correlation matrices were taken e.g. at different positions or time instants.

The CMD is bounded by zero and unity. It becomes zero if the compared correlation matrices are equal (up to a scaling factor), and unity if they differ to a maximum extent, i.e. if the spatial structures of both matrices are orthogonal to each other. Using synthetic data, it was found in [92, Chapter 4.4.1] that a CMD value below 0.2 indicates that the channel did not change largely, whereas a value of 0.4 or more signals significant changes. Moreover, changes in the spatial structure leading to CMD values larger than 0.2 show up as a significant performance reduction in MIMO transmission schemes using outdated channel side information.

Based on these findings, we can extend the significance of the CMD to our problem: Equation (5.17) represents also a proper metric for the experimental validation of channel models. If $||\mathbf{R_H}||_{\mathrm{F}}$ and $||\mathbf{R}_{\hat{\mathbf{H}}}||_{\mathrm{F}}$ denote the correlation matrices of the measured and synthesized channel, the CMD characterizes the difference in spatial channel correlation, or in other words, the difference between the spatial structure of both channels.

5.4 On the Statistics of the Measured Channels

The investigated channel models assume that the channel is sufficiently described by its second order moments, covered by the full MIMO correlation matrix $\mathbf{R_H}$ only. As a consequence, measurements used for the evaluations of these models have to fulfill this requirement, too. In particular, only scenarios where the corresponding MIMO matrices follow a multivariate zero-mean complex Gaussian distribution may be considered for validation purposes of these models.

A necessary condition is that the marginal distributions, i.e. the distributions of the channel matrix elements are also zero-mean complex Gaussian. Or equivalently, their magnitudes (amplitudes) are Rayleigh distributed. This was checked by plotting the fading statistics for each scenario [105], keeping in mind that this condition alone is not sufficient.

As a further check, the average mutual information of channels synthesized by using its full second order description,

$$\mathbf{H} = \text{unvec}\left\{\hat{\mathbf{R}}_{\mathbf{H}}^{1/2}\text{vec}\{\mathbf{G}\}\right\}, \tag{5.18}$$

is compared with the average mutual information of the respective measured channels. For this purpose, Monte-Carlo simulations of (5.18) were performed in analogy to Chapter 5.2. For convenience, we will call (5.18) simply 'full R_H-model'.

For the different MIMO systems, which were considered in the following, we restricted the set of scenarios such that only those scenarios were taken into account (a) which were explicitly Rayleigh fading, and (b) where the average mutual information of the full R_H-model shows a maximum relative deviation of about 2% with respect to the measurement. We tolerate a small mismatch since we deal with real measurements where we expect some deviation from theory. Also, statistical variance had to be considered. In Fig. 5.3, this restricted set of scenarios is indicated by green arrows. The rest, especially LoS and OLoS scenarios that experience Ricean-fading are excluded (crosses in Fig. 5.3).

5.5 Variation of Antenna Number

How do the basic analytical channel models perform when considering variable antenna number, but constant antenna inter-element spacing? This question will be investigated in this subsection.

The models' performances will be studied for 2×2, 4×4 and 8×8 systems each for fixed antenna spacing of 0.5λ at the transmit array and 0.4λ at the receive array.

For the 8×8 MIMO channel, the set of samples is formed by 193 frequency times 30 spatial realizations, resulting in a total number of 5790 different realizations. Similarly, for the 4×4 MIMO channel we get $193 \cdot 42 = 8106$ realizations, and in case of a 2×2 system $193 \cdot 66 = 12738$ realizations, respectively. Regarding the quality of these estimations, we think that the number of realizations (the ensemble size) is appropriate (c.f. Chapter 4.3.3).

5.5.1 Average Mutual Information

In Fig. 5.4, a scatter plot of *average* mutual information of the synthesized channels vs. the *average* mutual information estimated directly from the measurement data in case of 8×8 MIMO is shown. For each model, a specific marker corresponds to one of the selected scenarios. The green diamonds indicate results of the full R_H-model, plotted for the just mentioned checking purpose. Red crosses represent the Kronecker model, black circles the Weichselberger model and blue squares the virtual channel representation. The dashed line corresponds to identity, whereas the dotted lines indicate different levels of relative errors. As a reference, the average mutual information of an i.i.d. Rayleigh fading channel, resulting to

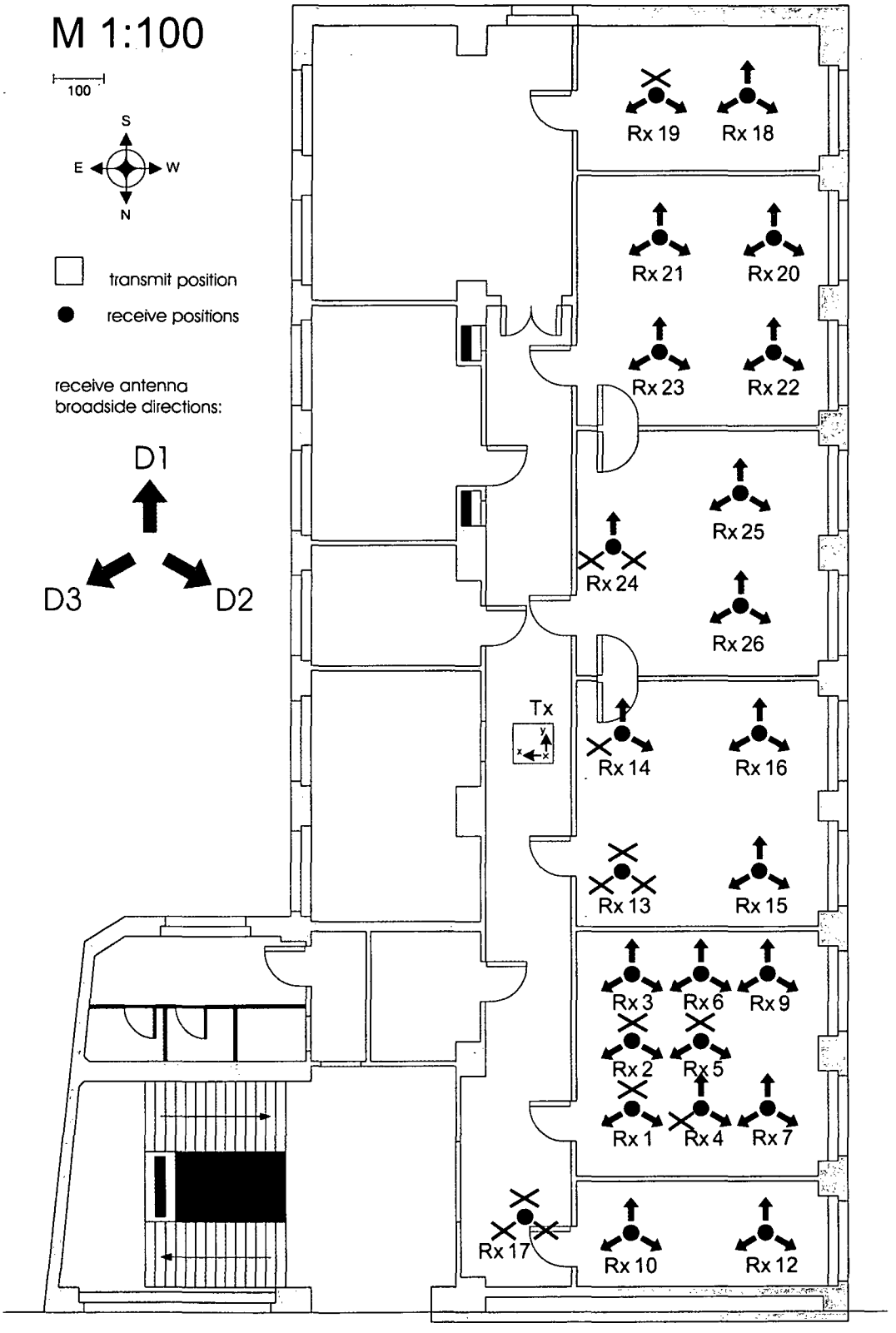

Figure 5.3: of the 5.2GHz measurement campaign. From a total of 72 different scenarios a restricted set of 58 Rayleigh-fading scenarios (indicated by green arrows) is used for the validation of analytical channel models. The excluded scenarios are denoted by crosses.

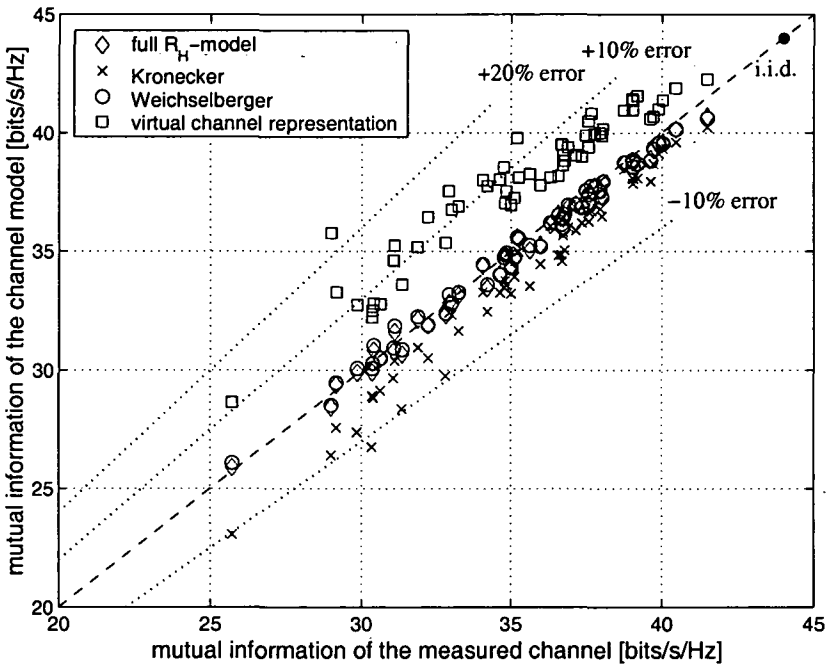

Figure 5.4: Average mutual information (for equal transmit power allocation) of synthesized vs. measured 8×8 MIMO channels @ 20dB receive SNR. The antenna inter-element spacings are 0.5λ at Tx and 0.4λ at Rx.

44.0bits/s/Hz at 20dB receive SNR, is represented by a black dot.

As can be seen, the Kronecker model underestimates the 'true' mutual information[1], i.e. the points lie below the identity (dashed) line. Moreover, the mismatch increases up to more than 10% with decreasing mutual information. A more detailed analysis in [106, 107] showed that scenarios with low mutual information correspond to high channel correlation. Thus, the Kronecker model, introduced to account for correlation, fails the more the more correlated the channel is.

The virtual channel representation overestimates the 'measured' mutual information significantly. Because of its fixed and predefined steering/response directions, the virtual channel representation is not able to reproduce any measured multipath components lying *between* fixed steering directions correctly. Instead, it assumes independently fading multipath components at the adjacent directions. In the worst case, a multipath component lying between two fixed DoDs and DoAs is modelled by four equal-powered, independently-fading multipath components. Thus, it tends to model the MIMO channel with more multipath components than the underlying channel really has, thereby reducing channel correlation and increasing the mutual information.

The Weichselberger model fits the measurements best with relative errors within the range of a few percents.

[1]Monte-Carlo simulations that we have performed with completely synthetic MIMO channels revealed the following. Although very seldom, the Kronecker model might also overestimate the 'true' mutual information. The probability of overestimation decreases with increasing antenna number.

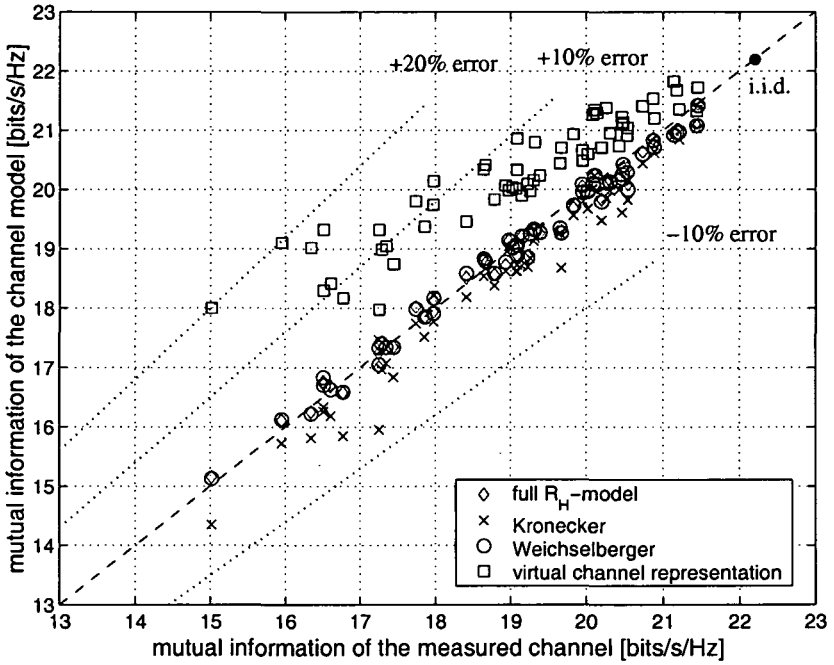

Figure 5.5: The same as Fig. 5.4, but for 4×4 MIMO channels.

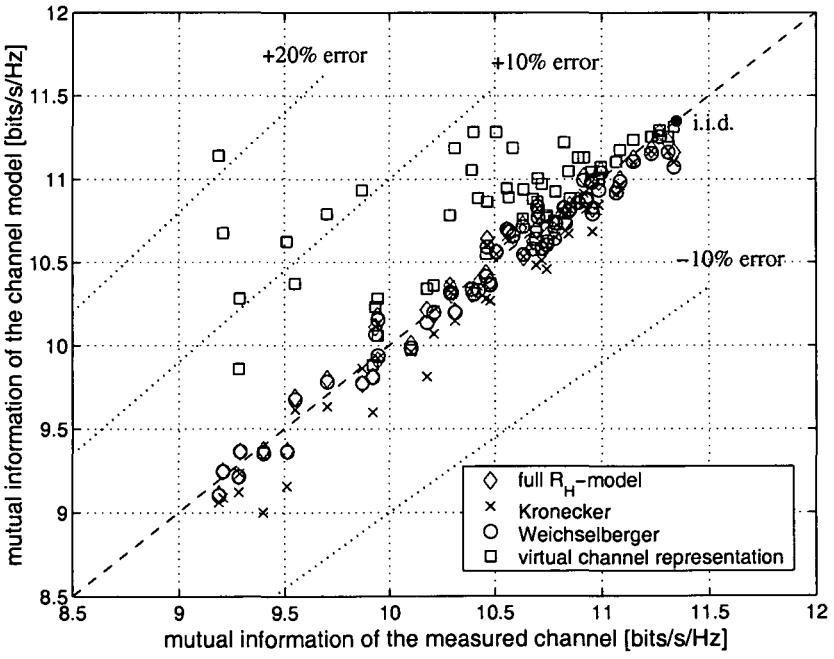

Figure 5.6: The same as Fig. 5.4, but for 2×2 MIMO channels.

In analogy to the 8×8 case, the average mutual information for 4×4 and 2×2 MIMO channels is shown in Fig. 5.5 and Fig. 5.6.

Evidently, the relative model error of the Kronecker model decreases with decreasing antenna number to a few percent. Although for 2×2 channels there exist some exceptional scenarios where the Kronecker model also overestimates the mutual information, a clear trend goes with underestimation of the mutual information.

The relative model errors of the virtual channel representation do not change significantly with the antenna number. The model overestimates mutual information of the measured channel systematically up to 20%.

The performance of the Weichselberger model does not change significantly, either. It still reflects the multiplexing gain of the measured channel best.

At this point, we want to mention that the mutual information of the Kronecker model was already investigated in several publications, e.g. in [108] or [109], where the performance of the model was found to be satisfactory for a 2×2 and 3×3 system. This is in agreement with our results. However, as demonstrated above, when the antenna size increases, thereby improving the angular resolution, the deficiency of the Kronecker model becomes worse.

5.5.2 Joint DoD-DoA Spectrum

Figure 5.7 plots the 8×8 Capon spectra evaluated for the example scenario Rx20D1. Rx20D1 (Fig. 5.7 (a)) was chosen because it is a scenario where the weaknesses of all three models become evident. The upper right plot shows the marginal DoD spectrum, whereas the left depicts shows the marginal DoA spectrum. What follows from the top to the bottom are the joint DoD-DoA spectra of the measured channel ('true' spectrum), the Kronecker model, the Weichselberger model and the virtual channel representation. The color-bar scales dB values with red color indicating high power and blue color corresponding to low power. Since our receive array was limited to 120° field-of-view the DoA spectrum is plotted only in the range from $-60°$ to $+60°$. Full 360° field-of-view is treated in [42].

In the measured channel, specific DoDs are clearly linked to specific DoAs such that the joint APS is *not separable* into a product of the DoD and the DoA APS. The Kronecker factorization, however, forces the joint spectrum of the Kronecker model to be separable, thus introducing artifact paths lying at the intersections of DoD and DoA spectral peaks. The resulting APS is the rank-one product of the two marginal spectra (c.f. Chapter 3.3.1.3).

In contrast, the Weichselberger model exposes this assumption to be too restrictive. Nevertheless, the Weichselberger model does not render the multipath structure completely correct either.

The virtual channel representation should, in principle, be able to cope with any arbitrary DoD-DoA coupling. The joint APS shows that it does not. The reason is again due to its fixed steering/response directions.

The Capon spectra for 4×4 and 2×2 channels are plotted in Fig. 5.8 and Fig. 5.9. All three models suffer from the same types of deficiencies, but, due to the reduced spatial resolution, these are differently pronounced.

In case of the Kronecker model, decreasing antenna numbers comes along with an improved performance. The reduced spatial resolution makes a Kronecker coupling of the measured

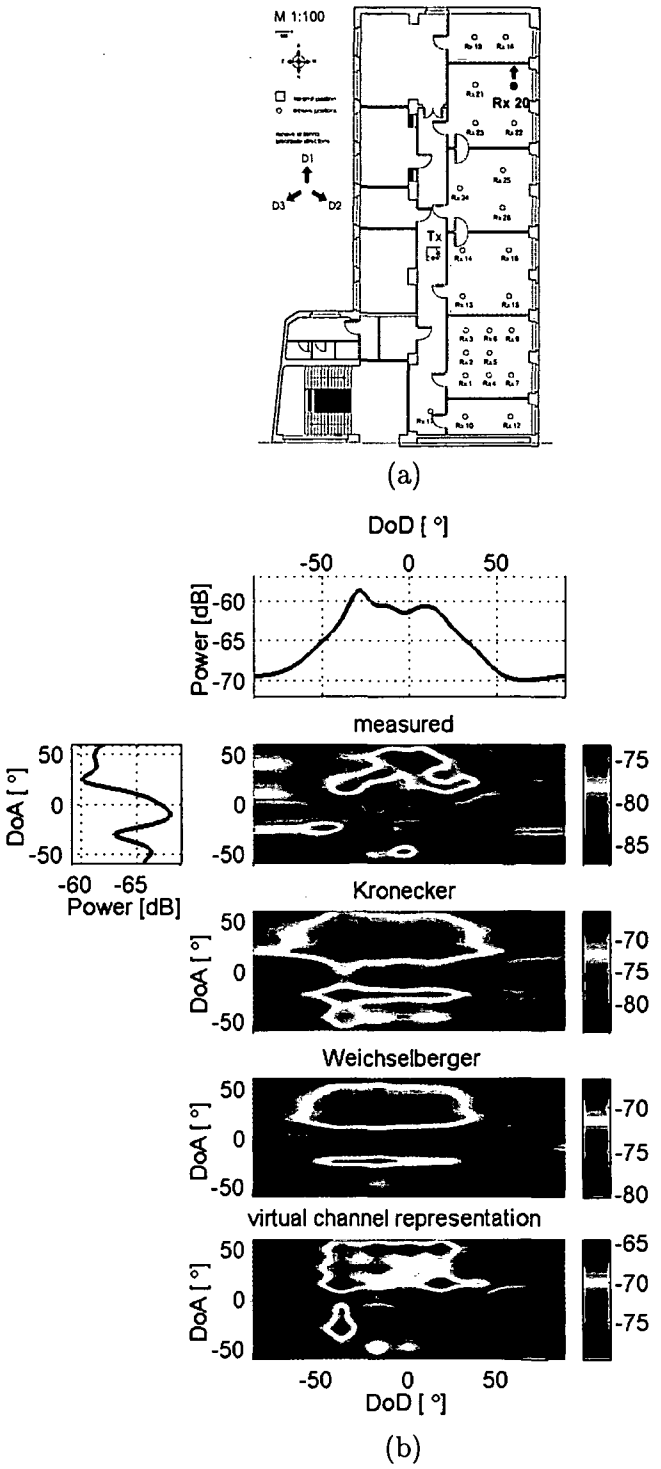

Figure 5.7: (a) Measurement scenario Rx20D1. (b) Joint DoD-DoA Capon spectra for 8 × 8 MIMO at scenario Rx20D1: The upper right (left) plot depicts the marginal DoD (DoA) spectrum. At the right-hand side, what follows from the top to the bottom are the joint DoD-DoA spectra of the measured channel, the Kronecker model, the Weichselberger model and the virtual channel representation.

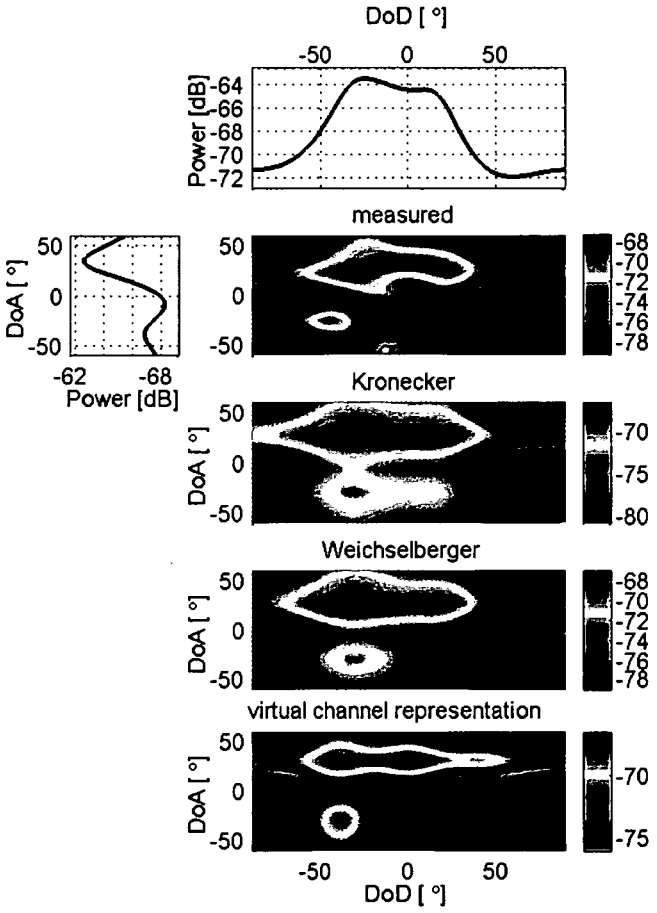

Figure 5.8: Joint DoD-DoA Capon spectra for 4 × 4 MIMO at scenario Rx20D1. The arrangements of the single APS follow Fig. 5.7.

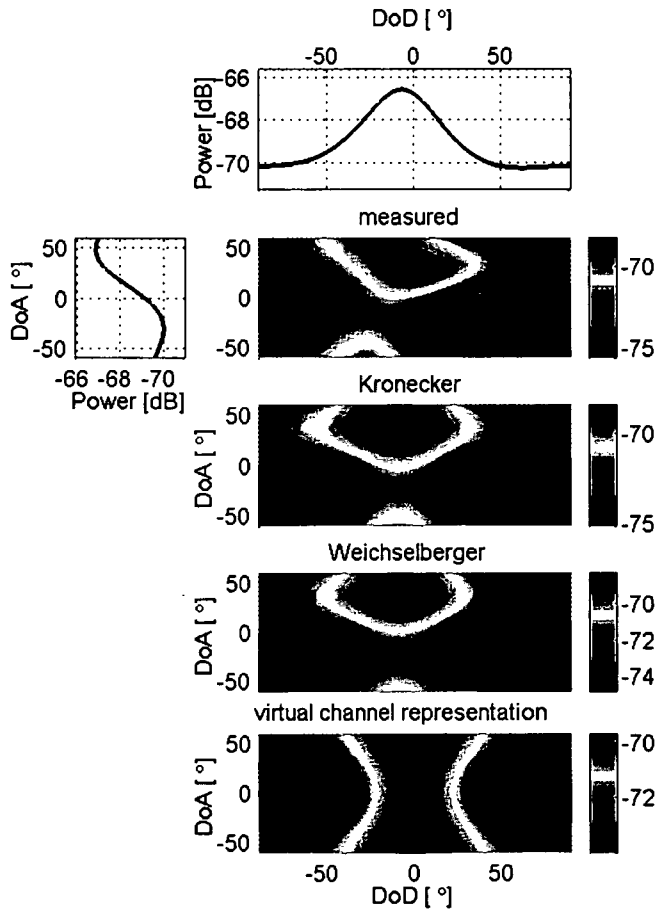

Figure 5.9: Joint DoD-DoA Capon spectra for 2×2 MIMO at scenario Rx20D1. The arrangements of the single APS follow Fig. 5.7.

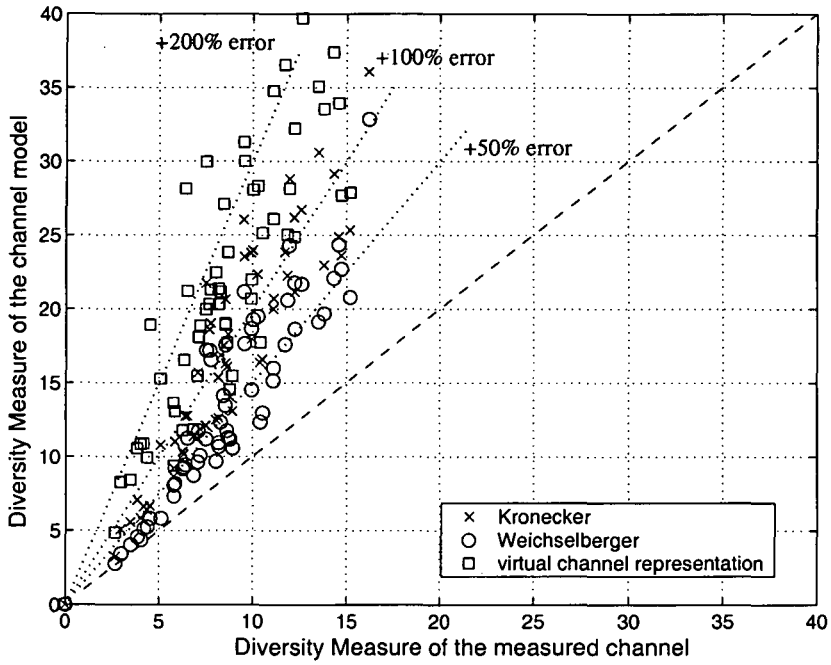

Figure 5.10: Diversity Measure of synthesized vs. measured 8×8 MIMO channels with inter-element spacings of 0.5λ at Tx and 0.4λ at Rx.

MIMO indoor channels more probable.

The same holds true for the Weichselberger model. Its match of reality gets also better with reduced antenna number. For the 4×4 system, it captures the spatial characteristics of this channel best of all three models.

On the other hand, the mismatch of the virtual channel representation increases since it now provides a decreasing number of steering/response directions to describe the underlying radio channel. In fact, for 2×2 it fails completely.

The joint DoD-DoA spectra of 8×8, 4×4 and 2×2 MIMO channels for all selected scenarios of the measurement campaign at our Institute are plotted in Appendix C.

5.5.3 Diversity Order

Figure 5.10 provides a scatter plot of the Diversity Measure of synthesized channels vs. the Diversity Measure estimated directly from the measurement data for each scenario in case of 8×8 MIMO channels. The blue dashed line indicates, again, the identity (no error), while the dotted line marks specific levels of relative error.

The synthetic channels either match or overestimate the Diversity Measures of the corresponding measured channels. Although the Weichselberger model (black circles) outperforms both the Kronecker model (red crosses) and the virtual channel model (blue squares) clearly, it shows relative errors of up to more than 100%. The worst performing virtual channel representation overestimates the diversity metric mostly by a factor of three.

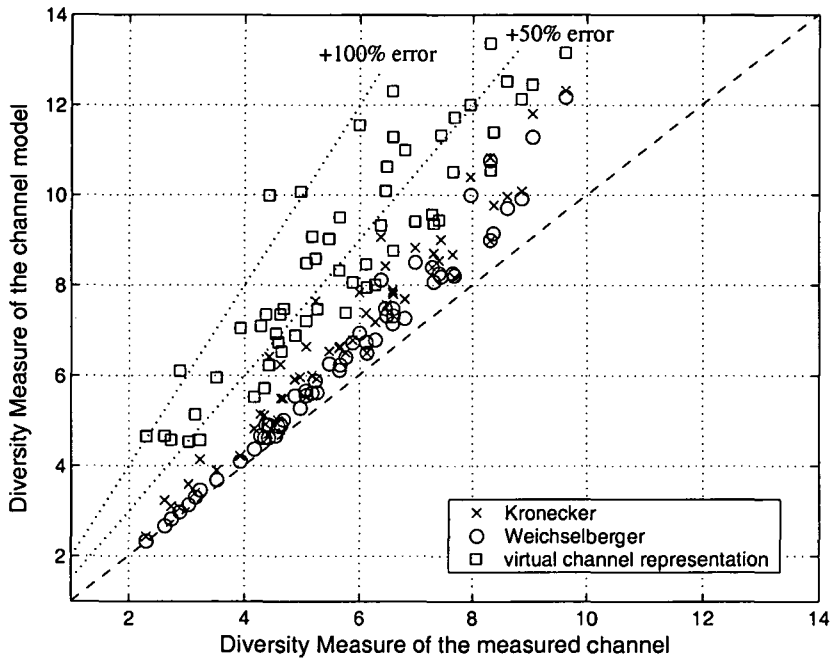

Figure 5.11: Diversity Measure of synthesized vs. measured 4×4 MIMO channels with inter-element spacings of 0.5λ at Tx and 0.4λ at Rx.

The Diversity Measures for 4×4 and 2×2 MIMO channels can be seen in Fig. 5.11 and Fig. 5.12. They show the same qualitative behavior as 8×8 channels, but decreasing relative errors with decreasing antenna numbers for all three models. Again, the Weichselberger model performs best. For the 2×2 channel, its match is almost perfect up to some negligible errors for higher diversity values. Also, the performance of the Kronecker model is quite tolerable within 10% relative error in this case. In contrast, the virtual channel representation, again, fails completely, even in the 2×2 case. It still overestimates the diversity significantly. The reason for the poor performance of the virtual channel representation is, again, its fixed, predefined steering directions. On the other hand, the mismatch of the Kronecker model is due to its deficiency of introducing artifact multipath components.

Although there is no direct relationship between diversity and spatial multiplexing, the overestimation of the diversity order can also be seen in the empirical cumulative density function (cdf) of the mutual information. The MIMO channel diversity affects the reliability (level of diversity) of the virtual parallel channel paths which is reflected by the slope of the capacity or mutual information cdf curve. As an example, the cdf of the mutual information for an 8×8 MIMO at Rx16D1 with an SNR of 20dB is plotted in Fig. 5.13.

The slopes of the Kronecker (red), Weichselberger (black) and virtual channel representation (blue) cdf curves are steeper than the one of the measured channel (green). This pretends higher reliability for the multiplexing gain. As a consequence, while the Weichselberger model reflects the average mutual information sufficiently, it does not so for the outage mutual information.

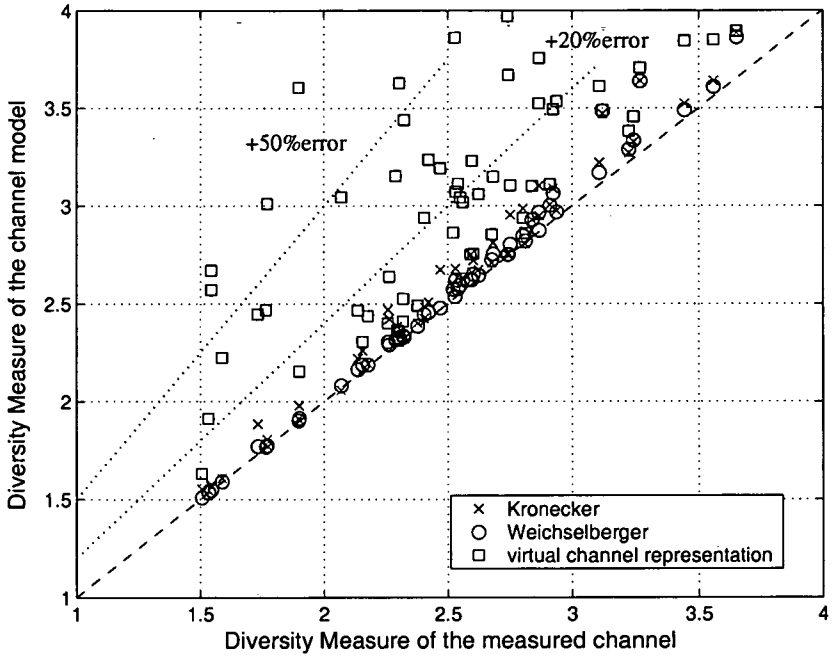

Figure 5.12: Diversity Measure of synthesized vs. measured 2×2 MIMO channels with inter-element spacings of 0.5λ at Tx and 0.4λ at Rx.

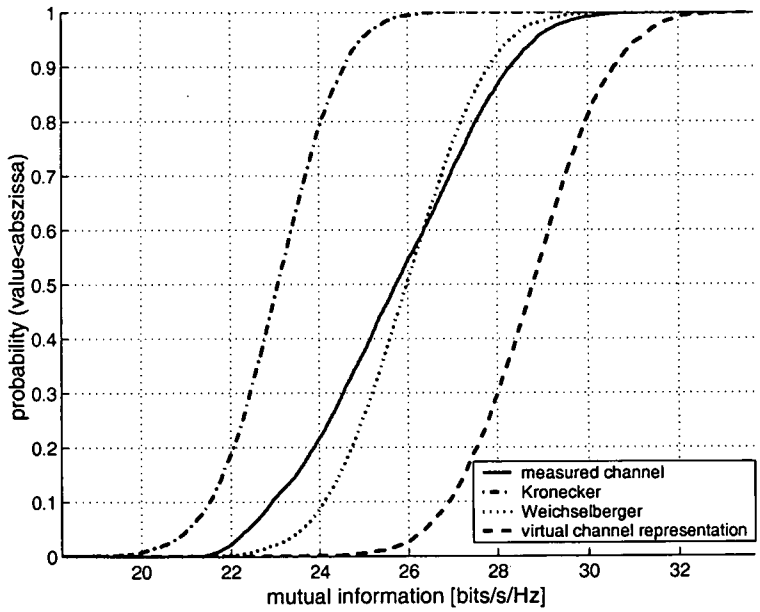

Figure 5.13: Empirical cdf of the 8×8 mutual information for example scenario Rx16D1 @ 20dB receive SNR. The inter-element spacings are 0.5λ at Tx and 0.4λ at Rx.

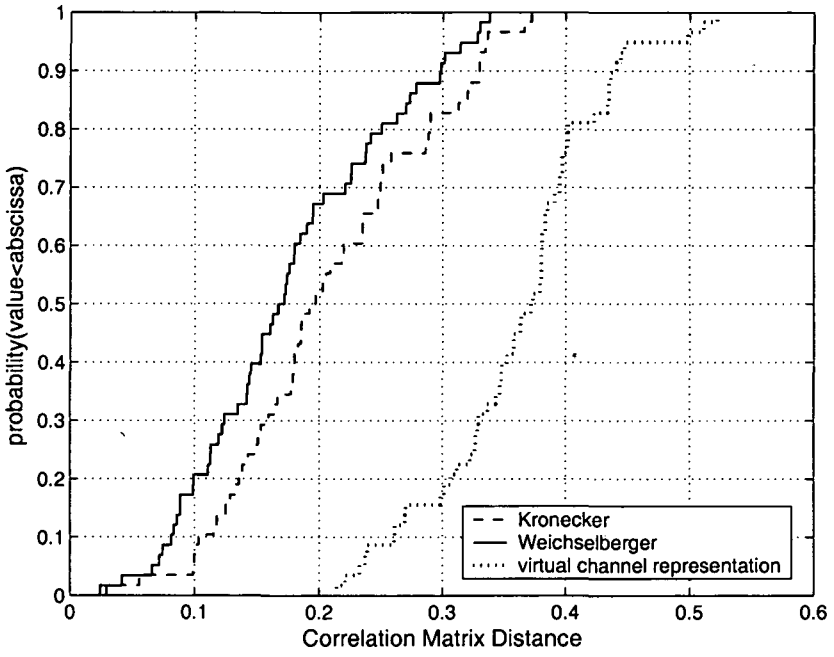

Figure 5.14: Empirical cdf of the Correlation Matrix Distance (CMD) between measured and synthesized 8×8 MIMO channels with inter-element spacings of 0.5λ at Tx and 0.4λ at Rx.

5.5.4 Correlation Matrix Distance

Figure 5.14 shows the empirical cdf of the CMD between the measured and synthesized 8×8 channels. With a mean CMD of 0.18 and a maximum of 0.34, the Weichselberger model (black) has the smallest deviation from the measurement. Although it renders the measured channel correlation best, it does not so sufficiently for all scenarios. Under the premise that a CMD value of 0.4 emphasizes significant deviations, as it was argued in [92, Chapter 4.4.1], the modeling of those scenarios that result in a CMD of 0.34 are critical with respect to the full channel correlation.

The performance of the Kronecker model (red) is slightly poorer. Its mean CMD results as 0.21, whereas its maximum CMD is 0.37. Evidently, the virtual channel representation (blue) shows the largest deviation from the measured channel correlation. With a mean CMD of 0.36 it is not advisable for modeling correlation of 8×8 channels.

The performances of all three models improve with decreasing antenna number, as it is shown for 4×4 channels in Fig. 5.15, and 2×2 channels in Fig. 5.16. Note the changing scale of the horizontal axis. The ranking of the models stays the same and can be listed with decreasing performance as: Weichselberger model, Kronecker model and virtual channel representation. In contrast to the virtual channel representation, both the Weichselberger and Kronecker model are able to reflect the full channel correlation sufficiently well when considering MIMO systems with 4×4 antennas or even less. In these cases, the evaluations exhibit a maximum CMD value of 0.15.

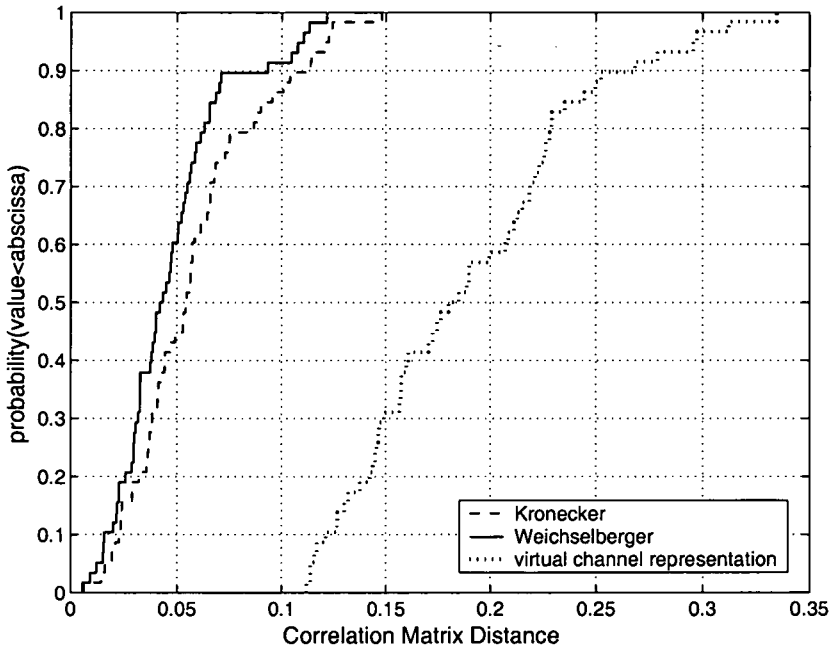

Figure 5.15: Empirical cdf of the Correlation Matrix Distance (CMD) between measured and synthesized 4×4 MIMO channels with inter-element spacings of 0.5λ at Tx and 0.4λ at Rx.

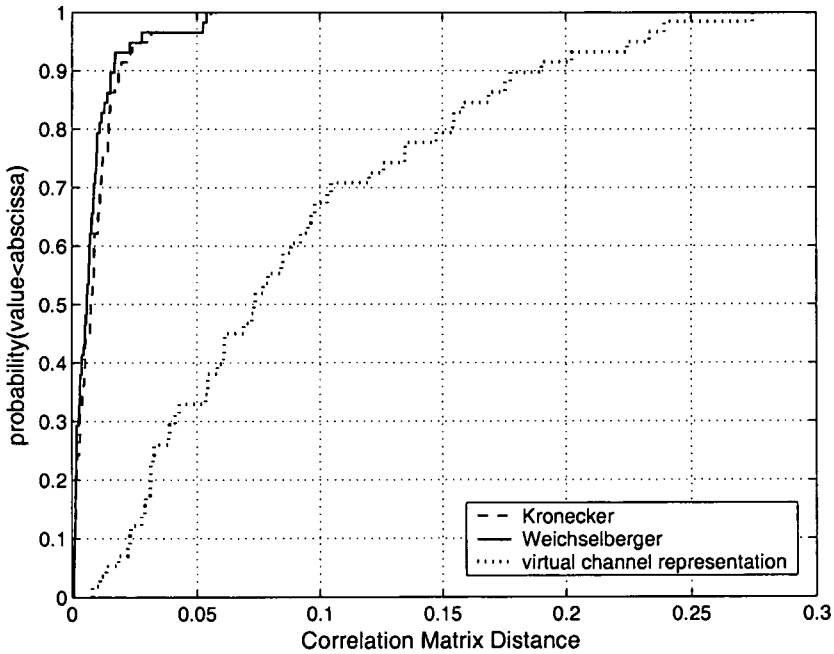

Figure 5.16: Empirical cdf of the Correlation Matrix Distance (CMD) between measured and synthesized 2×2 MIMO channels with inter-element spacings of 0.5λ at Tx and 0.4λ at Rx.

5.6 Variation of Antenna Spacing

It is well known that increasing antenna spacing can increase capacity. In [54] it is argued that increasing antenna separation may not only decorrelate the channel (and thus partially increase capacity as well) but also can directly contribute to increased capacity by efficiently increasing the number of parallel sub-channels. Therefore, it is more than likely that antenna separation of future indoor MIMO systems will not be limited to half-a-wavelength, which is critical for spatial sampling.

In this subsection we will analyze the models' performances when increasing inter-element spacing at both link ends. The limitation at the receive array allows only for the following evaluations: For 4×4 MIMO channels, the antenna spacing can be doubled with respect to the initial (minimum) antenna spacing, to one λ at Tx and 0.8λ at Rx. This reduces the set of samples to $193 \cdot 36 = 6948$ realizations.

For 2×2 MIMO channels, antenna spacings up to 3.5λ at Tx and 2.8λ at Rx can be set, thereby providing at least $193 \cdot 30 = 5790$ different channel matrix realizations.

Unfortunately, due to our restriction at the receive array, increasing the initial antenna separation of the 8×8 channels is not possible.

It is noteworthy that this time only the the mutual information, the Diversity Measure and the Correlation Matrix Distance will be used as metrics. Beamforming will not be regarded since it can not be performed uniquely for antenna spacings larger than half-a-wavelength because of the spatial aliasing effect (Shannon's sampling theorem).

5.6.1 Average Mutual Information

To investigate the effect of increased antenna spacing on the models' performances let us first inspect Fig. 5.17. In this figure, the average mutual information of synthesized vs. measured 4×4 MIMO channels for an antenna spacing of (a) 0.5λ at Tx and 0.4λ at Rx, and (b) one λ at Tx and 0.8λ at Rx is shown. The essential effects of increasing antenna separation, viz. *spatial zooming* and *spatial aliasing* (the latter for antenna spacings larger than half-a-wavelength) [54] make an increase in mutual information more likely. Of course, this does not mean that the mutual information of every single scenario has to increase. Although very seldom, it could happen that increasing antenna separation does not come along with increased mutual information. In fact, the average mutual information of the measured channels shift to a range of higher values. The bulk of the measured scenarios exhibit an average mutual information in a narrow range of 19 to 22bits/s/Hz.

As can be seen, the performance of the virtual channel representation improves significantly with increased antenna separation. Its relative errors reduce from 20% to about 10% as a consequence of the improved resolution of the fixed virtual angles. As explained in [54], more virtual angles couple to the scatterers enabling a better representation of the measured channel.

Regarding the Weichselberger model, increasing antenna separation does not affect its almost perfect match of the measurement.

Also the performance of the Kronecker model does not change significantly. Depending on the underlying physical propagation, the spatial aliasing effect could support a more uniform

joint APS, which complies with the Kronecker assumption. Evidently, this is not the case.

For 2×2 MIMO channels, Fig. 5.18 plots the average mutual information of synthesized vs. measured channels for antenna spacings of (a) 0.5λ at Tx and 0.4λ at Rx, (b) one λ at Tx and 0.8λ at Rx, and (c) 3.5λ at Tx and 2.8λ at Rx.

What changes with increasing antenna separation is again that the errors of the virtual channel representation decrease. For a spacing of 3.5λ at Tx and 2.8λ at Rx its maximum relative error reduces to less than 5%.

Note that a 2×2 MIMO system with very large antenna spacing could also be modeled as an i.i.d. channel. In this case the resulting relative error in the average mutual information would not exceed 10%.

5.6.2 Diversity Order

The impact of antenna separation on the Diversity Measure of measured and synthesized 4×4 channels is shown in Fig. 5.19, whereas Figure 5.20 depicts the same investigation for 2×2 channels.

In analogy to the mutual information, the diversity of the measured channels increases with increasing antenna separation.

As can be seen, the antenna separation does not affect the performance of the virtual channel representation significantly. The virtual channel representation overestimates the Diversity Measure of the measured channels up to 100% in case of 4×4 channels and and up to more than 50% in case of 2×2 channels, independently of the antenna separation.

Interestingly enough, match of the Weichselberger model and the Kronecker model becomes slightly poorer with increasing antenna separation.

5.6.3 Correlation Matrix Distance

Lastly, let us investigate the effect of antenna separation on the models' CMDs. For this purpose, Fig. 5.21 plots the empirical cdf of the CMD between the measured and synthesized 4×4 channels, and Fig. 5.22 shows 2×2 channels, respectively.

Evidently, the CMD of both the Weichselberger model and the Kronecker model increases with increasing antenna separation. The maximum CMD of both models increases to approximately 0.23 when doubling the initial antenna spacing of 4×4 channels. Similarly, the maximum CMD of 2×2 channels increases to about 0.1 for antenna spacings of 3.5λ at Tx and 2.8λ at Rx. Nevertheless, their performances are still sufficiently well, as CMD values smaller than 0.2 indicate only moderate deviations from the measured full channel correlation.

In contrast, there is no clear trend for the CMD of the virtual channel representation when increasing antenna separation.

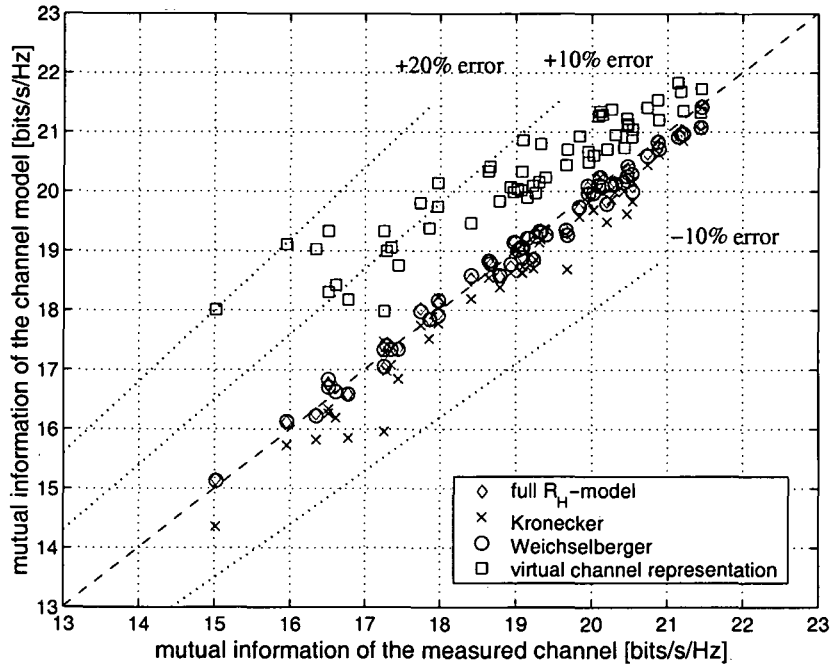

(a) Antenna spacings of 0.5λ at Tx and 0.4λ at Rx.

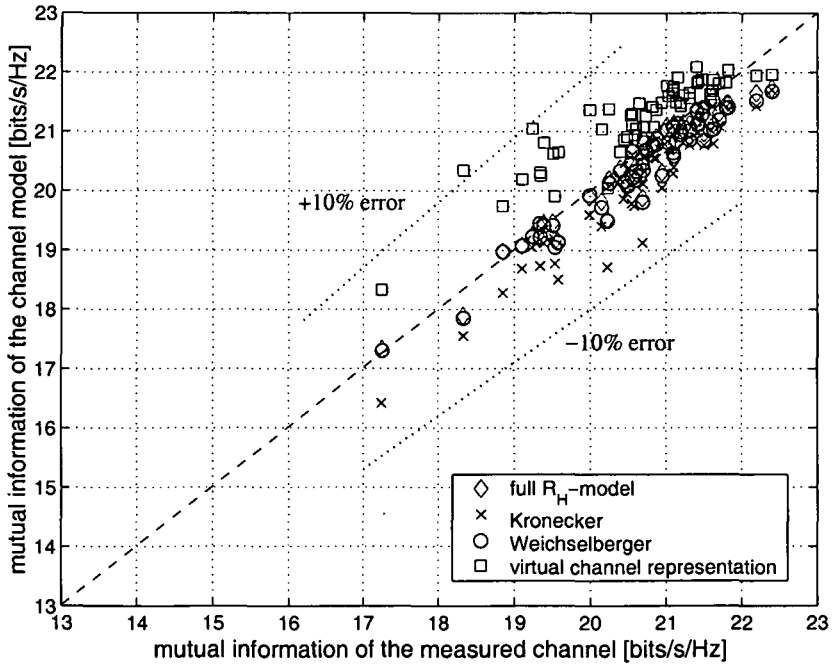

(b) Antenna spacings of one λ at Tx and 0.8λ at Rx.

Figure 5.17: Average mutual information of synthesized vs. measured 4×4 MIMO channels for varying antenna spacings. The receive SNR is set to 20dB.

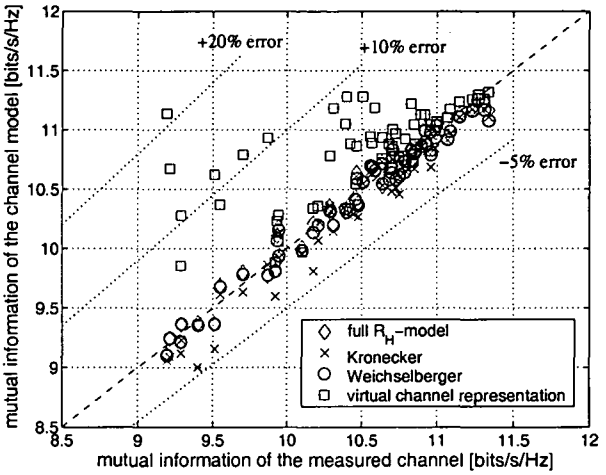

(a) Antenna spacings of 0.5λ at Tx and 0.4λ at Rx.

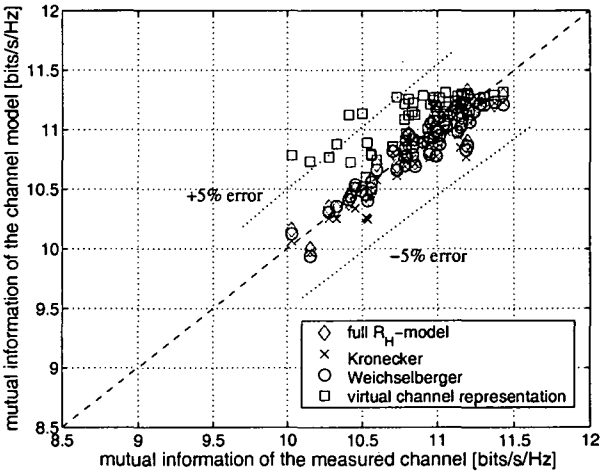

(b) Antenna spacings of one λ at Tx and 0.8λ at Rx.

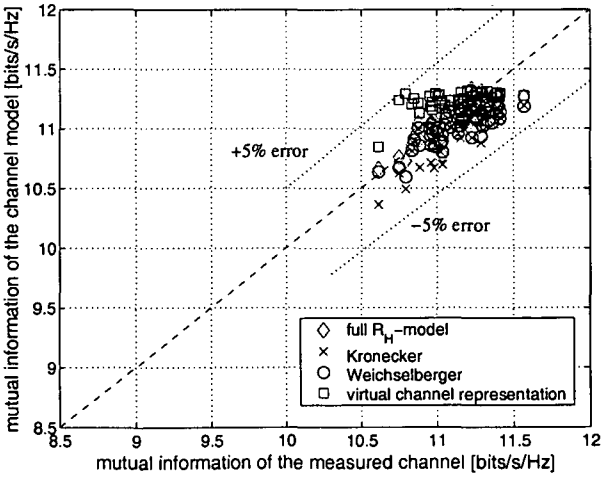

(c) Antenna spacings of 3.5λ at Tx and 2.8λ at Rx.

Figure 5.18: Average mutual information of synthesized vs. measured 2×2 MIMO channels for varying antenna spacings. The receive SNR is set to 20dB.

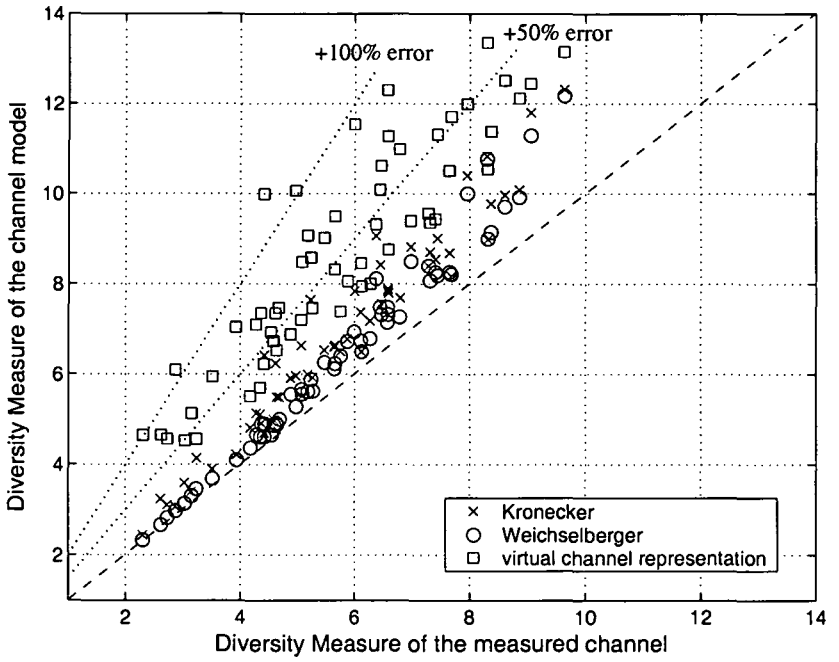

(a) Antenna spacings of 0.5λ at Tx and 0.4λ at Rx.

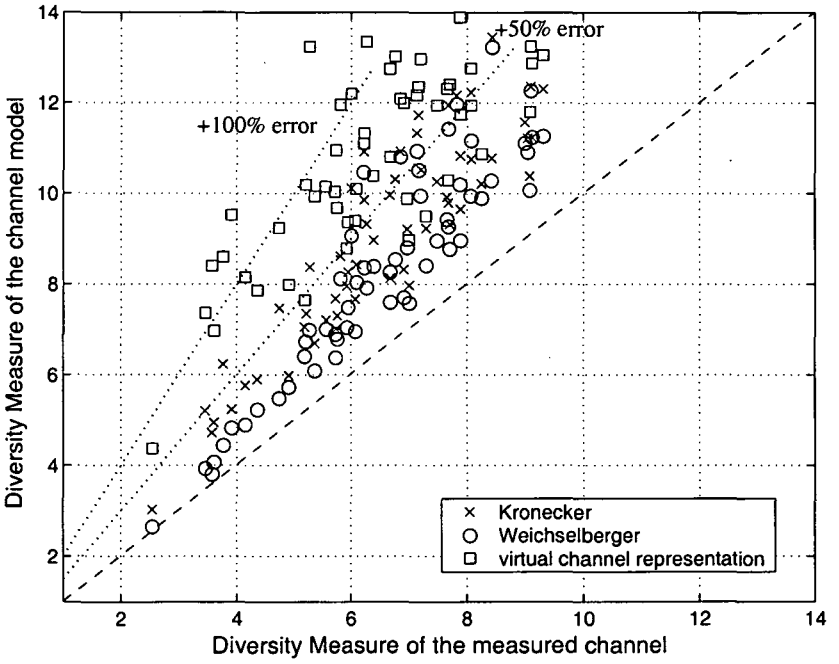

(b) Antenna spacings of one λ at Tx and 0.8λ at Rx.

Figure 5.19: Diversity Measure of synthesized vs. measured 4×4 MIMO channels.

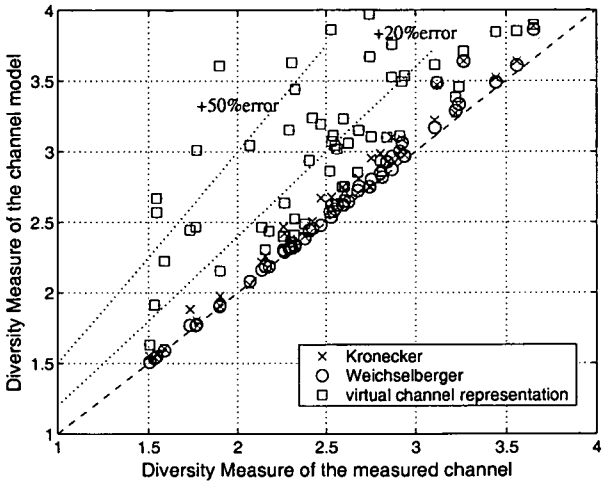

(a) Antenna spacings of 0.5λ at Tx and 0.4λ at Rx.

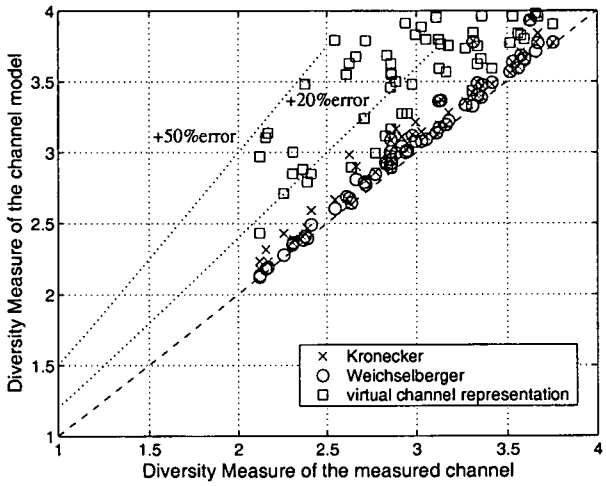

(b) Antenna spacings of one λ at Tx and 0.8λ at Rx.

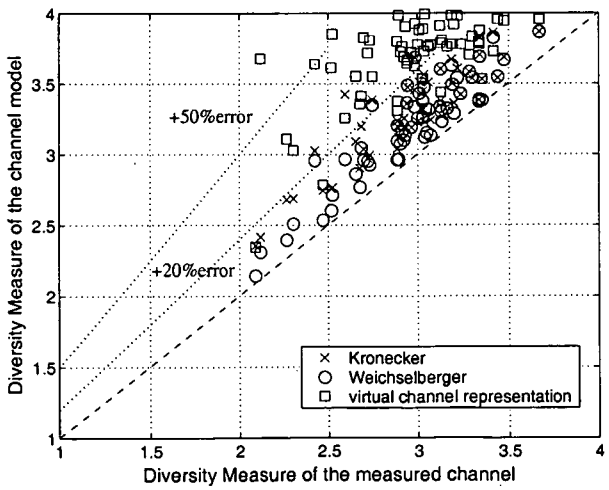

(c) Antenna spacings of 3.5λ at Tx and 2.8λ at Rx.

Figure 5.20: Diversity Measure of synthesized vs. measured 4×4 MIMO channels.

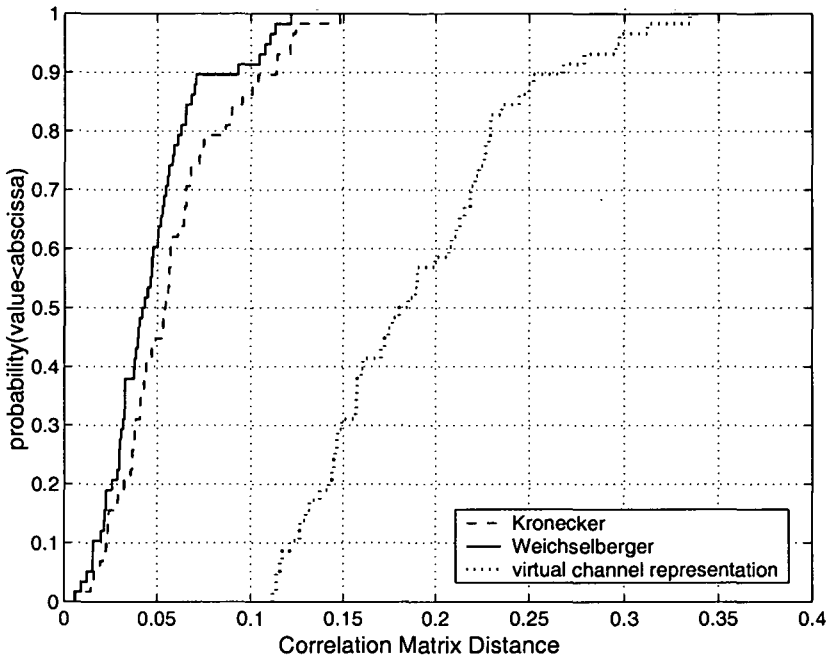

(a) Antenna spacings of 0.5λ at Tx and 0.4λ at Rx.

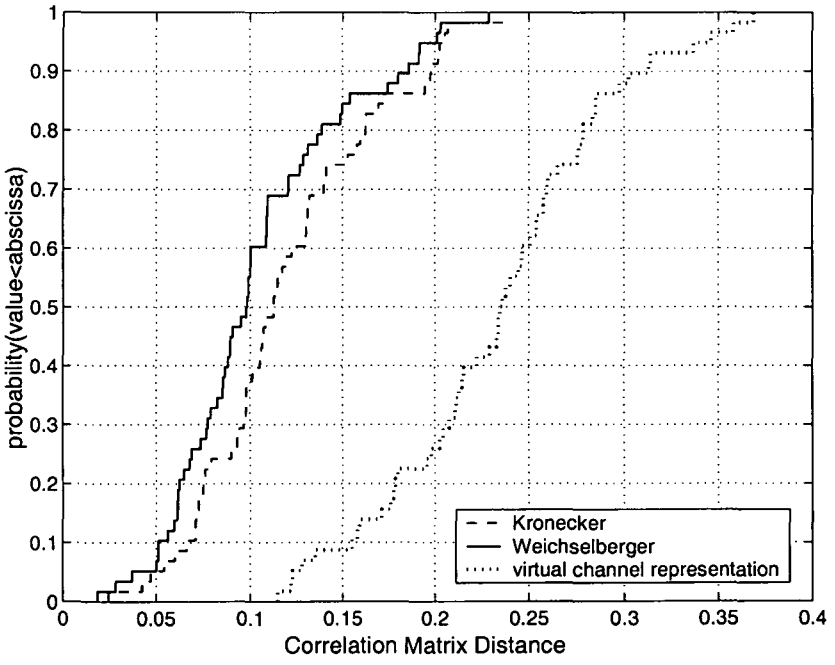

(b) Antenna spacings of one λ at Tx and 0.8λ at Rx.

Figure 5.21: Empirical cdfs of the Correlation Matrix Distance (CMD) between measured and synthesized 4×4 MIMO channels.

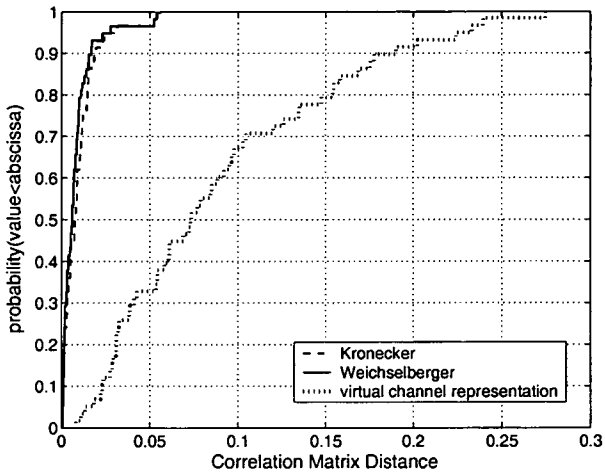

(a) Antenna spacings of 0.5λ at Tx and 0.4λ at Rx.

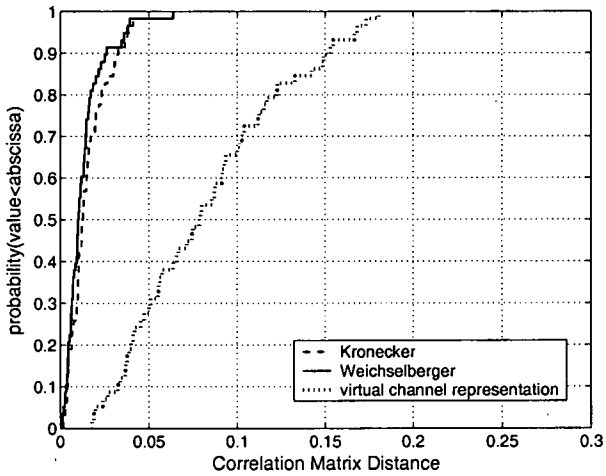

(b) Antenna spacings of one λ at Tx and 0.8λ at Rx.

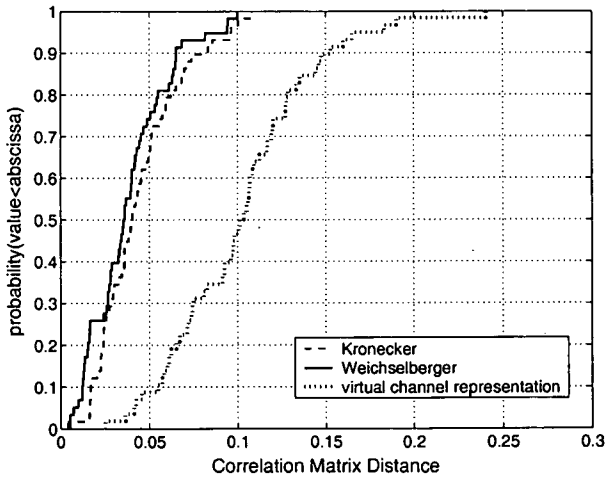

(c) Antenna spacings of 3.5λ at Tx and 2.8λ at Rx.

Figure 5.22: Empirical cdfs of the Correlation Matrix Distance (CMD) between measured and synthesized 4×4 MIMO channels.

Chapter 6

Summary and Conclusions

It is the radio channel that limits the capabilities of MIMO systems. Indeed, the benefits of MIMO, viz. spatial multiplexing, spatial diversity and beamforming, depend all on the structure of the underlying radio multipath propagation. This thesis has focused on *indoor* MIMO channel models, as they are of great importance for the design, simulation, and deployment of future high data-rate indoor MIMO systems such as WLANs.

Although radio propagation in indoor environments is characterized by the same propagation mechanisms as in outdoor, the situation is more complex. The specifics of indoor environments, where numerous objects may act as scatterers, result from both the smaller distances that are covered and the much larger variability of such environments. Extending conventional models (SISO or SIMO) to the MIMO case is not straightforward, since, in addition to the spatial characteristics at both link ends, also their *linkage* has to be considered.

Recent work on indoor MIMO modeling was briefly reviewed[1]. Note that the reported models were not exclusively indoor models. Models were categorized in *physical* and *analytical* models. The first characterize an environment on the basis of electromagnetic wave propagation by describing the (polarization dependent) double-directional multipath propagation between the location of the transmit array and receive array. As main drawbacks count the measurement and parameter extraction that is usually very tedious. As representatives of physical models, the extension of the Saleh-Valenzuela model and Zwick's model were addressed.

In contrast, analytical models describe the impulse response, or equivalently the transfer function, of the channel between the elements of the antenna arrays at the transmitter and receiver. These impulse responses are combined in a (delay dependent) channel matrix given by closed-form mathematical expressions. Analytical models provide an analytical framework for the design of transmit and receive techniques like space-time codes and the development of MIMO algorithms in general. They allow for reproducing various channel characteristics by changing only a limited number of modeling parameters.

The relationship between physical and analytical models is this: Starting from a physical model we arrive at analytical models, if we specify antenna arrays at both link ends by setting antenna elements, their geometrical configuration, and their polarizations, preferably by agreement to reference configurations. We emphasize that a physical model can be easily

[1]Parts of this will constitute a section of the first deliverable on 'Survey of existing channel models' of NEWCOM Department 2, Network of Excellence funded by the EU commission.

converted into an analytical model but not vice versa.

Various analytical narrowband models are based on the multivariate complex Gaussian distribution. Most popular examples include the i.i.d. model, Kronecker model, the Weichselberger model, and the virtual channel representation. Their commonness is that the elements of the channel matrix follow a joint multivariate zero-mean complex Gaussian distribution. Such channels are sufficiently described by their second order moments, covered by the full MIMO channel correlation matrix. However, they all rely on various simplifying assumptions regarding the underlying radio propagation. Benefits and shortcomings as consequences of those assumptions were detailed. Particularly, implications of the Kronecker separability assumption and the Weichselberger assumption were analyzed.

A recent finding about the correlation *across* the link, so-called 'diagonally correlated channels', shook the entrenched view that i.i.d. channels provide maximum ergodic capacity. We have shown how such channels would have to look like in physical terms (Appendix D).

For the purpose of experimental model validation, the Kronecker model, the Weichselberger model, and the virtual channel representation were compared with measurements. More specific, the following approach was used to validate the models: For each scenario (i) model parameters were extracted from measurement; (ii) synthesized channel matrices were generated with these parameters by Monte-Carlo simulations of the three models; (iii) different metrics calculated from the synthesized channels were compared with those extracted directly from the respective measurement.

The basis for our comparison was an extensive 5.2GHz measurement campaign in the offices of the Institut für Nachrichtentechnik und Hochfrequenztechnik. Within this campaign, a 20×10 virtual rectangular array with an inter-element spacing of half-a-wavelength was used at the transmit side, whereas a directional uniform linear array of 8 printed dipoles, spaced 0.4 wavelength and 3dB field-of-view, formed the receive array. The channel was probed at 193 equi-spaced frequencies over 120MHz of bandwidth. The measurements were used to create different spatial realizations of 2×2, 4×4 and 8×8 MIMO channels with varying inter-element spacings by moving a virtual uniform linear array across the whole transmit array.

Regarding the evaluation of the measurements, a particularly challenging problem was the proper choice of the statistical sample. The quality of statistical estimates depends on the number of measured statistical realizations - the more the better. On one hand, these realizations have to be sufficiently independent. On the other hand, the statistical samples must not span a region which exceeds the small-scale region of the statistics under consideration because this would mean averaging over multiple different statistics. Taking both limitations into consideration, the size of the used transmit array was reduced to a subset of 12×6. Since the investigated models assume that the channel is sufficiently described by its second order moments, measurements used for experimental validation of these models have to fulfill this requirement, too. Following this condition, only a restricted set of 58 scenarios (out of a total 72 measured scenarios) was considered for the validation. Ignoring these two caveats will yield misleading results about the measured channels.

In order to judge on the goodness of the models, metrics or performance measures were needed. Since the application of a specific metric implies a reduction of reality to some specific aspects, a single metric alone turned out not to be capable of capturing all properties of a MIMO channel. As a consequence, we used four different metrics covering different aspects

of MIMO systems to verify the suitability of the considered models: (i) the *average mutual information* (with equal transmit power allocation) describing the spatial multiplexing gain; (ii) the *double-directional angular power spectrum*, giving insight into the multipath structure and potential beamforming gain; (iii) a *Diversity Measure* describing the channel's diversity order; and (iv) the *Correlation Matrix Distance* in order to characterize the changes in the full channel correlation. We stress that the suitability of a metric strongly depends on the relevance of this metric to the MIMO system to be deployed.

The validation revealed that the Weichselberger model predicts the average mutual information, the Diversity Measure and the full channel correlation best of all three models, although it does not so sufficiently well in each case. Regarding average mutual information it shows an almost perfect match with the measurements, whereas the Kronecker model tends to underestimate the mutual information up to more than 10% (at a receive SNR of 20dB) especially for large arrays (8×8). The virtual channel representation, suffering from its fixed and predefined steering/response directions, overestimates the mutual information significantly. When we lower antenna numbers to 2×2 and increase antenna spacing, all considered models predict mutual information accurately, but the i.i.d. model is not farther off than 10% either.

Concerning the double-directional angular power spectrum none of the considered models can reproduce an arbitrary multipath structure accurately, independently of the array size. While the Weichselberger model can only cope with systems not larger than 4×4 sufficiently, the virtual channel representation improves its performance with increasing antenna numbers due to improved angular resolution. But 8×8 does not seem to be large enough. The Kronecker model forces the double-directional angular power spectrum to be separable and should, in general indoor environments with interdependent DoDs and DoAs, not be used for modeling the double-directional angular power spectrum. Exceptions are MIMO systems with low antenna numbers, e.g. as 2×2 or maybe 3×3 where the produced error is negligible, because of the very modest spatial resolution of such a system in first place.

Since the analyzed models are all based upon simplifying assumptions of the full MIMO correlation matrix, none of them is able to render the full correlation and diversity of the measured channels, independently of the antenna number and separation. Both the Kronecker model and the Weichselberger model are able to match the Diversity Measure and the full channel correlation matrix only for systems not larger than 4×4.

A general trend for all three models goes with this: the higher the number of antennas, the more the models deviate from the measurements.

The validation approach just discussed is the proper one to arrive at models that re-construct realistic MIMO channels, e.g. channels that are measured. This approach, though, is not the only one possible. Should one be interested in a *single* aspect of MIMO only, then models that contain proper parameters (that can be specified more or less freely) might perform better. For instance, the virtual channel representation allows for modeling channels with arbitrary multiplexing orders by choosing appropriate coupling matrices. Similarly, an appropriate choice of the Weichselberger coupling matrix enables the setting of arbitrary multiplexing *and* diversity orders.

Measurements made clear that the way MIMO channel matrices are normalized has a strong impact on the conclusions one draws. There are two meaningful ways of normalizing ensembles of measured channel matrices taken at different locations. The first ignores the pathloss at different locations by normalizing the channel matrix realizations at each location separately.

Since the receive SNR can then be set independently at different locations, this corresponds to a system with power control. Alternatively, a common normalization factor can be applied to all channel matrix realizations at all locations. This preserves the pathloss information and therefore corresponds to constant transmit power.

Appendix A

Proof of an Identity

Let $\mathbf{G}$ be an $m \times n$ complex Gaussian random matrix with unity power and independently distributed elements g_{ij}. For such a matrix

$$\mathbf{Y} = E\{\mathbf{G}\mathbf{X}\mathbf{G}^{\mathrm{H}}\} \tag{A.1}$$

is always equal to a scaled identity matrix $K \cdot \mathbf{I}_m$. Writing the matrix multiplication element-wise, the elements of $\mathbf{Y}$ become

$$y_{ij} = E\left\{\sum_{k=1}^{n} g_{ik} \sum_{l=1}^{n} x_{kl} g_{jl}^{*}\right\} = \sum_{k=1}^{n}\sum_{l=1}^{n} E\left\{g_{ik} x_{kl} g_{jl}^{*}\right\}. \tag{A.2}$$

Since the elements of $\mathbf{G}$ are independent and identically distributed, the expectation of the right hand side of (A.2) is non-zero only for $i = j$ and $k = l$, and therefore (A.2) simplifies to

$$y_{ij} = \begin{cases} E\left\{\sum_{k=1}^{n} |g_{ik}|^2 \cdot x_{kk}\right\} & i = j \\ 0 & i \neq j \end{cases} \tag{A.3}$$

Or equivalently with $P_g = E\{|g_{ik}|^2\}$

$$\mathbf{Y} = \left(P_g \cdot \sum_{k=1}^{n} x_{kk}\right) \cdot \mathbf{I}_m \tag{A.4}$$

Appendix B

Sample Eigenvalue Profiles

This appendix shows some sample eigenvalue profiles of the MIMO channel correlation matrix. For each of the chosen scenarios, the profiles are calculated for the measured channel and respective channels synthesized by the Kronecker model, the Weichselberger model and the virtual channel representation. Figure captions also include values for the Diversity Measure of the considered channels. The Diversity Measures of the measured channel, Kronecker model, Weichselberger model and virtual channel representation are denoted by Ψ_{meas}, Ψ_{kron}, Ψ_{weichsel} and Ψ_{virt}.

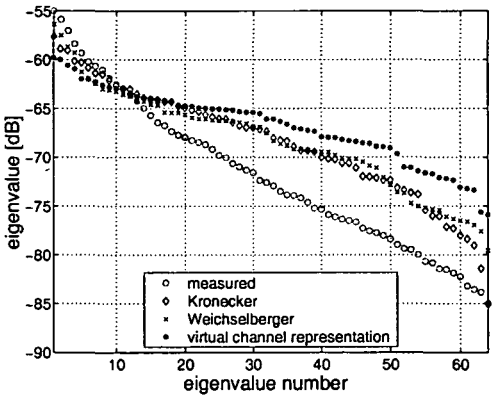

Figure B.1: Eigenvalue Profile of the 8×8 MIMO channel at Rx4D2: $\Psi_{\text{meas}} = 12.6$, $\Psi_{\text{kron}} = 26.7$, $\Psi_{\text{weichsel}} = 21.7$, $\Psi_{\text{virt}} = 39.7$.

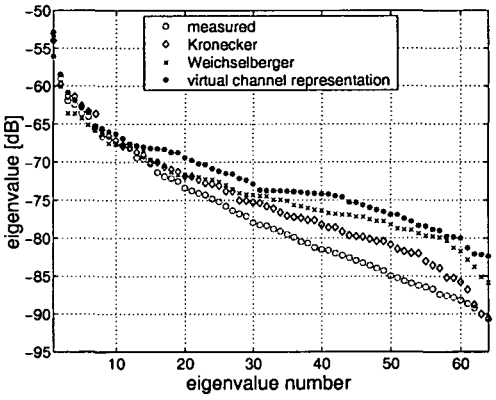

Figure B.2: Eigenvalue Profile of the 8×8 MIMO channel at Rx12D1: $\Psi_{\text{meas}} = 4.0$, $\Psi_{\text{kron}} = 5.8$, $\Psi_{\text{weichsel}} = 4.4$, $\Psi_{\text{virt}} = 10.8$.

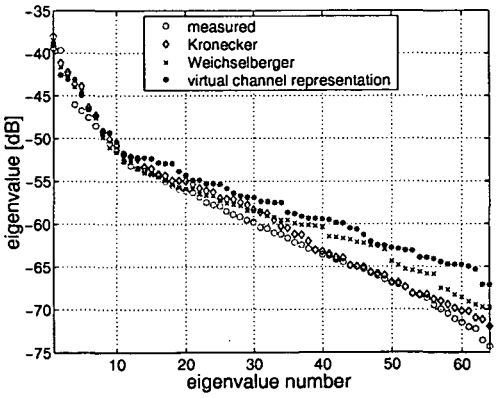

Figure B.3: Eigenvalue Profile of the 8×8 MIMO channel at Rx15D1: $\Psi_{\text{meas}} = 5.8$, $\Psi_{\text{kron}} = 8.6$, $\Psi_{\text{weichsel}} = 7.3$, $\Psi_{\text{virt}} = 9.4$.

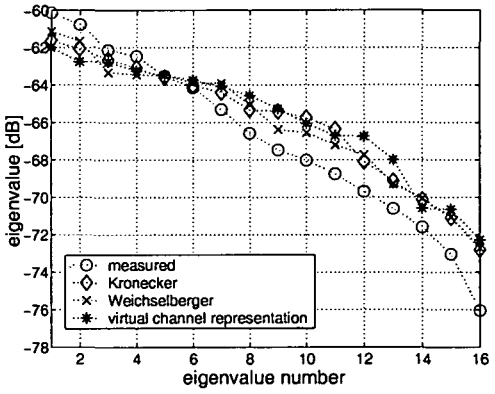

Figure B.4: Eigenvalue Profile of the 4 × 4 MIMO channel at Rx4D2: $\Psi_{\text{meas}} = 9.0$, $\Psi_{\text{kron}} = 11.8$, $\Psi_{\text{weichsel}} = 11.3$, $\Psi_{\text{virt}} = 12.4$.

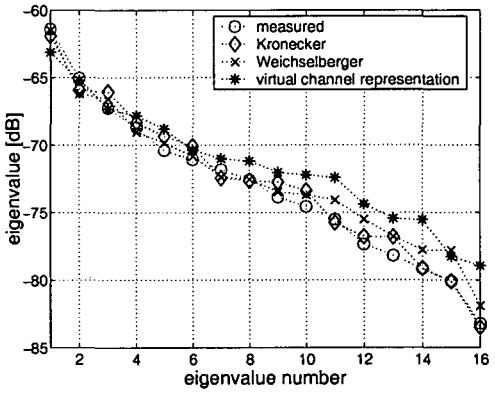

Figure B.5: Eigenvalue Profile of the 4 × 4 MIMO channel at Rx12D1: $\Psi_{\text{meas}} = 4.7$, $\Psi_{\text{kron}} = 5.5$, $\Psi_{\text{weichsel}} = 5.0$, $\Psi_{\text{virt}} = 7.5$.

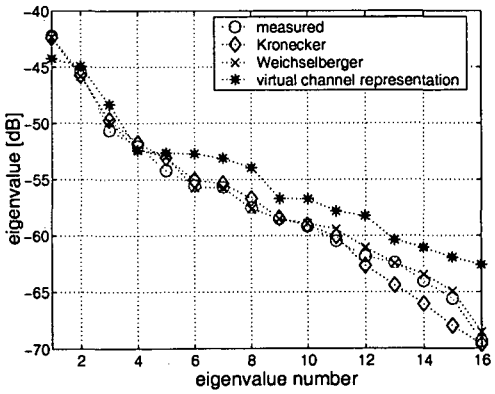

Figure B.6: Eigenvalue Profile of the 4 × 4 MIMO channel at Rx15D1: $\Psi_{\text{meas}} = 3.2$, $\Psi_{\text{kron}} = 3.4$, $\Psi_{\text{weichsel}} = 3.3$, $\Psi_{\text{virt}} = 5.1$.

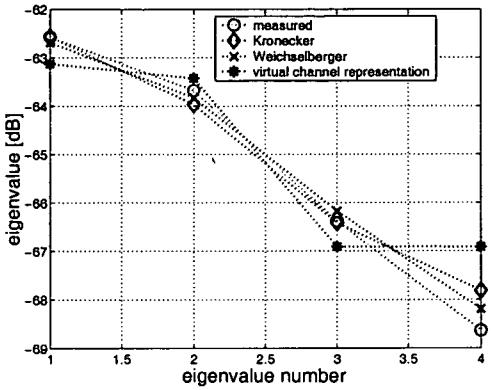

Figure B.7: Eigenvalue Profile of the 2×2 MIMO channel at Rx4D2: $\Psi_{\text{meas}} = 3.2$, $\Psi_{\text{kron}} = 3.3$, $\Psi_{\text{weichsel}} = 3.3$, $\Psi_{\text{virt}} = 3.5$.

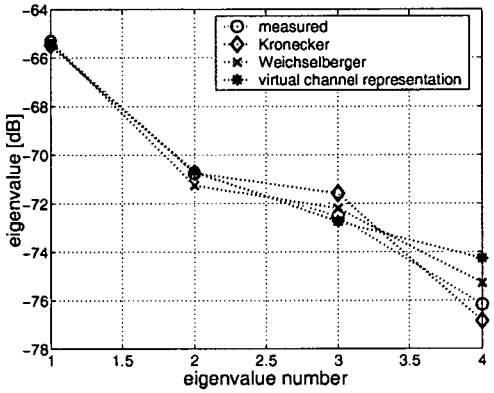

Figure B.8: Eigenvalue Profile of the 2 × 2 MIMO channel at Rx12D1: $\Psi_{\text{meas}} = 2.2$, $\Psi_{\text{kron}} = 2.3$, $\Psi_{\text{weichsel}} = 2.2$, $\Psi_{\text{virt}} = 2.3$.

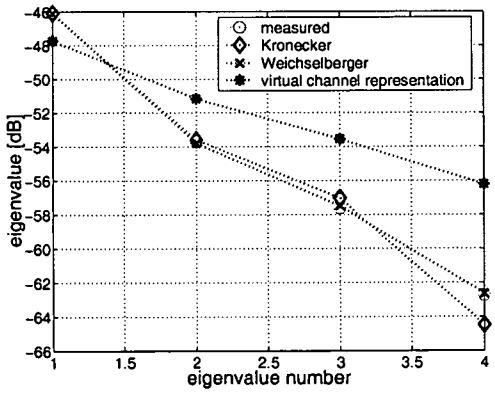

Figure B.9: Eigenvalue Profile of the 2 × 2 MIMO channel at Rx15D1: $\Psi_{\text{meas}} = 1.5$, $\Psi_{\text{kron}} = 1.6$, $\Psi_{\text{weichsel}} = 1.5$, $\Psi_{\text{virt}} = 2.7$.

Appendix C

Joint DoD-DoA Capon spectra

In this appendix the joint DoD-DoA Capon spectra of 8×8, 4×4 and 2×2 MIMO channels are shown for 58 Rayleigh-fading scenarios of the 5.2GHz measurement campaign at our Institute. To recap, the complete floor plan of the measurement campaign is again plotted in Fig. C.1.

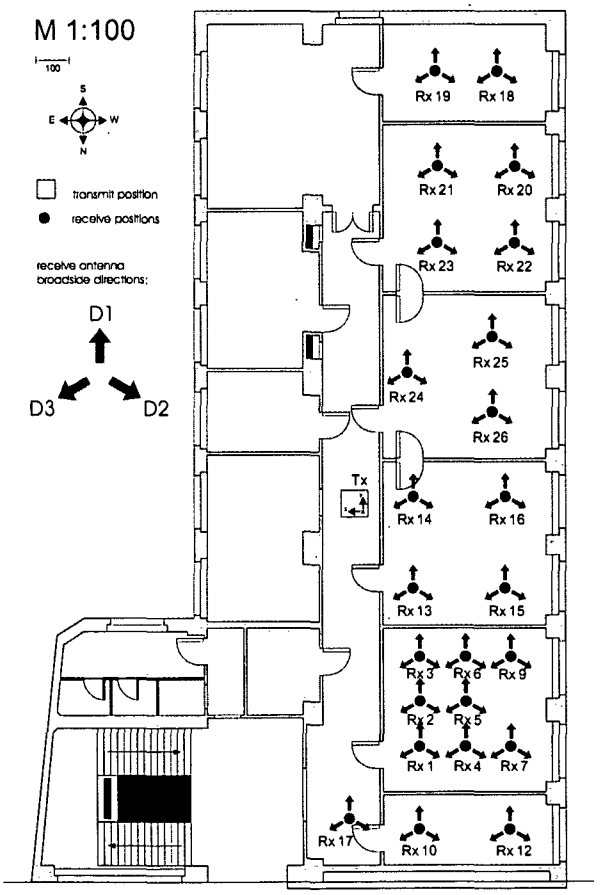

Figure C.1: Floor plan of the 5.2GHz measurement campaign. In total, 72 different scenarios, i.e. Rx positions and directions, were measured.

The arrangement of the individual sub-plots for each scenario is as follows. The upper right plot shows the marginal DoD spectrum, the left plot shows the marginal DoA spectrum. What follows from the top to the bottom are the joint DoD-DoA spectra of the measured channel, the Kronecker model, the Weichselberger model and the virtual channel representation. The color-bar scales dB values with red color indicating high power and blue color corresponding to low power. The DoD is plotted in the range from $-90°$ to $+90°$, whereas the DoA is in the range from $-60°$ to $+60°$

C.1 Capon spectra for 8×8 MIMO systems

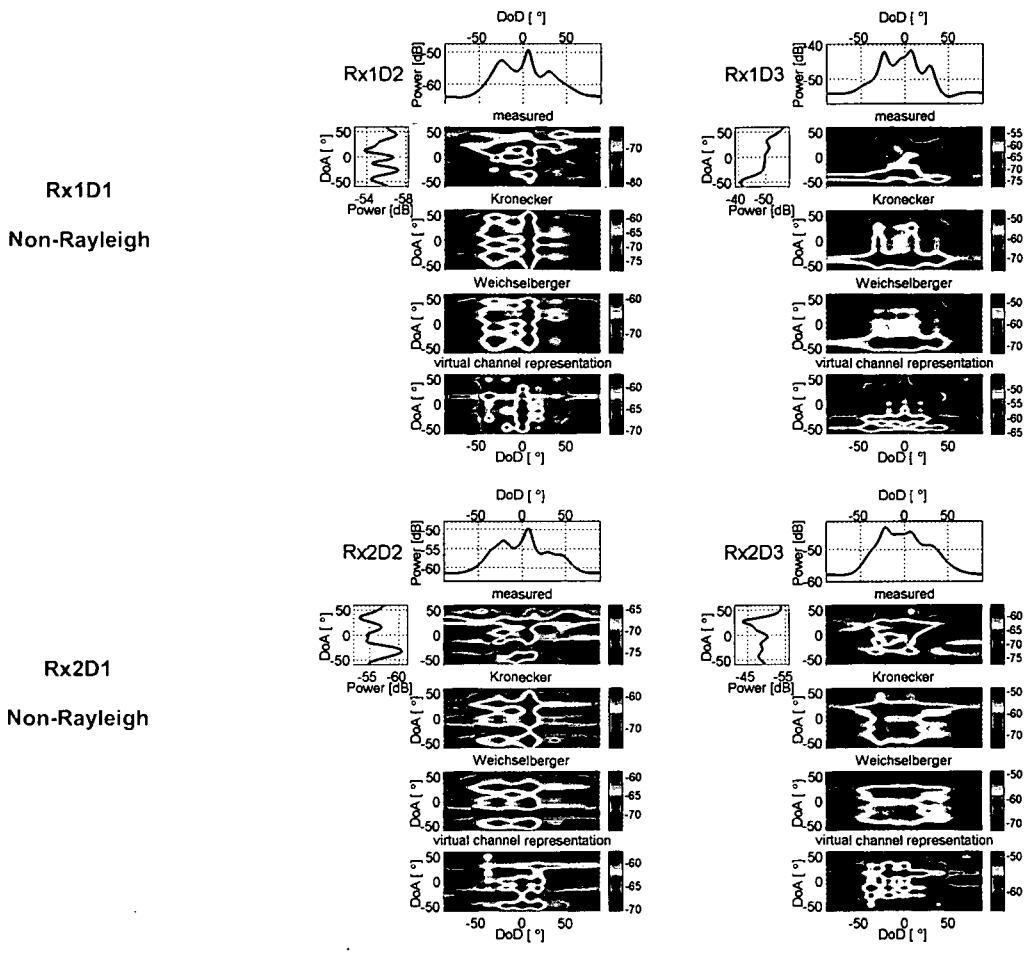

Figure C.2: Joint 8×8 DoD-DoA Capon spectra.

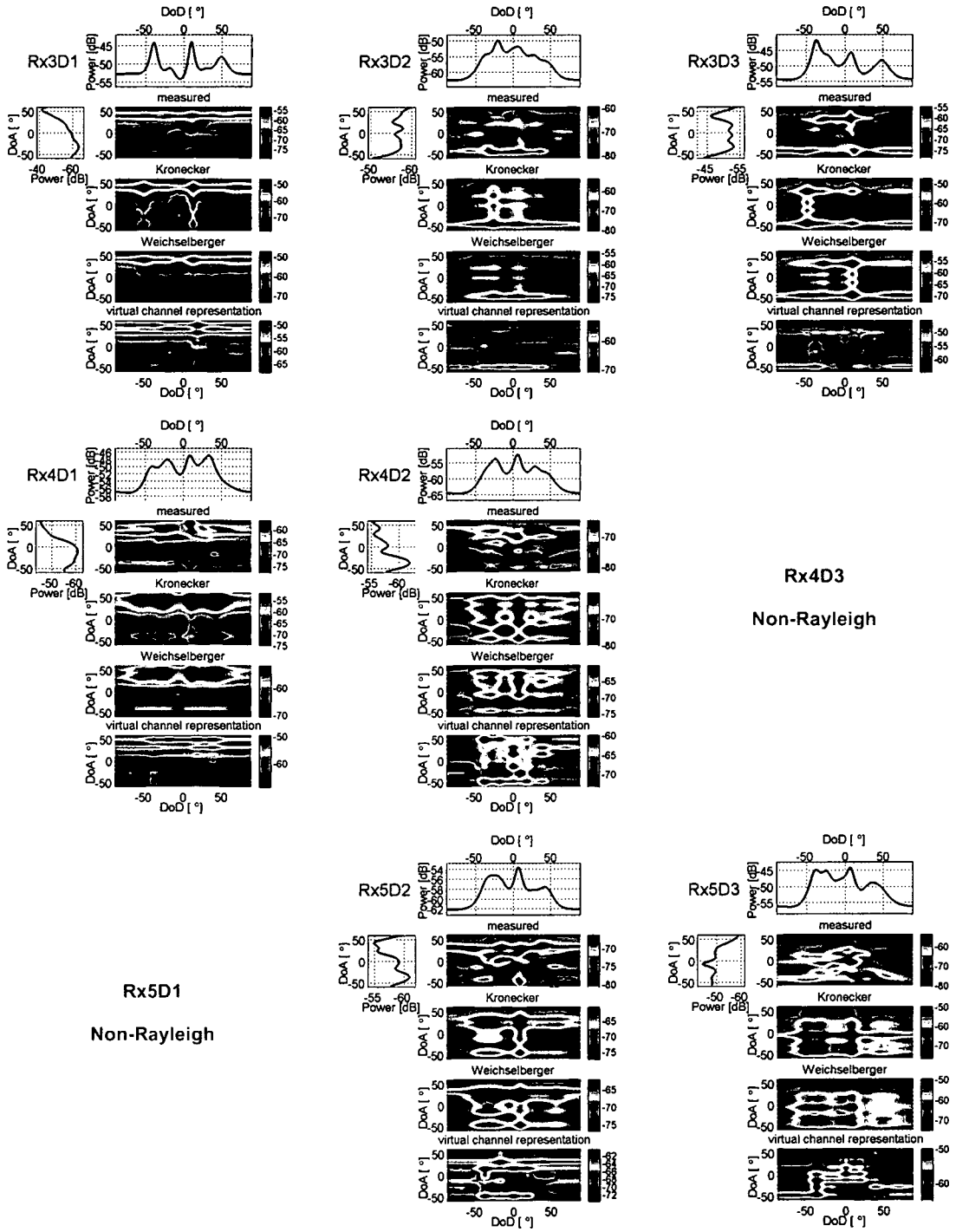

Figure C.3: Joint 8 × 8 DoD-DoA Capon spectra (cont'd).

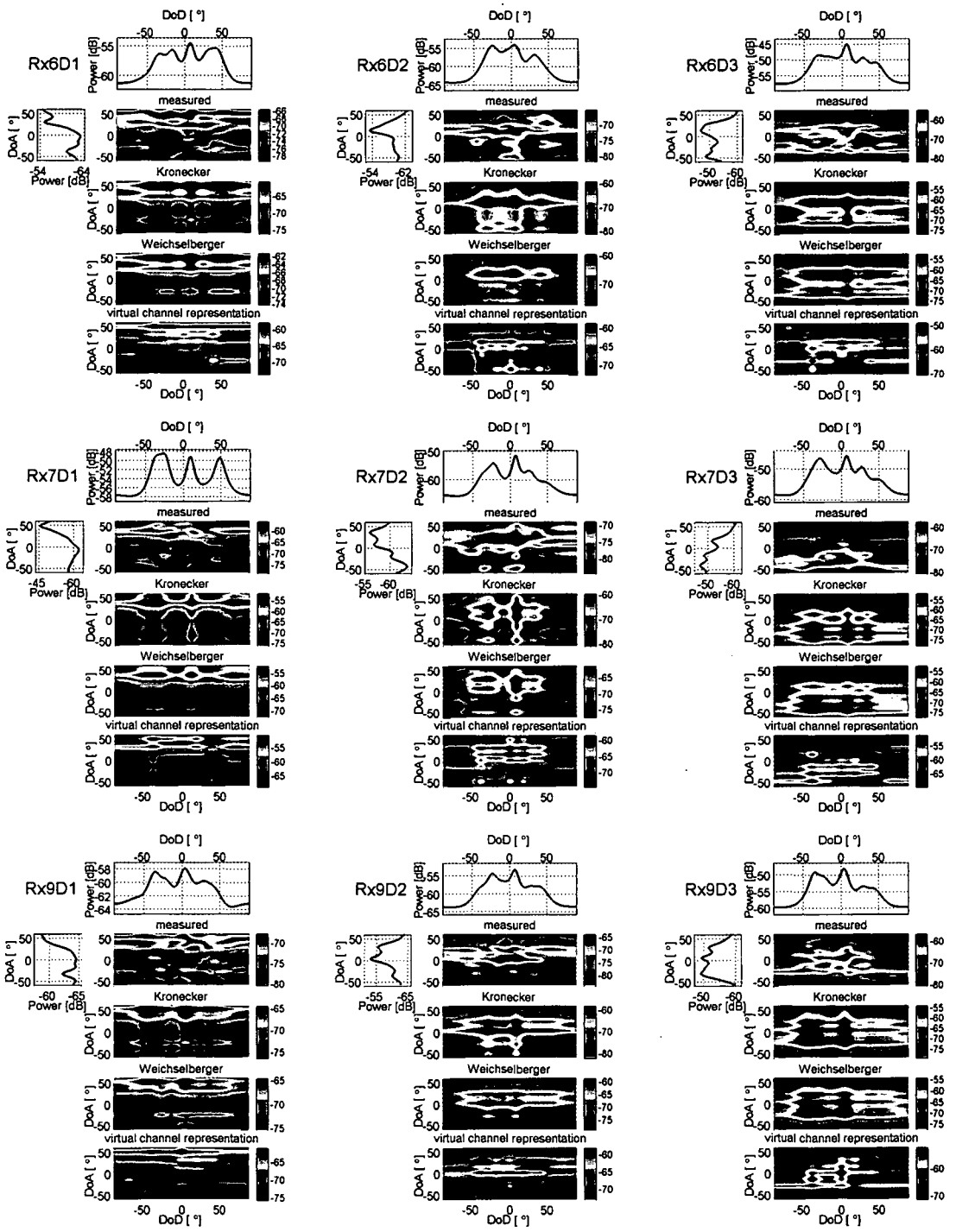

Figure C.4: Joint 8 × 8 DoD-DoA Capon spectra (cont'd).

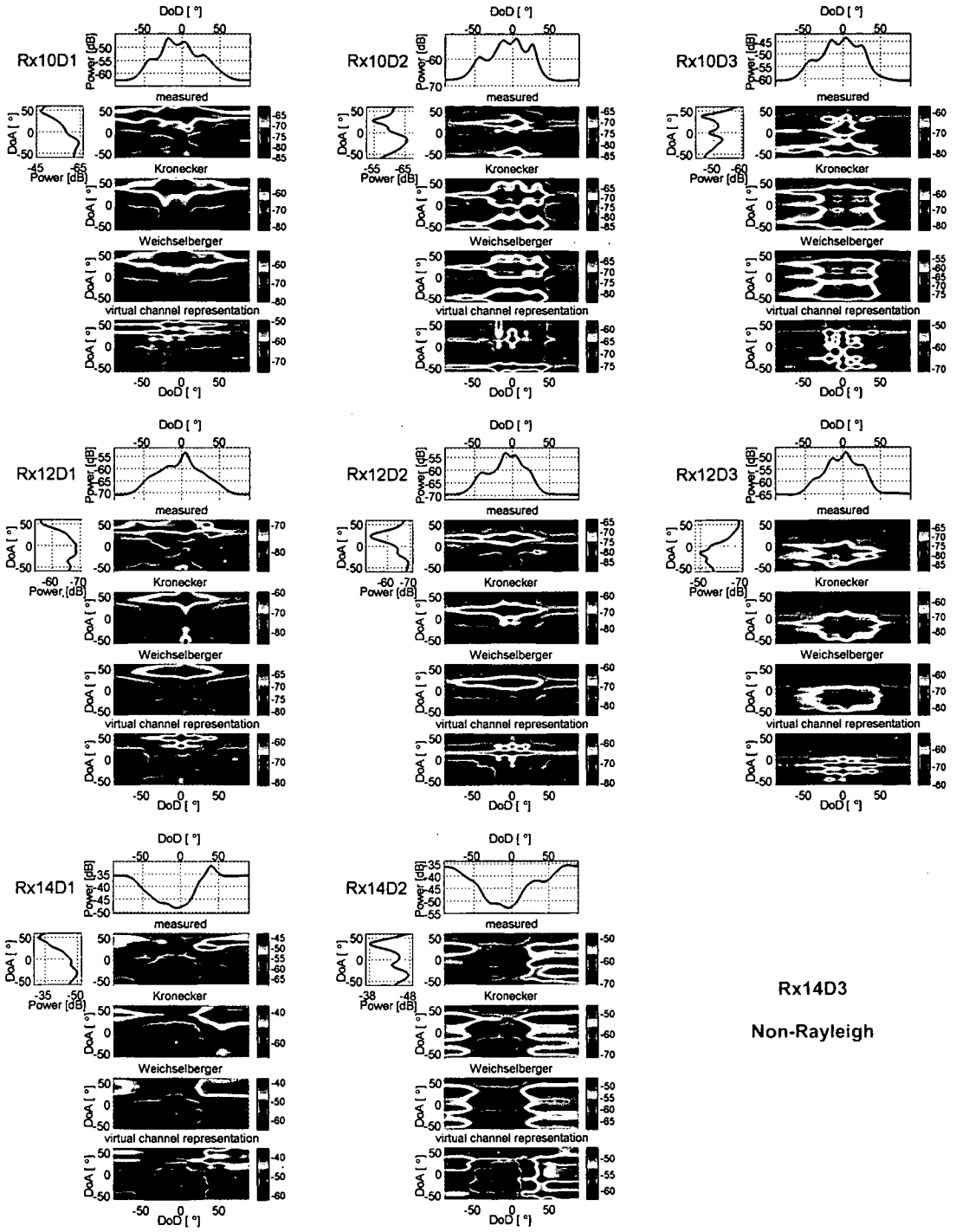

Figure C.5: Joint 8 × 8 DoD-DoA Capon spectra (cont'd).

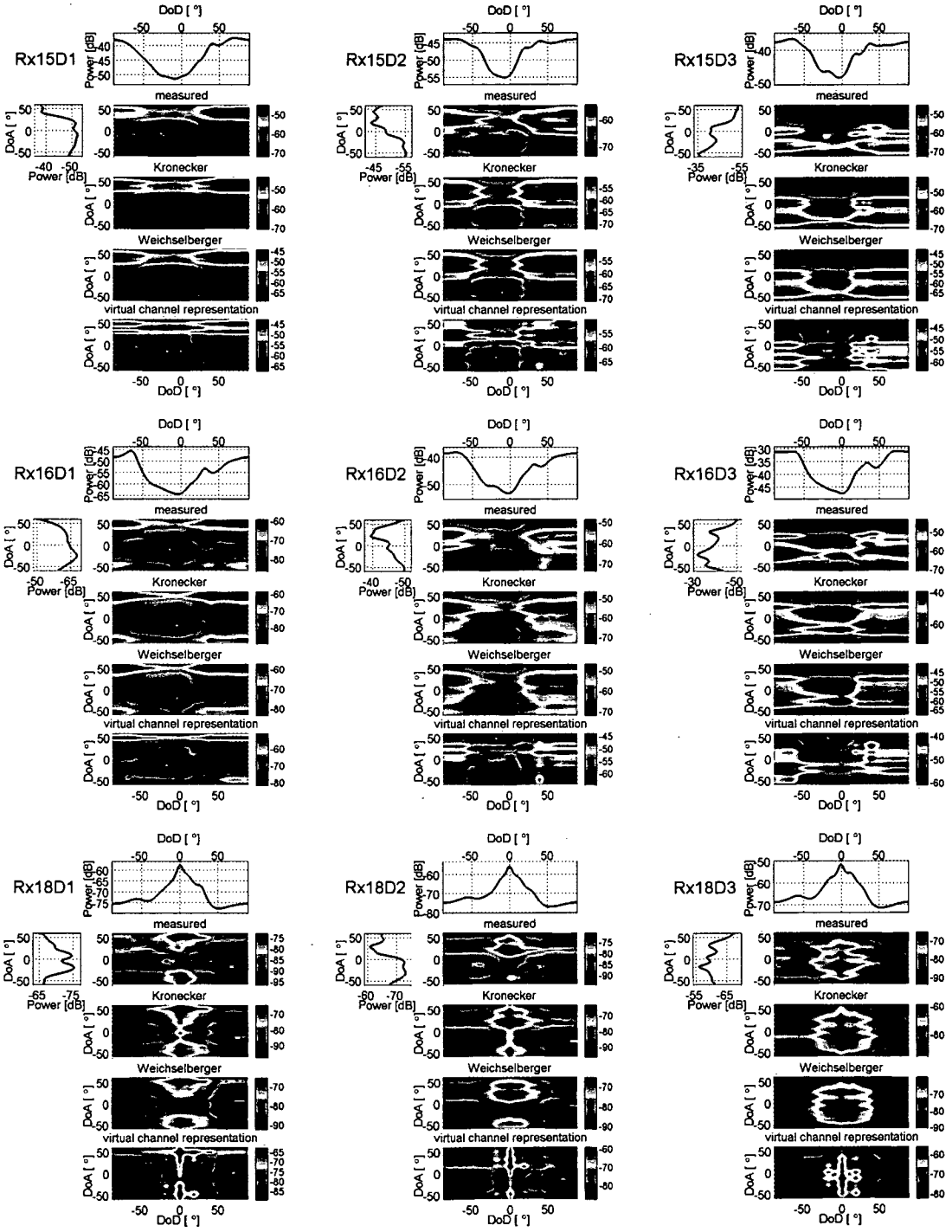

Figure C.6: Joint 8 × 8 DoD-DoA Capon spectra (cont'd).

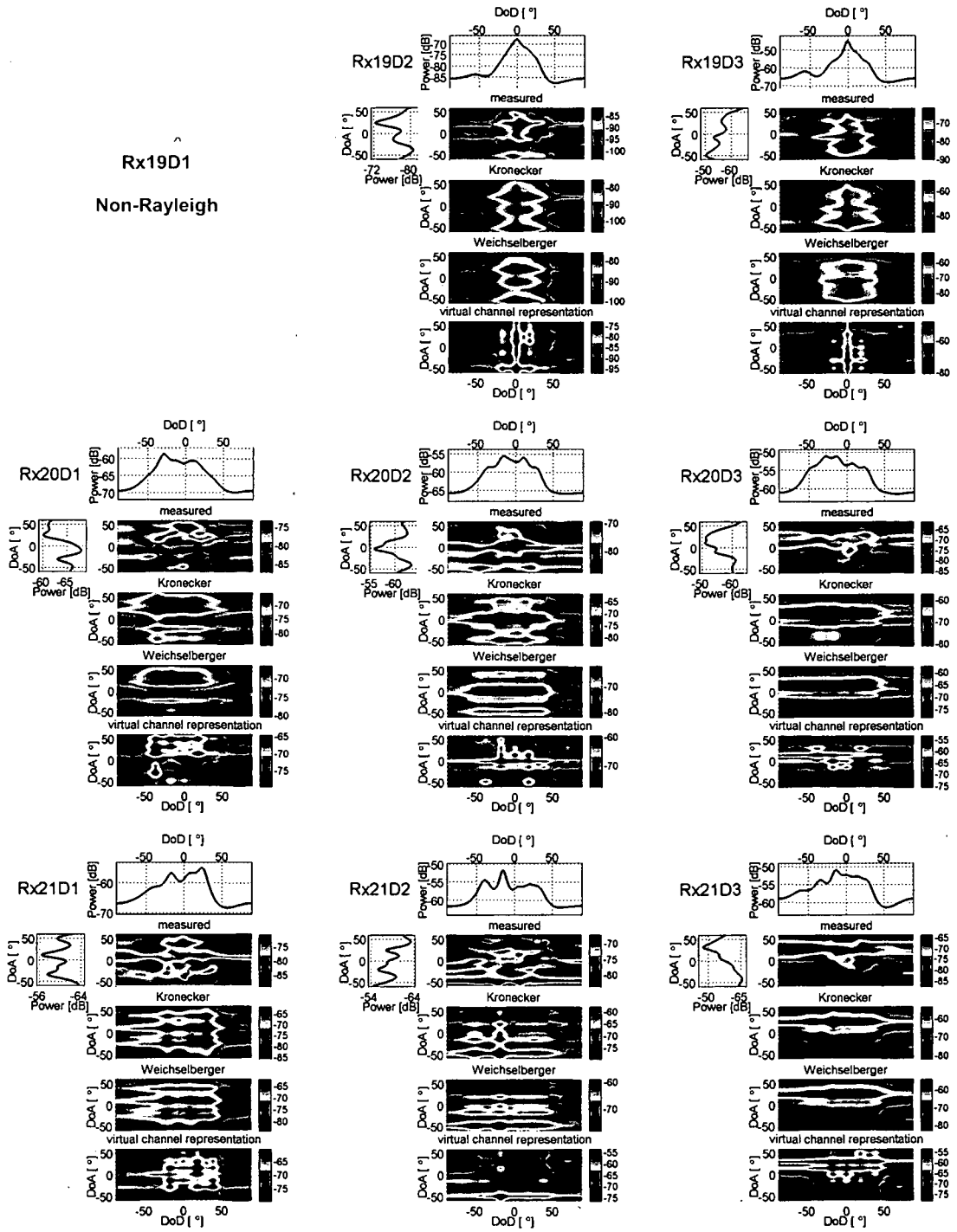

Figure C.7: Joint 8 × 8 DoD-DoA Capon spectra (cont'd).

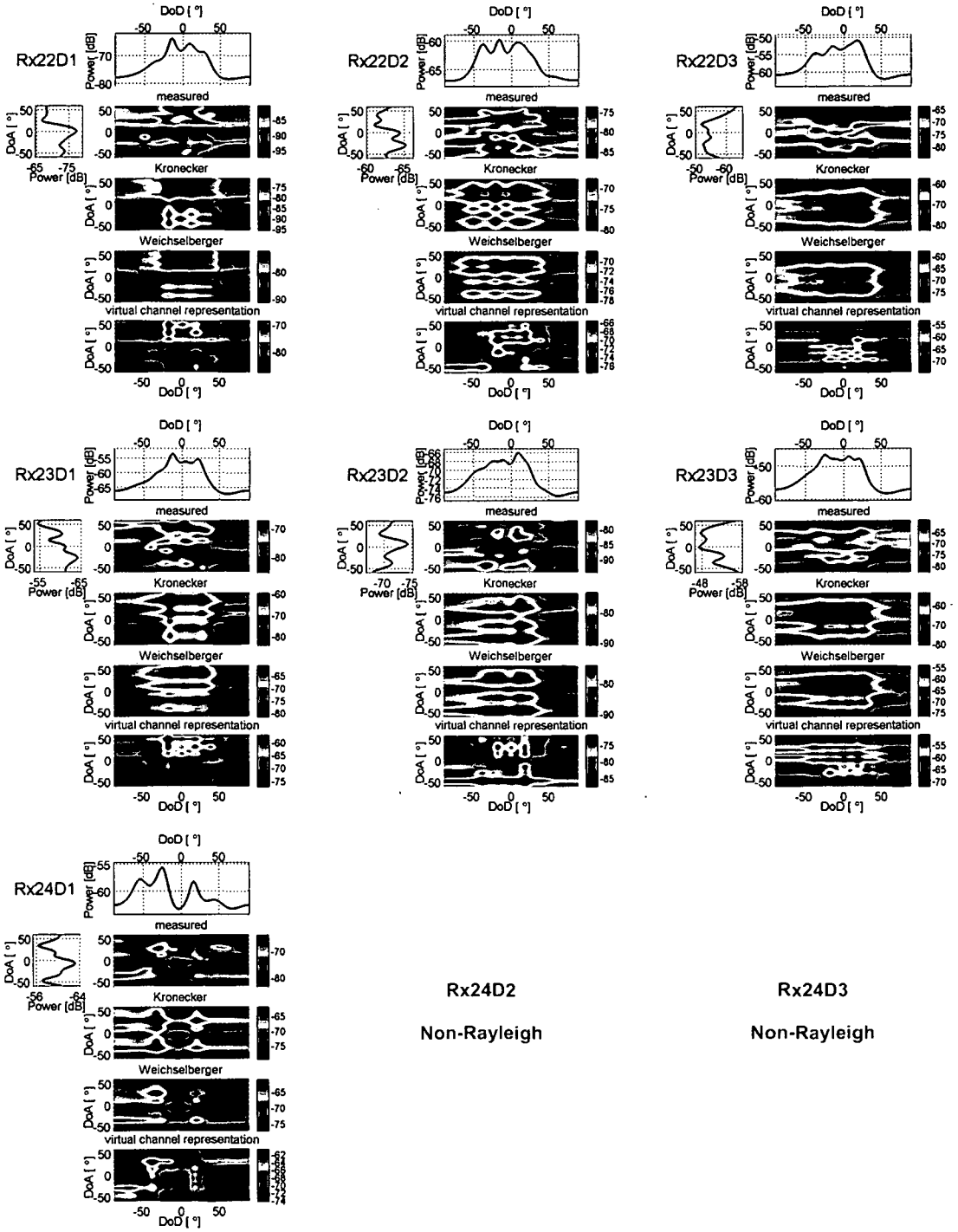

Figure C.8: Joint 8 × 8 DoD-DoA Capon spectra (cont'd).

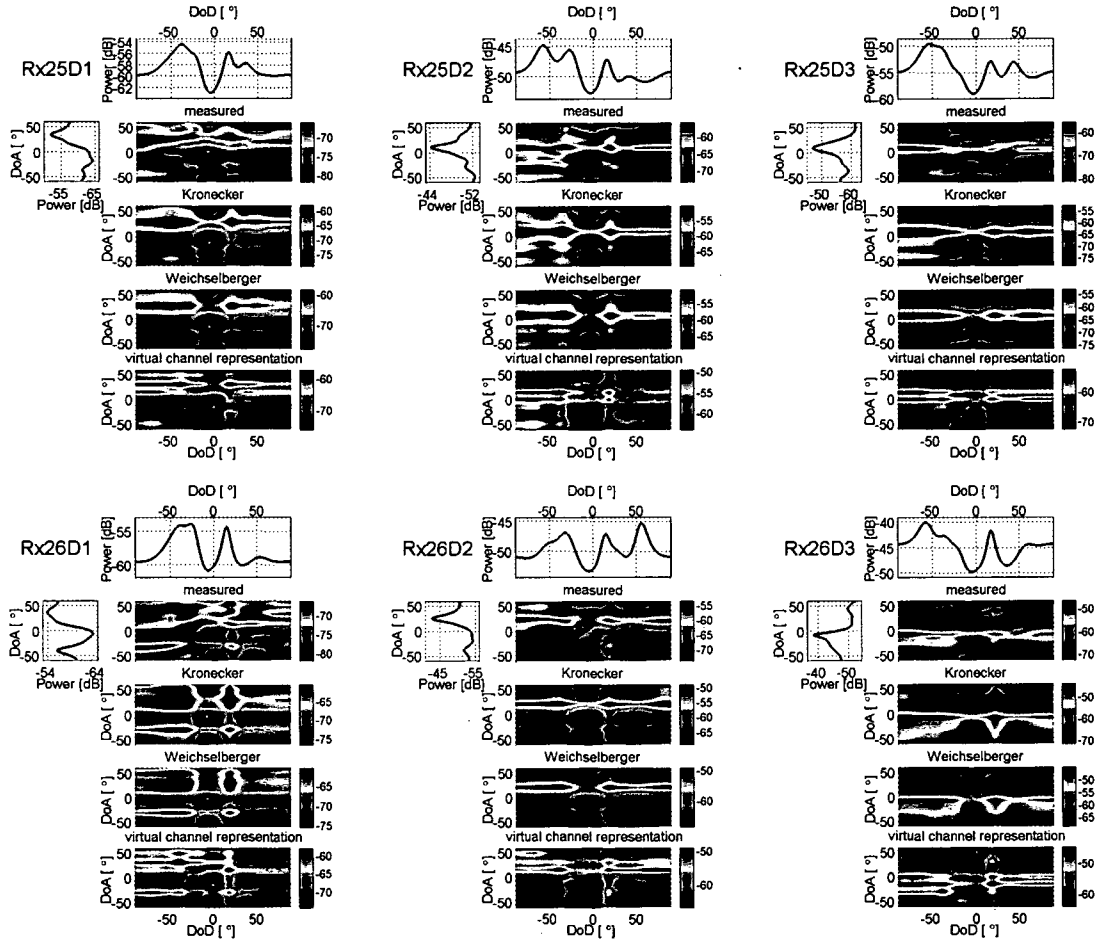

Figure C.9: Joint 8 × 8 DoD-DoA Capon spectra (cont'd).

C.2 Capon spectra for 4×4 MIMO systems

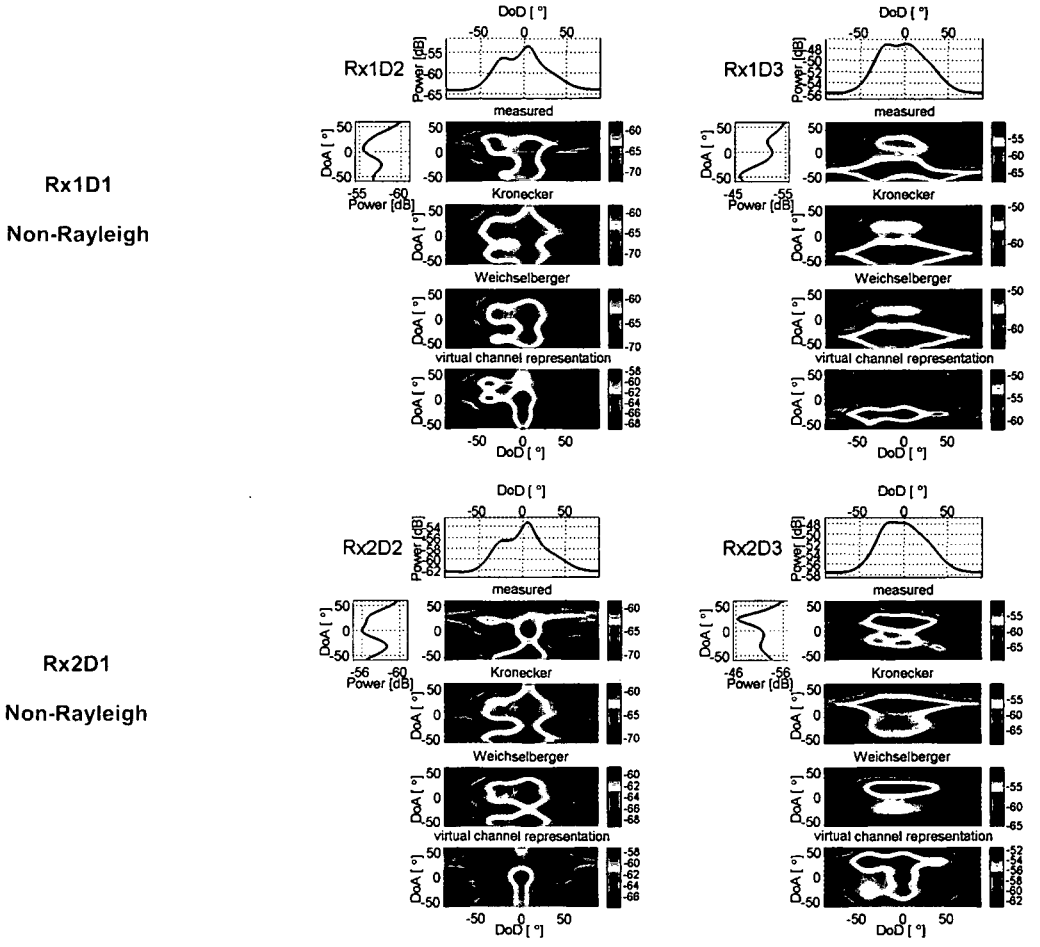

Figure C.10: Joint 4×4 DoD-DoA Capon spectra.

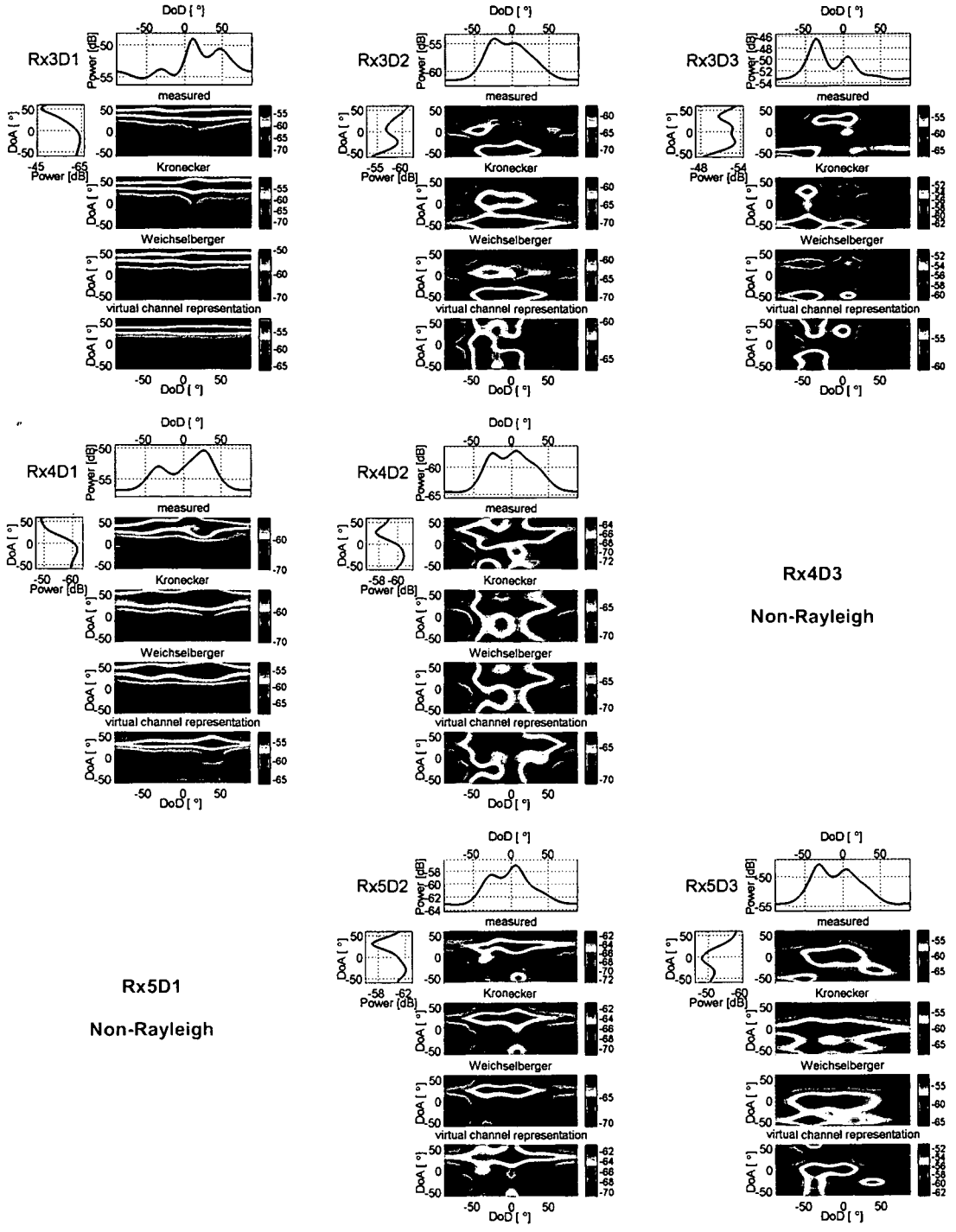

Figure C.11: Joint 4 × 4 DoD-DoA Capon spectra (cont'd).

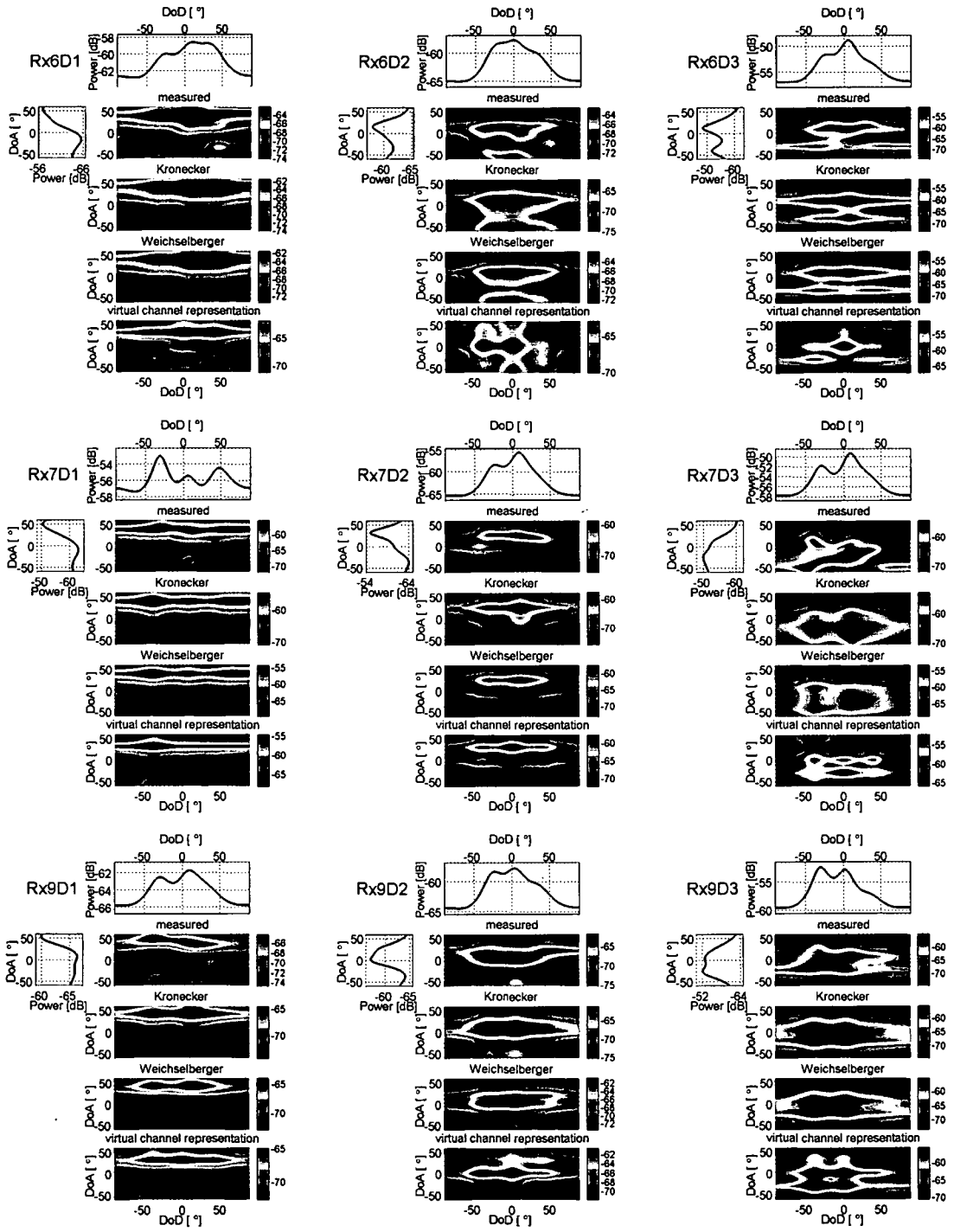

Figure C.12: Joint 4 × 4 DoD-DoA Capon spectra (cont'd).

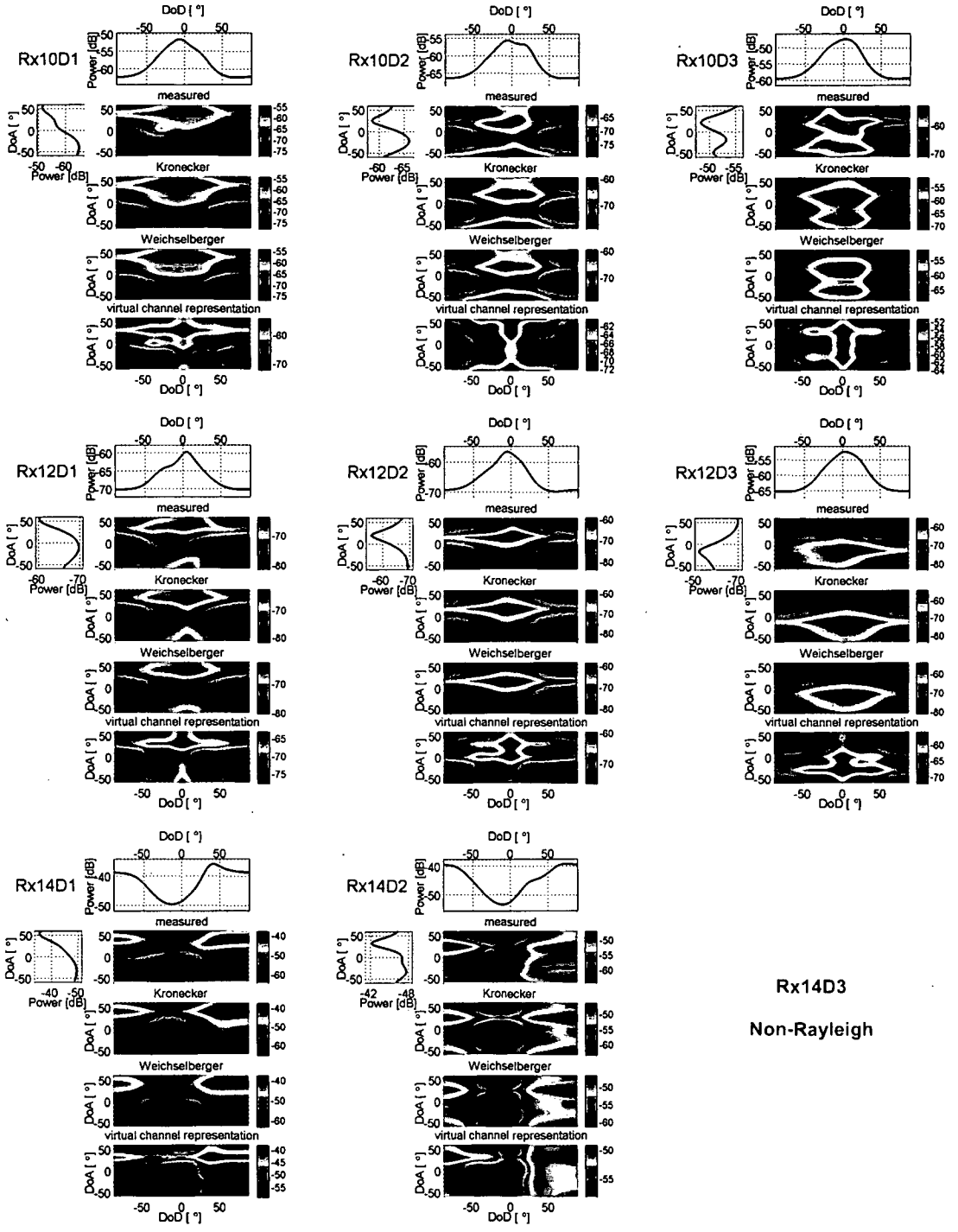

Figure C.13: Joint 4 × 4 DoD-DoA Capon spectra (cont'd).

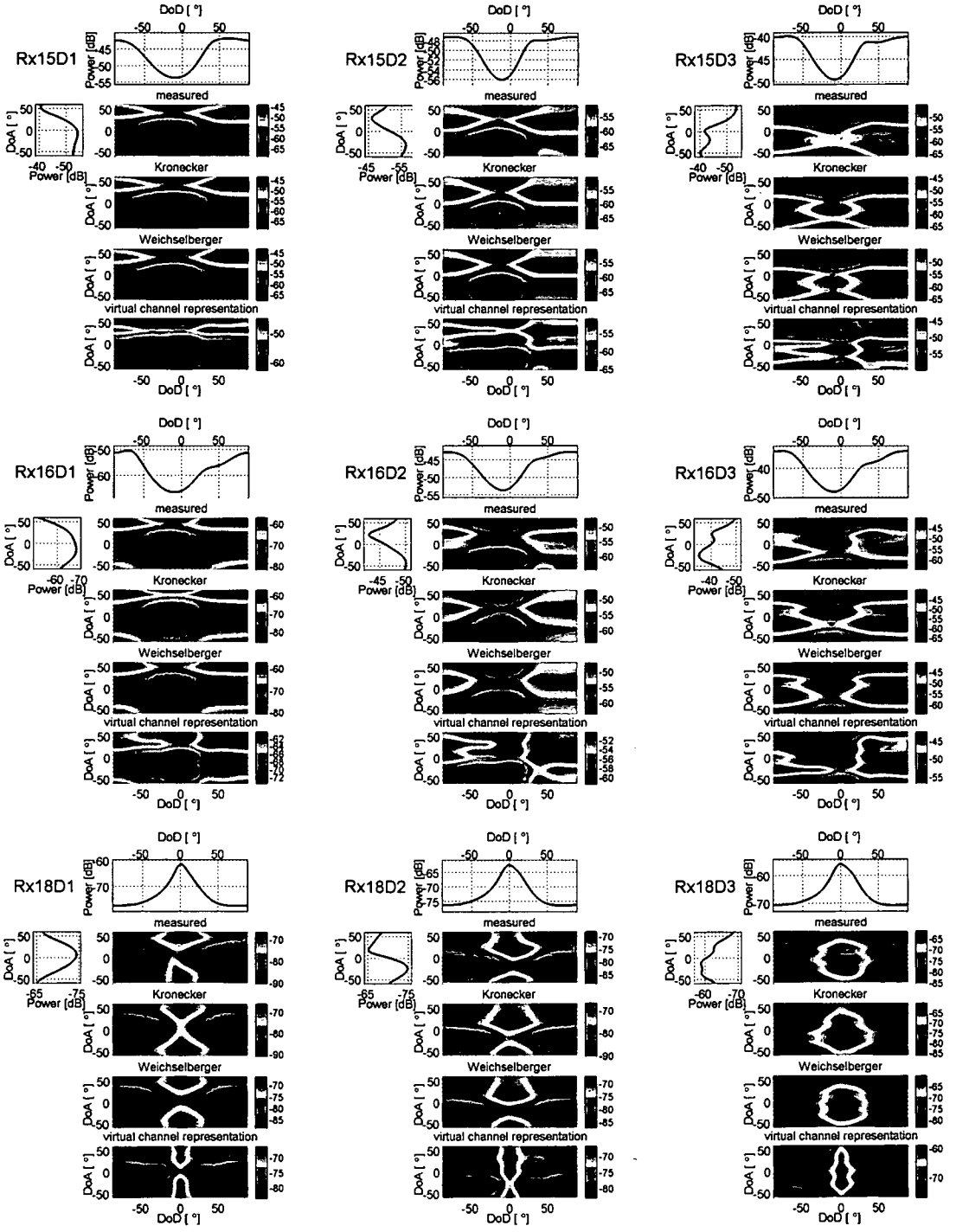

Figure C.14: Joint 4 × 4 DoD-DoA Capon spectra (cont'd).

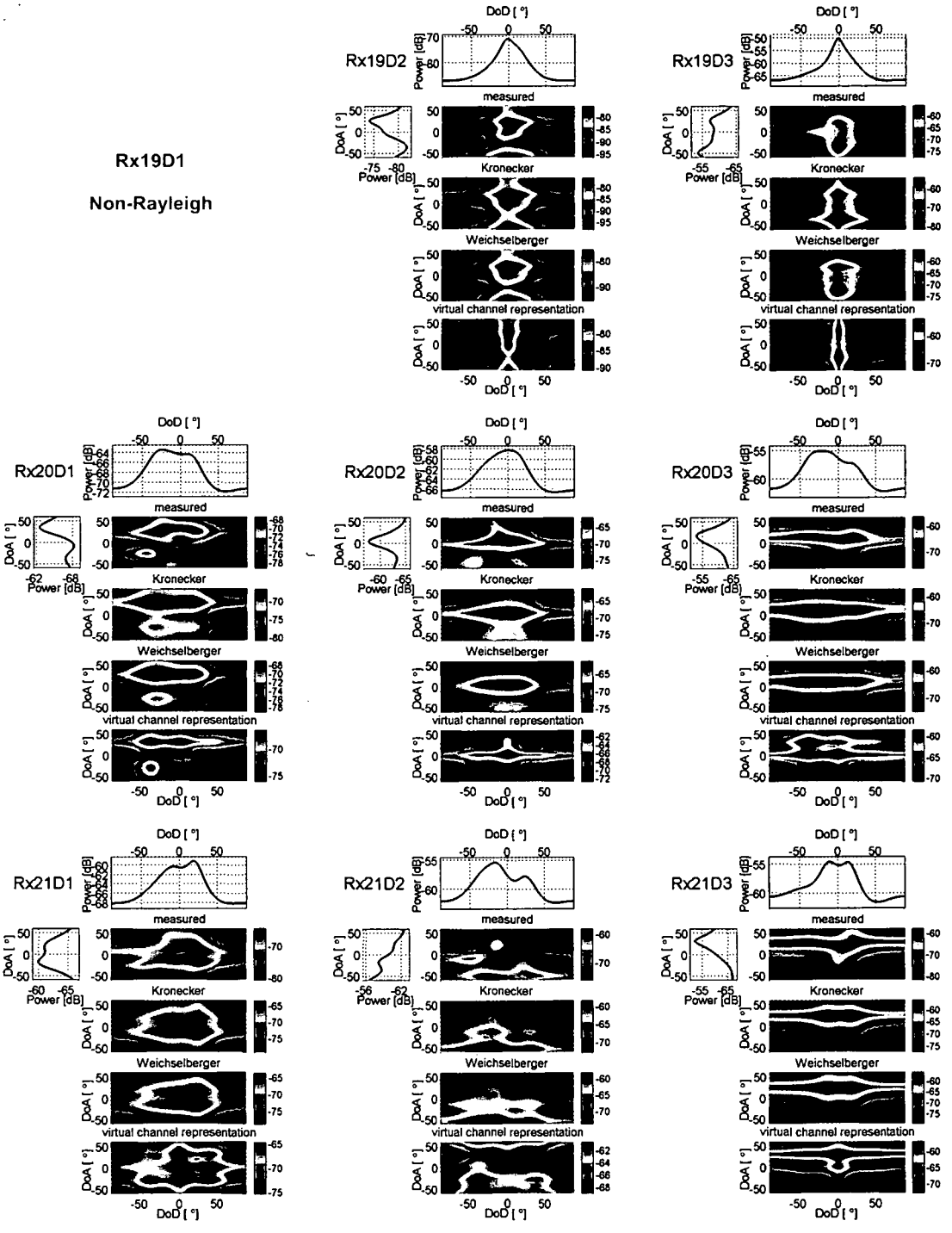

Figure C.15: Joint 4 × 4 DoD-DoA Capon spectra (cont'd).

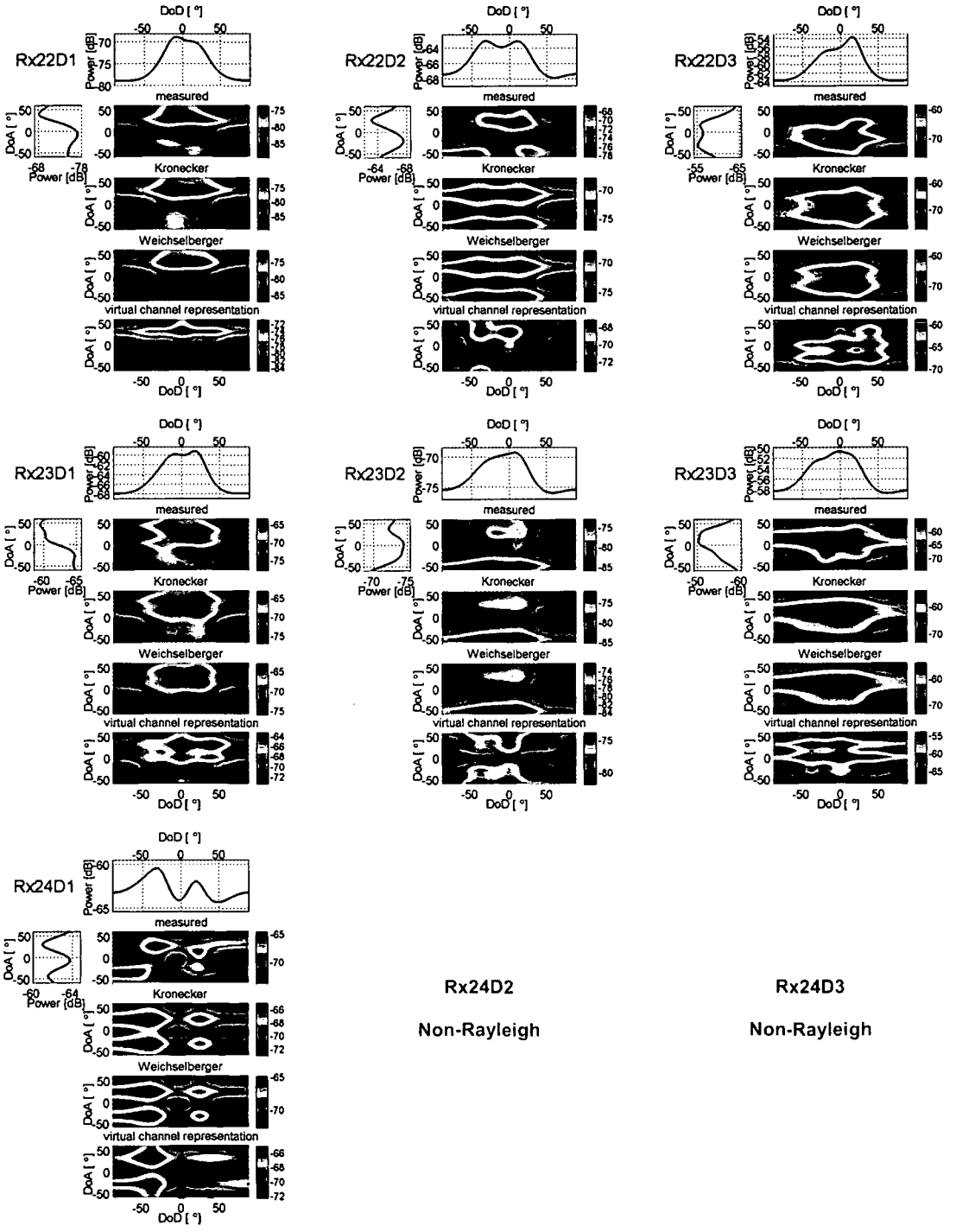

Figure C.16: Joint 4 × 4 DoD-DoA Capon spectra (cont'd).

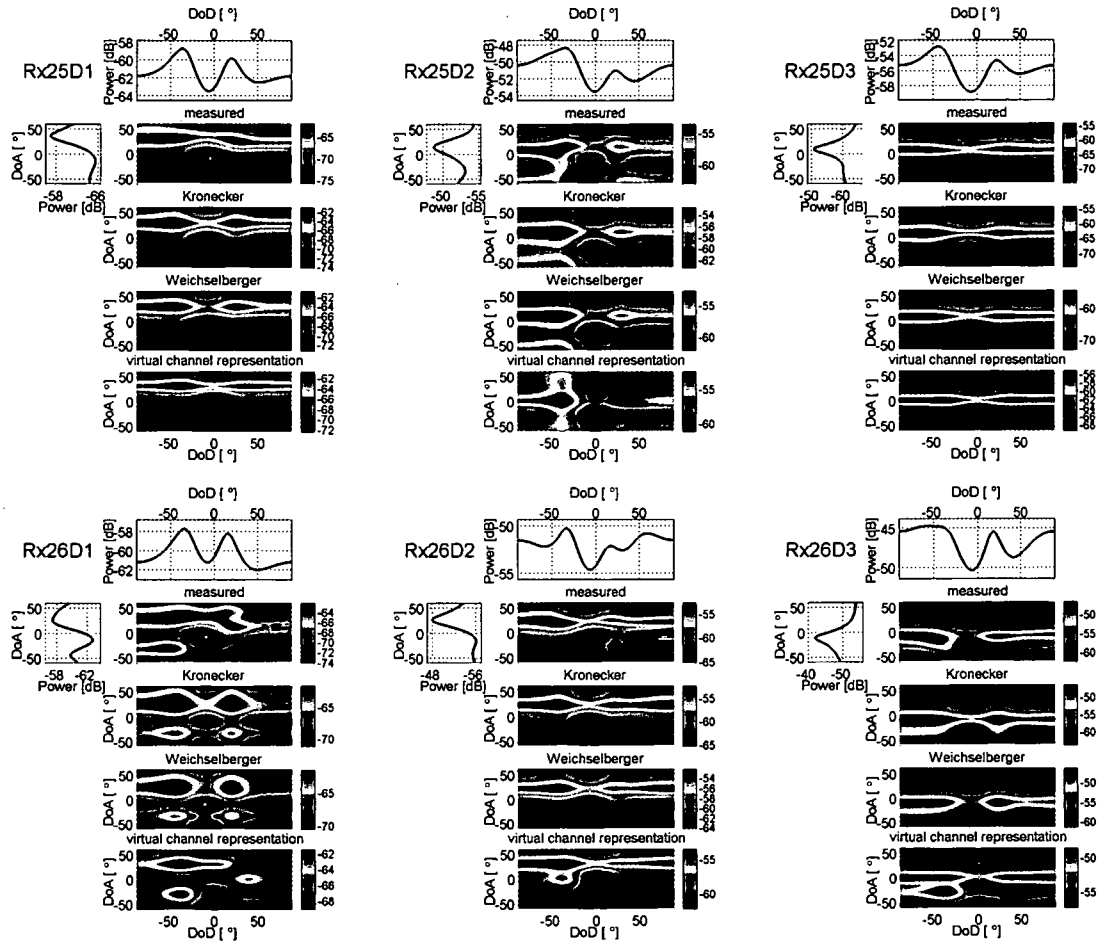

Figure C.17: Joint 4 × 4 DoD-DoA Capon spectra (cont'd).

C.3 Capon spectra for 2×2 MIMO systems

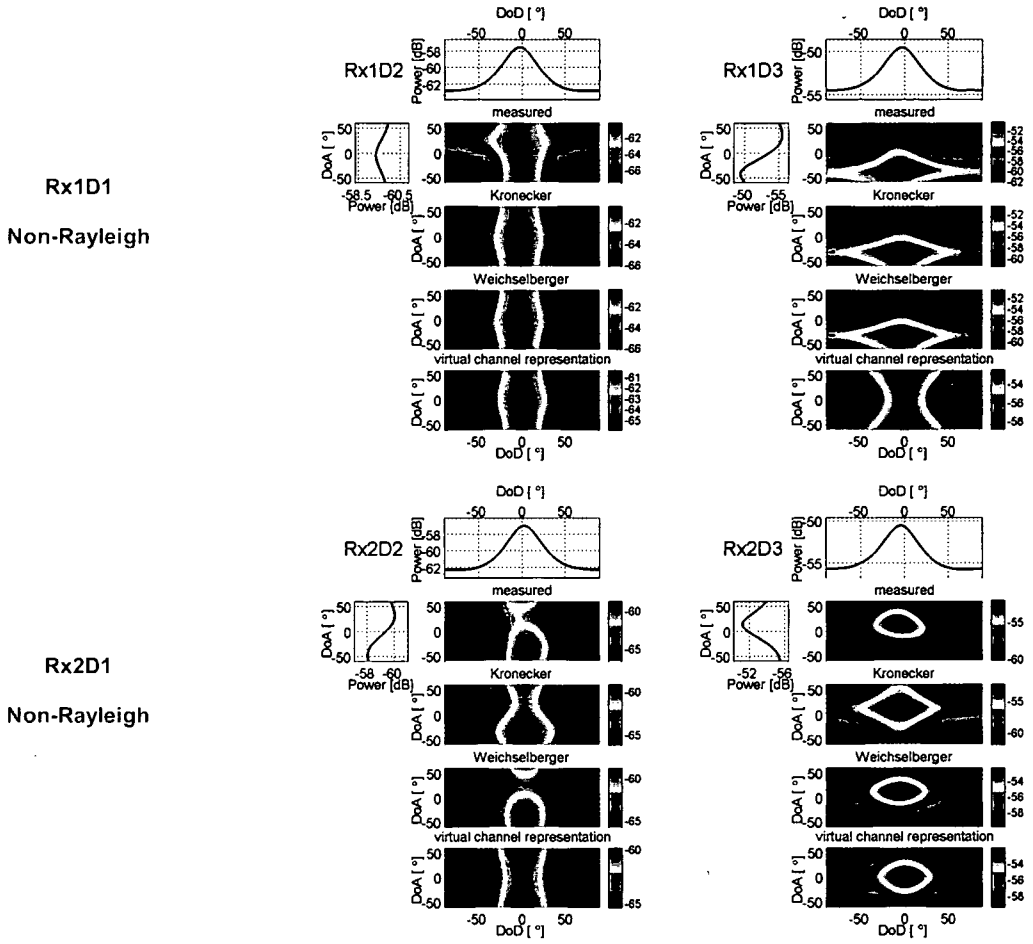

Figure C.18: Joint 2×2 DoD-DoA Capon spectra.

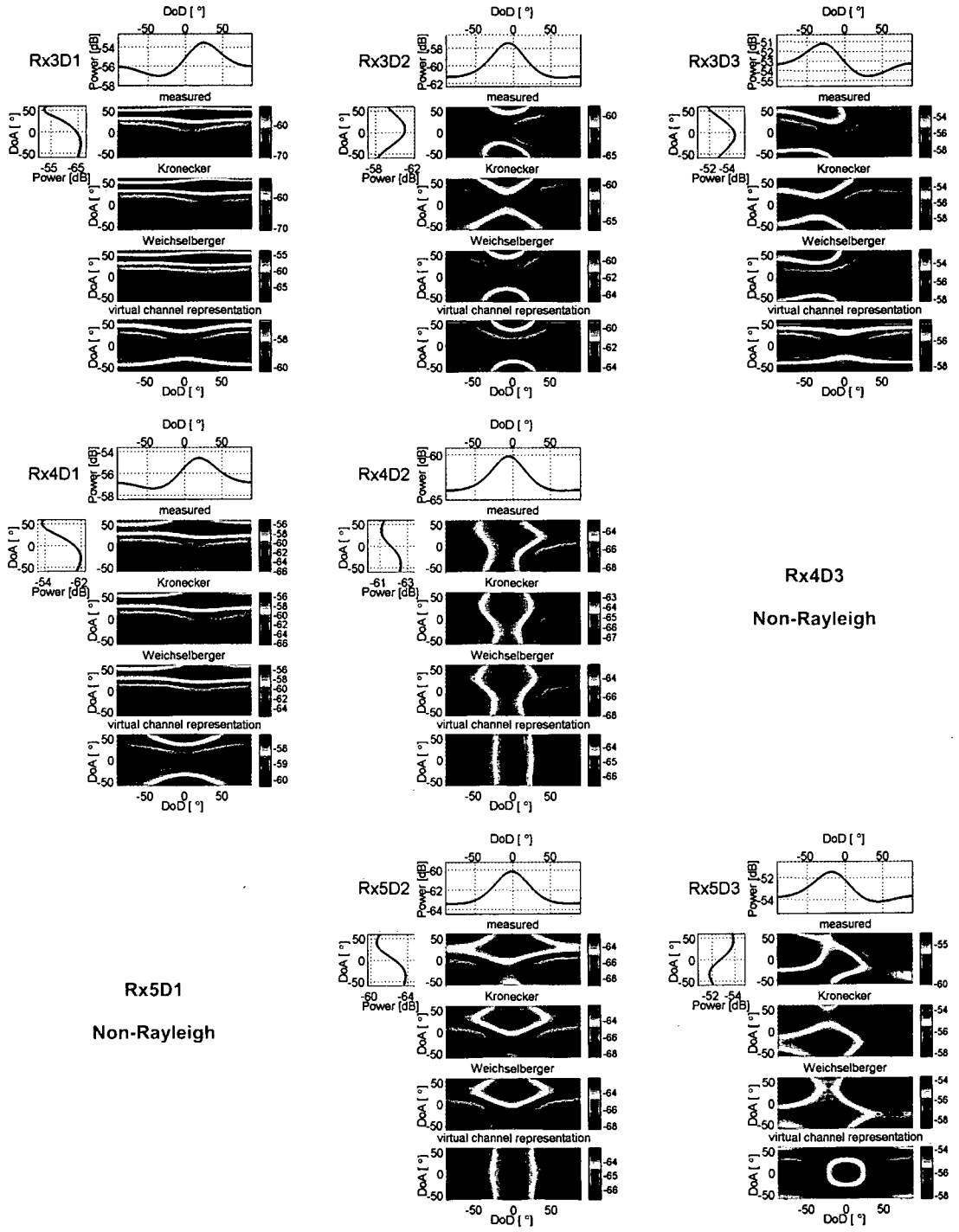

Figure C.19: Joint 2 × 2 DoD-DoA Capon spectra (cont'd).

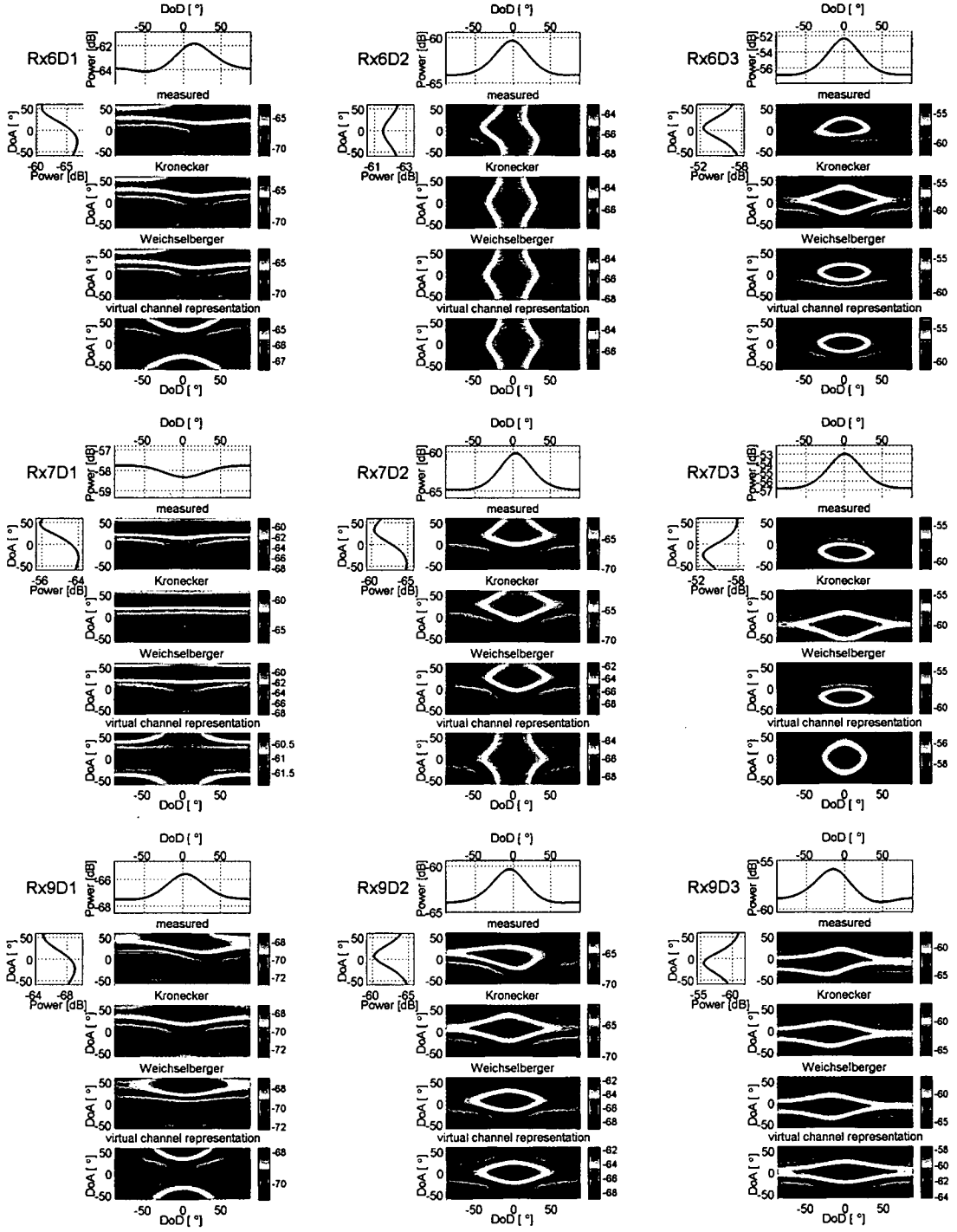

Figure C.20: Joint 2 × 2 DoD-DoA Capon spectra (cont'd).

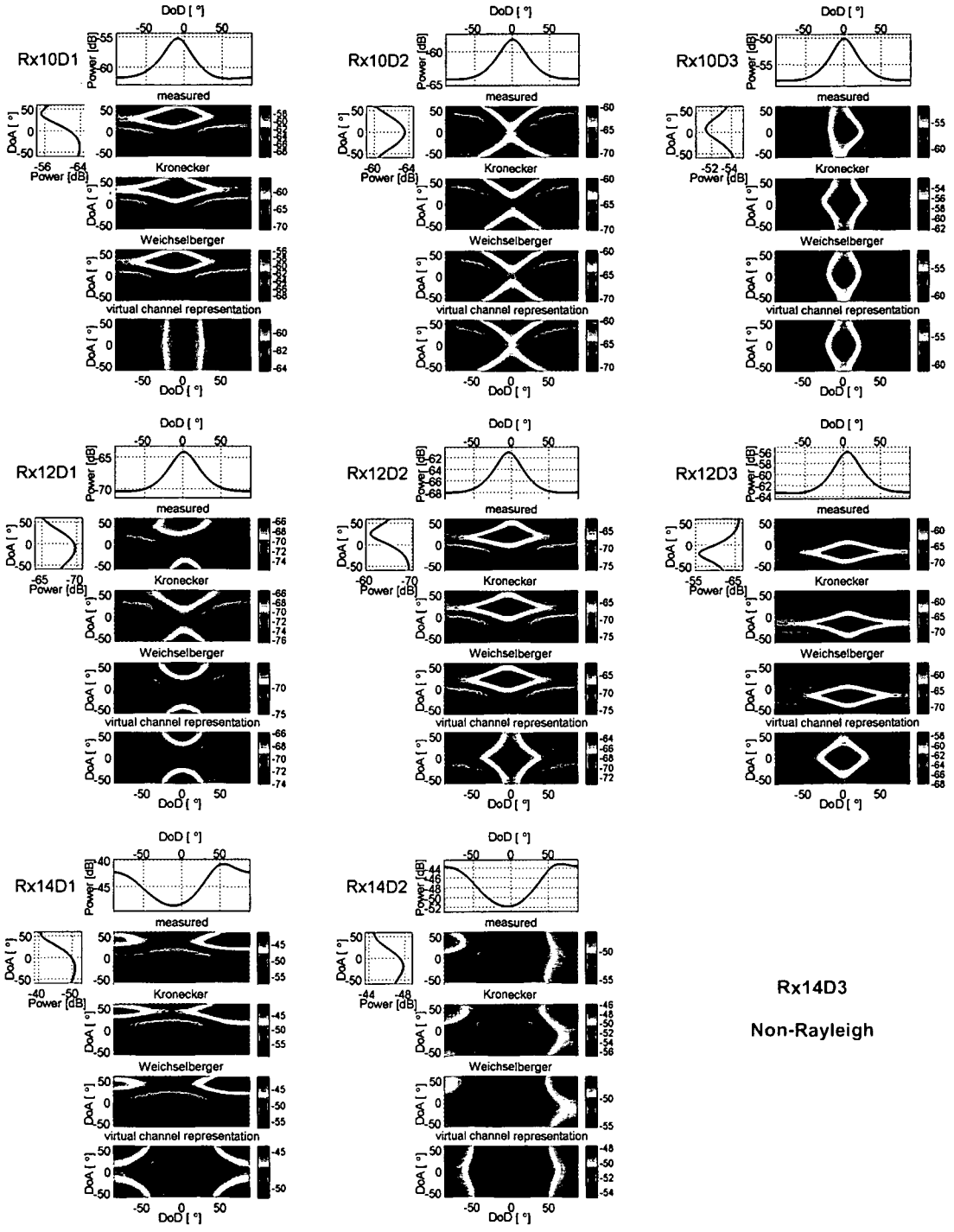

Figure C.21: Joint 2 × 2 DoD-DoA Capon spectra (cont'd).

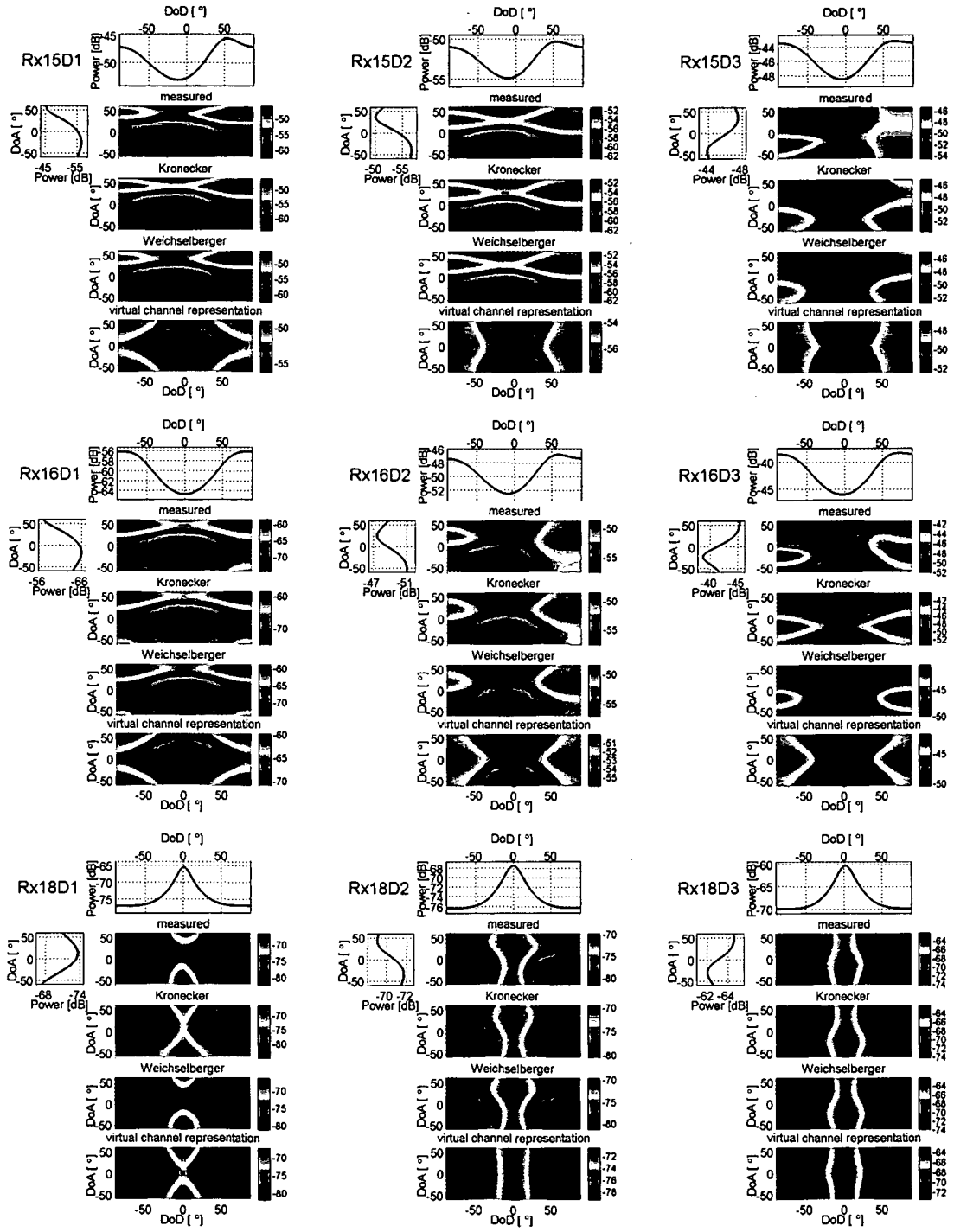

Figure C.22: Joint 2 × 2 DoD-DoA Capon spectra (cont'd).

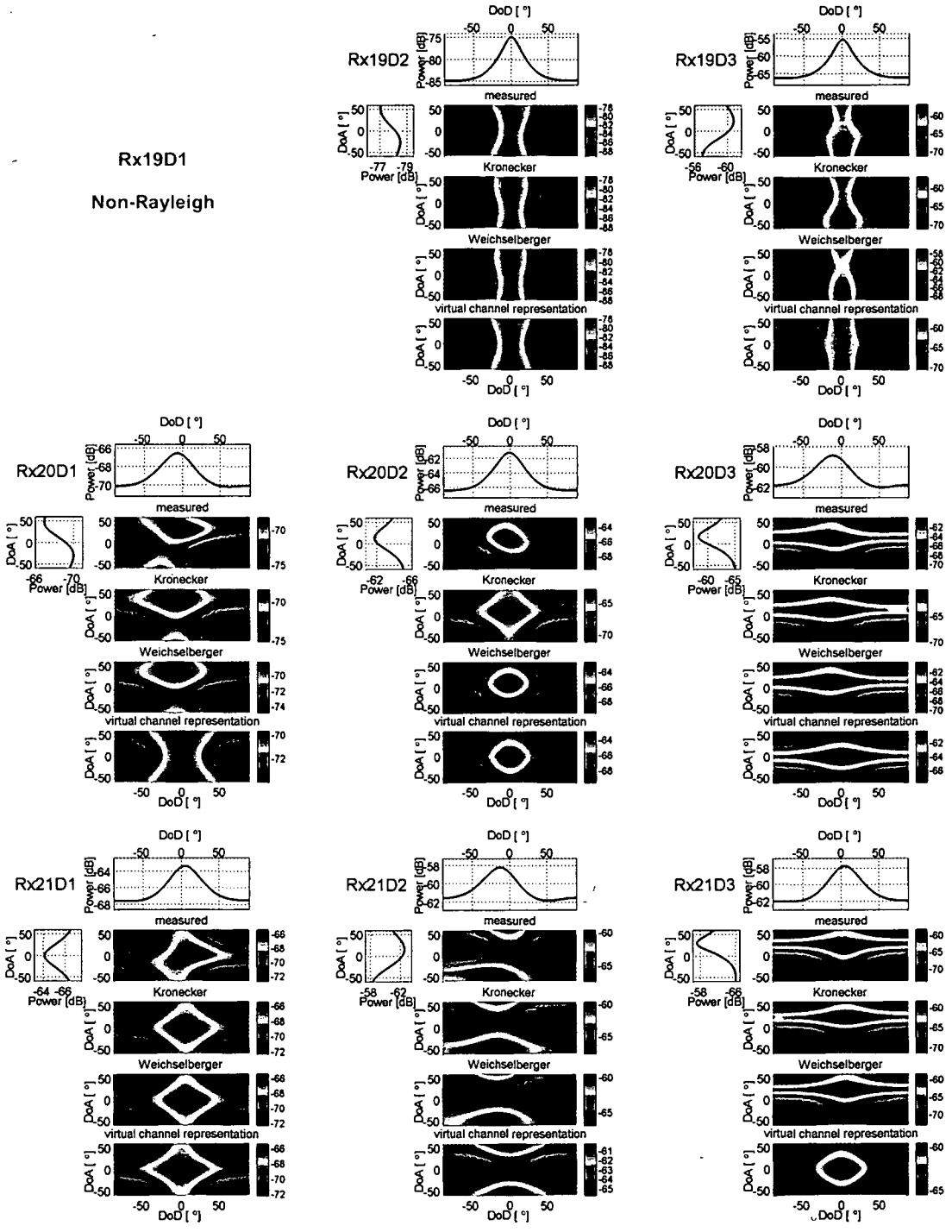

Figure C.23: Joint 2 × 2 DoD-DoA Capon spectra (cont'd).

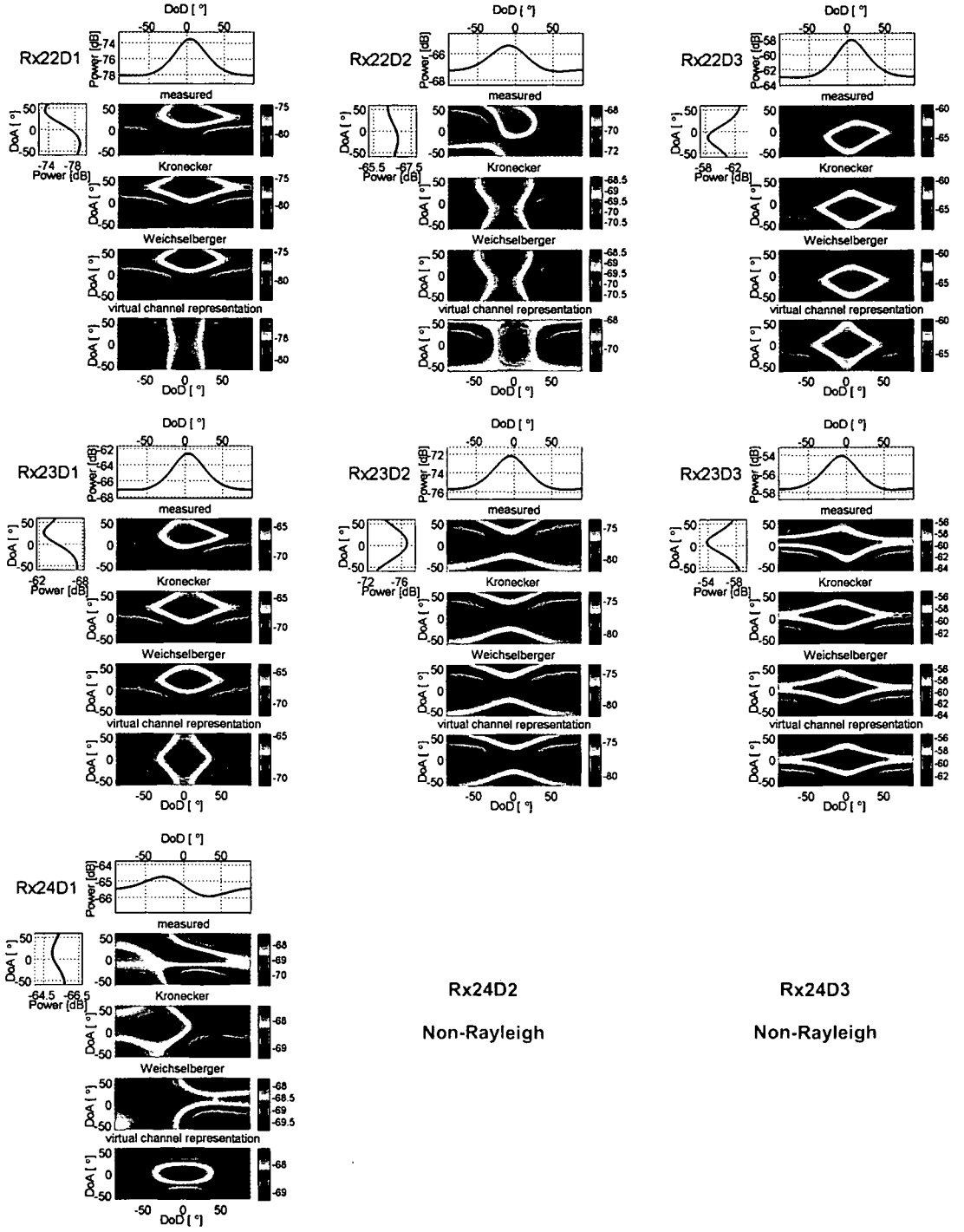

Figure C.24: Joint 2 × 2 DoD-DoA Capon spectra (cont'd).

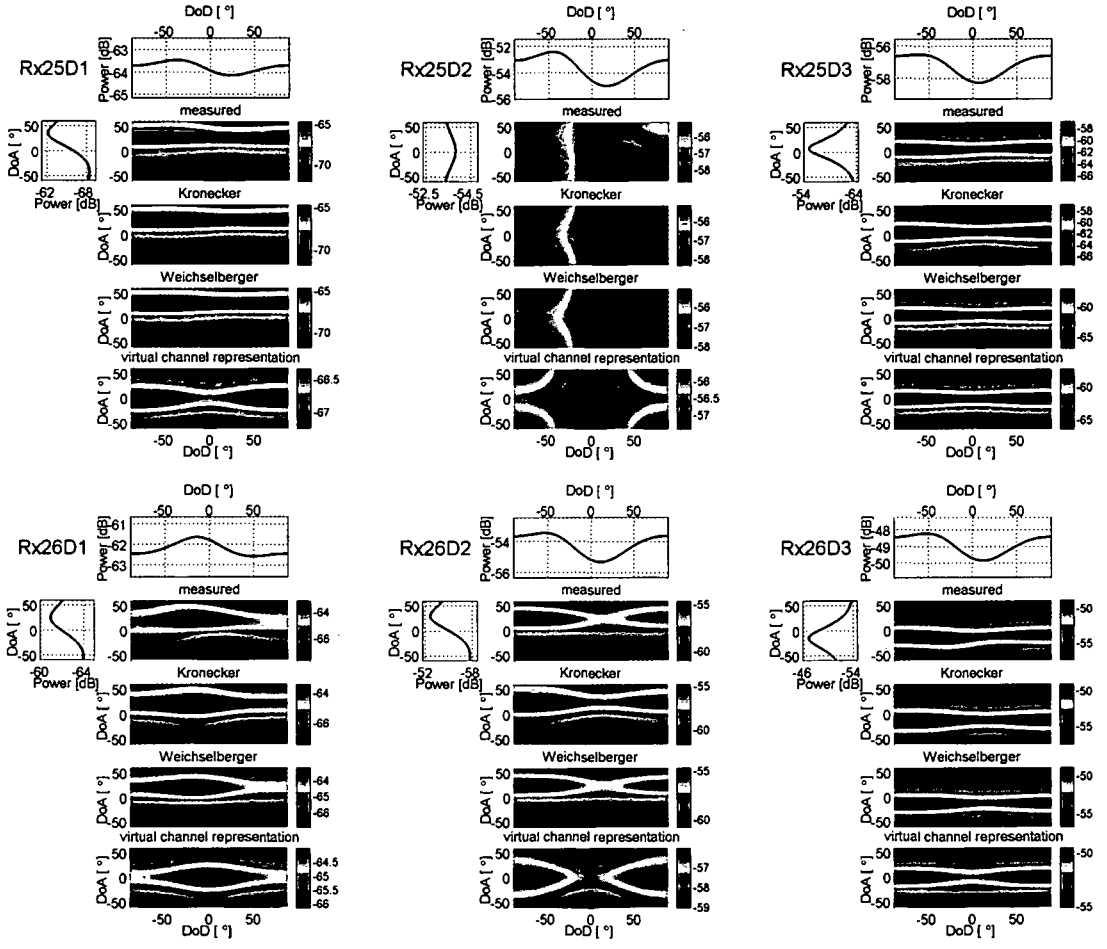

Figure C.25: Joint 2 × 2 DoD-DoA Capon spectra (cont'd).

Appendix D

Diagonally Correlated Channels

It is well known that the ergodic MIMO capacity grows asymptotically linearly with the minimum number of transmit and receive antennas in a sufficiently rich multipath environment[10, 11]. For Rayleigh-fading channels, it is usually believed that channel correlations always reduce capacity and that therefore i.i.d. channels would yield maximum ergodic capacity. In case of n antennas at both link ends and narrowband, the ergodic capacity can be expressed as [10, 11] (c.f. Chapter 2.3.1.3)

$$\bar{C}_{\text{iid}} = \mathrm{E}_{\mathbf{H}} \left\{ \log_2 \det \left[\mathbf{I} + \frac{\rho}{n} \mathbf{H}\mathbf{H}^H \right] \right\}. \tag{D.1}$$

However, by introducing a simple metric for the ergodic MIMO capacity, the most surprising result of [110, 111] was that ergodic capacity is not maximized under i.i.d. fading conditions. After exchanging the expectation and the $\log_2$ operation (Jensen's inequality) in (D.1), the proposed metric can be expressed as

$$\bar{\kappa} = \det \left[\mathrm{E}_{\mathbf{H}} \left\{ \mathbf{I} + \frac{\rho}{n} \mathbf{H}\mathbf{H}^H \right\} \right]. \tag{D.2}$$

As a beneficial property, the metric allows for analysis of ergodic MIMO capacity as a function of the correlations between different channel matrix elements. Interestingly enough, channels with so called *diagonal correlations* [110] could exhibit higher ergodic capacity than i.i.d. fading channels. These findings have met skepticism.

This appendix will characterize such channels. In the sequel, we will introduce so-called *diagonally correlated* 2×2 MIMO channels that exhibit higher ergodic capacity (in strict Shannon sense) than i.i.d. channels. Further, we will extend this approach to a general $n \times n$ channel.

D.1 Diagonally Correlated 2×2 MIMO Channels

D.1.1 Derivation and Modeling

In case of a 2×2 MIMO channel the channel matrix reads as

$$\mathbf{H} = \begin{bmatrix} h_{11} & h_{12} \\ h_{21} & h_{22} \end{bmatrix}, \tag{D.3}$$

and the full MIMO channel correlation matrix can be expressed as

$$\mathbf{R_H} = \begin{bmatrix} \mathrm{E}\{h_{11}h_{11}^*\} & \mathrm{E}\{h_{11}h_{21}^*\} & \mathrm{E}\{h_{11}h_{12}^*\} & \mathrm{E}\{h_{11}h_{22}^*\} \\ \mathrm{E}\{h_{21}h_{11}^*\} & \mathrm{E}\{h_{21}h_{21}^*\} & \mathrm{E}\{h_{21}h_{12}^*\} & \mathrm{E}\{h_{21}h_{22}^*\} \\ \mathrm{E}\{h_{12}h_{11}^*\} & \mathrm{E}\{h_{12}h_{21}^*\} & \mathrm{E}\{h_{12}h_{12}^*\} & \mathrm{E}\{h_{12}h_{22}^*\} \\ \mathrm{E}\{h_{22}h_{11}^*\} & \mathrm{E}\{h_{22}h_{21}^*\} & \mathrm{E}\{h_{22}h_{12}^*\} & \mathrm{E}\{h_{22}h_{22}^*\} \end{bmatrix}. \tag{D.4}$$

The diagonal entries in (D.4) represent the antenna powers, the $\mathrm{E}\{h_{ij}h_{lj}^*\}$ with $i \neq j \neq l$ the receive antenna correlations, and the $\mathrm{E}\{h_{ij}h_{il}^*\}$, again with $i \neq j \neq l$, the transmit antenna correlations, respectively. Thus, following [110], we will call the remaining matrix entries *diagonal correlations.*

From (D.2) it becomes clear that, in the case of a 2×2 MIMO Rayleigh fading channel, the ergodic channel capacity is maximized if the absolute value $|\mathbf{R_H}|$ of the full channel correlation matrix fulfills

$$|\mathbf{R_H}| = \begin{bmatrix} 1 & 0 & 0 & 1 \\ 0 & 1 & 1 & 0 \\ 0 & 1 & 1 & 0 \\ 1 & 0 & 0 & 1 \end{bmatrix}, \tag{D.5}$$

i.e. if the antenna amplitude correlations are zero, but the magnitudes of the diagonal correlations are equal to unity. We call this type of channels a 2×2 *diagonally correlated channel.* Thus, the amplitudes of its matrix elements read as

$$|\mathbf{H}| = \begin{bmatrix} |h_{11}| & |h_{12}| \\ |h_{12}| & |h_{11}| \end{bmatrix}. \tag{D.6}$$

An illustration of a diagonally correlated 2×2 MIMO channel is shown in Fig. D.1. Such a channel occurs in scenarios where only two, nearly equally-powered, independent Rayleigh-fading multipath components with orthogonal DoDs and DoAs exist. If a single DoD couples into a single DoA and vice versa, then the diagonally correlated channel results [112]. Note that 'orthogonal' in this sense does not imply right angles, but orthogonality of the corresponding steering/response vectors.

Using the formalism of the finite scatterer model [53] or the approach presented by [54], the diagonally correlated channel $\mathbf{H}$ can be expressed as

$$\mathbf{H} = \mathbf{A}_{\mathrm{Rx}} \left(\mathbf{D} \odot \mathbf{G}\right) \mathbf{A}_{\mathrm{Tx}}^T. \tag{D.7}$$

Here, $\mathbf{G}$ is a 2×2 i.i.d. fading matrix with zero-mean, complex circularly symmetric Gaussian entries. The two columns of the unitary matrix $\mathbf{A}_{\mathrm{Tx}}$ ($\mathbf{A}_{\mathrm{Rx}}$) constitute orthogonal steering (response) vectors of DoDs (DoAs). The 2×2 coupling matrix $\mathbf{D}$ is either a diagonal or anti-diagonal matrix with identical entries, producing the equally-powered, one-to-one coupling between DoDs and DoAs. Almost identical entries of the coupling matrix $\mathbf{D}$ work fine as well. Note that (D.7) is identical to the virtual channel representation with a diagonal coupling

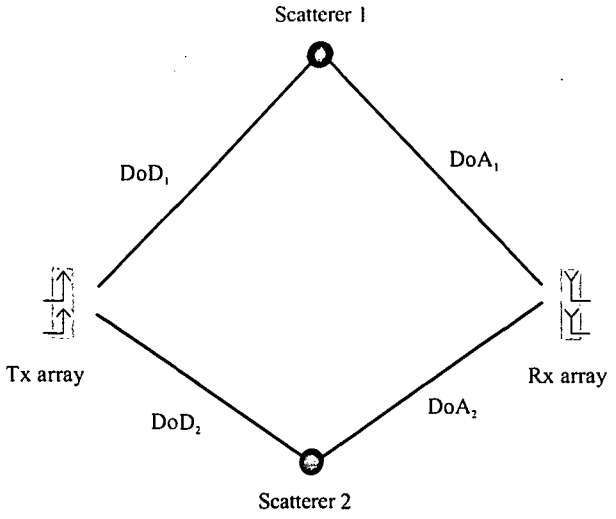

Figure D.1: Illustration of a 2×2 diagonally correlated channel: Two nearly equally powered, independent Rayleigh-fading multipath components with orthogonal DoDs and DoAs exist such that a single DoD couples into a single DoA and vice versa.

matrix. In fact, also the Weichselberger model with a diagonal coupling matrix exhibits diagonal correlations.

D.1.2 Capacity

A closer look at (D.7) reveals the distribution of the singular values of $\mathbf{H}$. The orthogonal steering (response) vectors of the unitary matrix $\mathbf{A}_{\mathrm{Tx}}$ ($\mathbf{A}_{\mathrm{Rx}}$) constitute the right (left) singular vectors, except a constant phase term. The magnitudes of the singular values of $\mathbf{H}$, $|s_i|$, are given by the magnitudes of the complex-Gaussian distributed, non-zero elements of $\mathbf{D} \odot \mathbf{G}$. Hence, $|s_i|$ follows a Rayleigh distribution. As a consequence, the eigenvalues $\lambda_i = |s_i|^2$ of the Gramian $\mathbf{H}\mathbf{H}^H$ are Chi-squared distributed with two degrees of freedom.

Before calculating the ergodic capacity, the channel has to be normalized properly. Its normalization to unity average power of each channel matrix coefficient leads to a Rayleigh parameter for $|s_i|$ of unity, too.

The ergodic capacity of a 2×2 diagonally correlated channel is exactly given by [113]

$$\begin{aligned} \bar{C} &= \mathrm{E}_x \left\{ \sum_{k=1}^{2} \log_2 \left(1 + \frac{\rho}{2} x^2\right) \right\} = 2 \cdot \mathrm{E}_x \left\{ \log_2 \left(1 + \frac{\rho}{2} x^2\right) \right\} \\ &= 2 \int_0^\infty \log_2 \left(1 + \frac{\rho}{2} x^2\right) x e^{-\frac{x^2}{2}} dx \\ &= 2 \log_2(e) e^{\frac{1}{\rho}} \mathrm{E}_1 \left(\frac{1}{\rho}\right), \end{aligned} \tag{D.8}$$

where x denotes a random realization of the identically distributed eigenvalues λ_i, and $\mathrm{E}_1(z)$

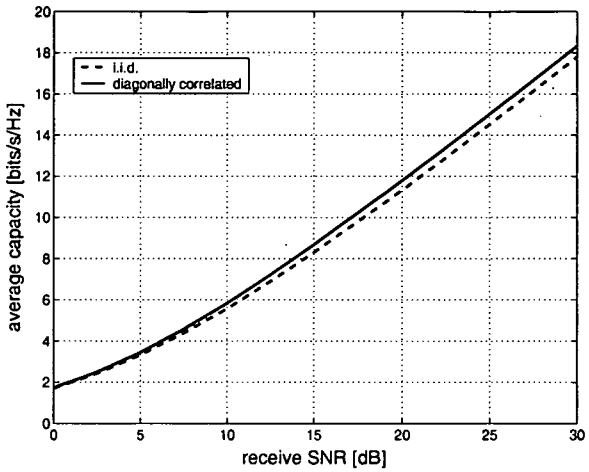

Figure D.2: Average capacity of a 2×2 i.i.d. and diagonally correlated channel as a function of the average receive SNR.

is the En-Function [114] for n $\neq$ 1 that satisfies $\mathrm{E}_1(z) = \int_1^\infty \frac{e^{-tz}}{t} dt$. For the special case of n = 1, the En-Function can also be expressed in terms of the Exponential Integral Function Ei(z), i.e. $\mathrm{E}_1(z) = -\mathrm{Ei}(-z)$.

Close scrutiny of (D.8) reveals that the diagonally correlated channel exhibits a higher ergodic capacity than the corresponding i.i.d. channel. Monte-Carlo simulations with $5 \cdot 10^5$ realizations for each SNR value were performed to show that this is indeed the case.

Figure D.2 plots the resulting average[1] 2×2 MIMO capacity of a diagonally correlated and an i.i.d. channel as a function of the receive SNR ρ. Evidently, the diagonally correlated channel exhibits a higher ergodic capacity. (Of course, both channels have the same channel power.) The difference is small, but it discusses the general statement that i.i.d. gives maximum ergodic capacity.

Further, we compared the capacity cdf of a diagonally correlated channel with the one of an i.i.d. channel at an SNR-level of 20dB. Figure D.3 shows the outcome. Despite the fact that the diagonally correlated channel (solid line) provides a higher average capacity than the i.i.d. channel (dashed line), we observe that the slope of its capacity cdf is flatter. Its *outage capacity* is lower for outage levels higher than approximately 85%.

D.1.3 Fading Behavior

As already mentioned before, for diagonally correlated channels $|h_{11}| = |h_{22}|$ and $|h_{12}| = |h_{21}|$. As a consequence, the channel amplitudes fade in tandem, either in pairs of $|h_{11}| - |h_{22}|$ (Fig. D.5) or $|h_{12}| - |h_{21}|$ (Fig. D.4), respectively. But these pairs fade Rayleigh independently of each other.

In case of i.i.d. Rayleigh-fading in contrast, each *single* channel matrix entry h_{ij} fades independently (according to a Rayleigh distribution).

[1]Please recall that we use the term ergodic only with respect to random variables. When dealing with realizations of a random variable, the expected value can be estimated by the arithmetic mean or average.

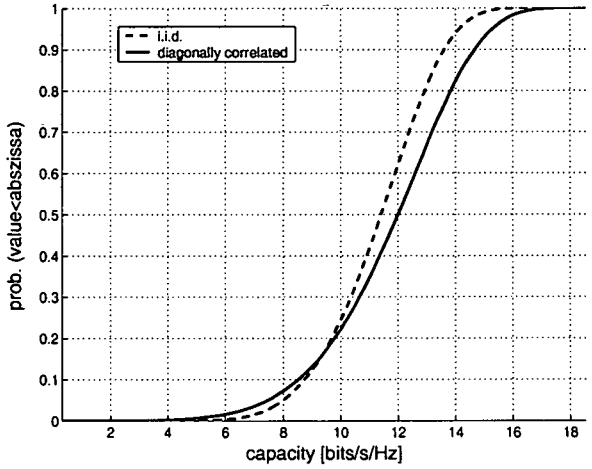

Figure D.3: Capacity cdf of a 2×2 i.i.d. and diagonally correlated channel at 20dB receive SNR.

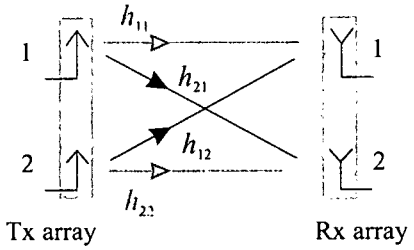

Figure D.4: The 2×2 diagonally correlated channel: fading pair $|h_{21}| - |h_{12}|$.

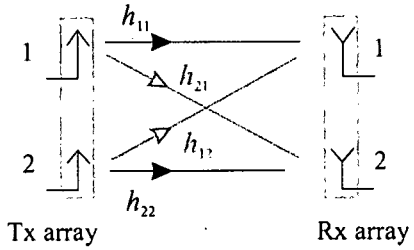

Figure D.5: The 2×2 diagonally correlated channel: fading pair $|h_{11}| - |h_{22}|$.

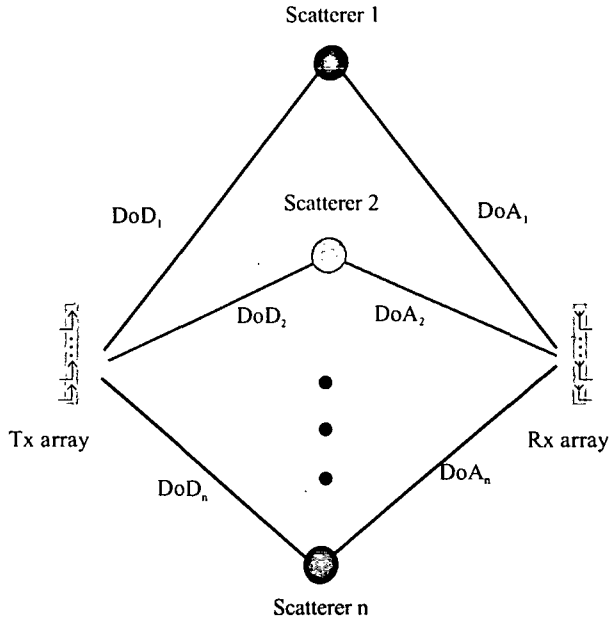

Figure D.6: Illustration of an $n \times n$ diagonally correlated channel: A channel with n orthogonal DoDs and n orthogonal DoAs such that each single DoD couples with equal power into a single DoA and vice versa.

An intuitively appealing reason for the capacity increase is as follows. Each of the independent fading pairs of a diagonally correlated channel provide perfectly separated virtual sub-channels on their own. This improved separation of the sub-channels result in a higher *ergodic* capacity. But, since the degrees of freedom reduces from four to two, diversity in diagonally correlated channels is lower than for i.i.d., leading to a flatter slope of the cdf, i.e. lower outage capacity for high outage levels.

D.2 Diagonally Correlated $n \times n$ MIMO Channels

The concept of the 2×2 diagonally correlated channel can be generalized as follows. Consider a symmetric $n \times n$ MIMO channel with n orthogonal DoDs and n orthogonal DoAs. We call such a channel *diagonally correlated* if each single DoD couples into a single DoA and vice versa. This is illustrated in Fig. D.6.

The analytical modeling stays the same and follows (D.7). Of course, the dimensions of the unitary steering and response matrices $\mathbf{A}_{\mathrm{Tx}}$ and $\mathbf{A}_{\mathrm{Rx}}$, the coupling matrix, and the random fading matrix $\mathbf{G}$ must change to $n \times n$. Further, $\mathbf{D}$ is a sparse matrix with only one entry in each row and column, producing the one-to-one coupling between DoDs and DoAs. The entries of $\mathbf{D}$ have to be identical. Again, almost identical entries work fine as well. The actual shape of $\mathbf{D}$ determines the appearance of the channel matrix and therefore the full channel correlation matrix. Interestingly enough, the amplitudes of the corresponding channel matrix entries exhibit a specific symmetry. It can be shown that the rows of these amplitudes have to be cyclically right- or left- shifted versions of each other.

As an example for 3×3 MIMO, the amplitudes of the channel matrix may result, for a given choice of D, in

$$|\mathbf{H}| = \begin{bmatrix} |h_{11}| & |h_{12}| & |h_{13}| \\ |h_{12}| & |h_{13}| & |h_{11}| \\ |h_{13}| & |h_{11}| & |h_{12}| \end{bmatrix}, \tag{D.9}$$

with the corresponding full channel correlation matrix

$$|\mathbf{R_H}| = \begin{bmatrix} 1 & 0 & 0 & 0 & 1 & 0 & 0 & 0 & 1 \\ 0 & 1 & 0 & 0 & 0 & 1 & 1 & 0 & 0 \\ 0 & 0 & 1 & 1 & 0 & 0 & 0 & 1 & 0 \\ 0 & 0 & 1 & 1 & 0 & 0 & 0 & 1 & 0 \\ 1 & 0 & 0 & 0 & 1 & 0 & 0 & 0 & 1 \\ 0 & 1 & 0 & 0 & 0 & 1 & 1 & 0 & 0 \\ 0 & 1 & 0 & 0 & 0 & 1 & 1 & 0 & 0 \\ 0 & 0 & 1 & 1 & 0 & 0 & 0 & 1 & 0 \\ 1 & 0 & 0 & 0 & 1 & 0 & 0 & 0 & 1 \end{bmatrix}, \tag{D.10}$$

or

$$|\mathbf{H}| = \begin{bmatrix} |h_{11}| & |h_{12}| & |h_{13}| \\ |h_{13}| & |h_{11}| & |h_{12}| \\ |h_{12}| & |h_{13}| & |h_{11}| \end{bmatrix}, \tag{D.11}$$

with

$$|\mathbf{R_H}| = \begin{bmatrix} 1 & 0 & 0 & 0 & 1 & 0 & 0 & 0 & 1 \\ 0 & 1 & 0 & 0 & 0 & 1 & 1 & 0 & 0 \\ 0 & 0 & 1 & 1 & 0 & 0 & 0 & 1 & 0 \\ 0 & 0 & 1 & 1 & 0 & 0 & 0 & 1 & 0 \\ 1 & 0 & 0 & 0 & 1 & 0 & 0 & 0 & 1 \\ 0 & 1 & 0 & 0 & 0 & 1 & 1 & 0 & 0 \\ 0 & 1 & 0 & 0 & 0 & 1 & 1 & 0 & 0 \\ 0 & 0 & 1 & 1 & 0 & 0 & 0 & 1 & 0 \\ 1 & 0 & 0 & 0 & 1 & 0 & 0 & 0 & 1 \end{bmatrix}. \tag{D.12}$$

However, the eigenvalues $\lambda_i = |s_i|^2$ of the Gramian $\mathbf{HH}^H$ are still independently identical Chi-squared distributed with two degrees of freedom, independent of the actual shape of $\mathbf{D}$. If the channel is normalized to unity average power of each channel matrix coefficient, the variance of the Rayleigh distributed $|s_i|$ increases linearly with the number of antennas. For n antennas at both link ends, it equals $\frac{n}{2}$. Hence, the ergodic capacity of an $n \times n$ diagonal channel with its identically distributed eigenvalues is exactly given by [113]

$$\begin{aligned}\bar{C} &= \mathrm{E}\left\{\sum_{k=1}^{n}\log_2\left(1+\frac{\rho}{n}x^2\right)\right\} = n\cdot\mathrm{E}\left\{\log_2\left(1+\frac{\rho}{n}x^2\right)\right\} \\ &= n\int_0^\infty \log_2\left(1+\frac{\rho}{n}x^2\right)\frac{2x}{n}e^{-\frac{x^2}{n}}dx \\ &= n\log_2(e)e^{\frac{1}{\rho}}\mathrm{E}_1\left(\frac{1}{\rho}\right), \end{aligned} \tag{D.13}$$

where $\mathrm{E}_1(z)$, again, is the En-Function for n = 1 that satisfies $\mathrm{E}_1(z) = \int_1^\infty \frac{e^{-tz}}{t}dt$.
Note that in the above expression the capacity grows exactly linearly with the number of antennas while the capacity of i.i.d. channels grows in n only asymptotically.

Bibliography

[1] The Economics of Mobile Wireless Data, Qualcomm Incorporated, March 2001.

[2] http://www.itu.int/rec/recommendation.asp?type=folders&lang=e&parent=R-REC-M.1645.

[3] J.H. Winters. Smart Antennas for Wireless Systems. *IEEE Personal Communications*, 5(1):23–27, Feb. 1998.

[4] L.C. Godara. Applications of Antenna Arrays to Mobile Communications, Part I: Performance Improvements, Feasibility, and System Considerations. *Proceedings of the IEEE*, 85(7):1031–1060, July 1997.

[5] L.C. Godara. Applications of Antenna Arrays to Mobile Communications, Part II: Beam-Forming and Direction-of-Arrival Considerations. *Proceedings of the IEEE*, 85(8):1195–1245, Aug. 1997.

[6] P.H. Lehne and M. Pettersen. An Overview of Smart Antenna Technology for Mobile Communication Systems. *IEEE Communications Surveys*, 2(4):2–13, 2000.

[7] H. Krim and M. Viberg. Two Decades of Array Signal Processing Research: The Parametric Approach. *IEEE Signal Processing Magazine*, 13(4):67–94, July 1996.

[8] B.D. Van Veen and K.M. Buckley. Beamforming: A Versatile Approach to Spatial Filtering. *IEEE Acoustic, Speech, and Signal Processing Magazine*, 5(2):4–24, Apr. 1988.

[9] J. Winters. On the Capacity of Radio Communication Systems with Diversity in a Rayleigh Fading Environment. *IEEE Journal on Selected Areas in Communications*, 5(5):871–878, June 1987.

[10] I.E. Telatar. Capacity of Multi-Antenna Gaussian Channels. *Technical Memorandum, Bell Laboratories, Lucent Technologies*, Oct. 1998. Published in *European Transactions on Telecommunications*, vol. 10, no. 6, pp. 585–595, Nov./Dec. 1999.

[11] G.J. Foschini and M.J. Gans. On Limits of Wireless Communications in Fading Environments when Using Multiple Antennas. *Wireless Personal Communications*, 6:311–335, 1998.

[12] H. Bölcskei, D. Gesbert, and A.J. Paulraj. On the Capacity of OFDM-Based Spatial Multiplexing Systems. *IEEE Transactions on Communications*, 50(2):225–234, Feb. 2002.

[13] A. Goldsmith, S.A. Jafar, N. Jindal, and S. Vishwanath. Capacity Limits Of MIMO Channels. *IEEE Journal on Selected Areas in Communications*, 21(5):684–702, June 2003.

[14] N. Jindal, S. Vishwanath, and A. Goldsmith. On the Capacity of Multiple Input Multiple Output Broadcast Channels. In *IEEE International Conference on Communications, ICC'02*, volume 3, pages 1444–1450, Apr. 2002.

[15] J. Kotecha and A. Sayeed. On the Capacity of Correlated MIMO Channels. In *IEEE International Symposium on Information Theory, 2003*, pages 355–355, Yokohama, Japan, June 2003.

[16] G.G. Raleigh and J.M. Cioffi. Spatio-Temporal Coding for Wireless Communication. *IEEE Transactions on Communications*, 46:357–366, Mar. 1998.

[17] V. Tarokh, N. Seshadi, and A.R. Calderbank. Space-Time Codes for High Data Rate Wireless Communication: Performance Criterion and Code Construction. *IEEE Transactions on Information Theory*, 44(2):744–765, March 1998.

[18] V. Tarokh, H. Jafarkhani, and A.R. Calderbank. Space-Time Block Codes from Orthogonal Designs. *IEEE Transactions on Information Theory*, 45(5):1456–1467, July 1999.

[19] Youjian Liu, M.P. Fitz, and O.Y. Takeshita. Space-Time Codes Performance Criteria and Design for Frequency Selective Fading Channels. In *IEEE International Conference on Communications, ICC'01*, volume 9, pages 2800–2804, Helsinki, Finland, 2001.

[20] B.M. Hochwald and T.L. Marzetta. Unitary Space-Time Modulation for Multiple-Antenna Communications in Rayleigh Flat Fading. *IEEE Transactions on Information Theory*, 46(2):543–462, Feb. 2000.

[21] V. Tarokh, A. Naguib, N. Seshadi, and A.R. Calderbank. Combined Array Processing and Space-Time Coding. *IEEE Transactions on Information Theory*, 45(4):1121–1128, May 1999.

[22] R. Vaughan and J.B. Andersen. *Channels, Propagation and Antennas for Mobile Communications.* IEE, 2003.

[23] D. Gesbert, M. Shafi, Da-shan Shiu, P.J. Smith, and A. Naguib. From Theory to Practice: An Overview of MIMO Space-time Coded Wireless Systems. *IEEE Journal on Selected Areas in Communications*, 21(3):281–302, Apr. 2003.

[24] A.J. Paulraj, D.A. Gore, R.U. Nabar, and H. Bölcskei. An Overview of MIMO Communications - A Key to Gigabit Wireless. *Proceedings of the IEEE*, 92(2):198–218, Feb. 2004.

[25] M. Steinbauer, A.F. Molisch, and E. Bonek. The Double-Directional Radio Channel. *IEEE Magazine in Antennas and Propagation*, 43(4):51–63, Aug. 2001.

[26] M. Steinbauer. *The Radio Propagation Channel - A Non-Directional, Directional and Double-Directional Point-of-View.* PhD thesis, Institut für Nachrichtentechnik

und Hochfrequenztechnik, Vienna University of Technology, 2001. downloadable from http://www.nt.tuwien.ac.at/mobile.

[27] M. Steinbauer. A Comprehensive Transmission and Channel Model for Directional Radio Channel. In *COST 259 TD (98) 027*, Bern, Switzerland, Feb. 1998.

[28] M. Steinbauer, D. Hampicke, G. Sommerkorn, A. Schneider, A.F. Molisch, R. Thomä, and E. Bonek. Array Measurement of the Double-Directional Mobile Radio Channel. In *Vehicular Technology Conference, VTC 2000-Spring*, volume 3, pages 1656–1662, Tokio, Japan, May 2000.

[29] W. Weichselberger. *Spatial Structure of Multiple Antenna Radio Channels.* PhD thesis, Institut für Nachrichtentechnik und Hochfrequenztechnik, Vienna University of Technology, Dec. 2003. downloadable from http://www.nt.tuwien.ac.at/mobile.

[30] J.W. Wallace and M.A. Jensen. Modeling the Indoor MIMO Wireless Channel. *IEEE Transactions on Antennas and Propagation*, 50(5):591–599, May 2002.

[31] T. Zwick, C. Fischer, and W. Wiesbeck. A Stochastic Multipath Channel Model Including Path Directions for Indoor Environments. *IEEE Journal on Selected Areas in Communications*, 20(6):1178–1192, Aug. 2002.

[32] T. Svantesson. A Wideband Statistical Model for NLOS Indoor MIMO Channels. In *IEEE 56th Vehicular Technology Conference, VTC Fall 2002*, volume 2, pages 691–695, Sep. 2002.

[33] Kai Yu, M. Bengtsson, B. Ottersten, D. McNamara, P. Karlsson, and M. Beach. A Wideband Statistical Model for NLOS Indoor MIMO Channels. In *IEEE Vehicular Technology Conference, VTC Spring 2002*, volume 1, pages 370–374, Birmingham, AL, USA, May 2002.

[34] Shuangquan Wang, K. Raghukumar, A. Abdi, J. Wallace, and M. Jensen. Indoor MIMO Channels: A Parametric Correlation Model and Experimental Results. In *IEEE/Sarnoff Symposium on Advances in Wired and Wireless Communication*, pages 1–5, Apr. 2004.

[35] S.R. Saunders. *Antennas and Propagation for Wireless Communication Systems.* John Wiley & Sons, New Jork, USA, 1999.

[36] A.F. Molisch, H. Asplund, R. Heddergott, M. Steinbauer, and T. Zwick. The COST 259 Directional Channel Model - I. Philosophy and General Aspects. IEEE Transactions on Wireless Communications, accepted pending revisions.

[37] A.G. Burr. Capacity of Multi-element Transmit/Receive Antenna (MIMO) Wireless Communication Systems. Technical report, FTW, Forschungszentrum Telecommunication Wien, 1999. alister@ohm.york.ac.uk.

[38] M. Herdin, H. Özcelik, H. Hofstetter, and E. Bonek. Variation of Measured Indoor MIMO Capacity with Receive Direction and Position at 5.2GHz. *Electronics Letters*, 38(21):1283–1285, Oct. 2002.

[39] A. Saleh and R. Valenzuela. A Statistical Model for Indoor Multipath Propagation. *IEEE Journal on Selected Areas in Communications*, 5(2):128–137, Feb. 1987.

[40] Chia-Chin Chong, Chor-Min Tan, D.I. Laurenson, M.A. Beach, and A.R. Nix. A New Statistical Wideband Spatio-temporal Channel Model for 5-GHz Band WLAN Systems. *IEEE Journal on Selected Areas in Communications*, 21(2):139–150, Feb. 2003.

[41] Q.H. Spencer, B.D. Jeffs, M.A. Jensen, and A.L. Swindlehurst. Modeling the Statistical Time and Angle of Arrival Characteristics of an Indoor Multipath Channel. *IEEE Journal on Selected Areas in Communications*, 18(3):347–360, Mar. 2000.

[42] N. Czink, M. Herdin, H. Özcelik, and E. Bonek. Number of Multipath Components in Indoor MIMO Propagation Environments. *Electronics Letters*, 40(23):1498–1499, Nov. 2004.

[43] A. Richter and R.S. Thomä. Parametric Modeling and Estimation of Distributed Diffuse Scattering Components of Radio Channels. In *COST 273 TD (03) 198*, Prague, Czech Republic, Sep. 2003.

[44] A.F. Molisch. Modeling the MIMO Propagation Channel. *Belgian Journal of Electronics and Communications*, 4:5–14, 2003.

[45] T. Zwick, D.J. Cichon, and W. Wiesbeck. Microwave Propagation Modeling in Indoor Environments. In *Microwaves and Optronics International Conference*, pages 629–633, Sindelfingen, Germany, May 1995.

[46] J. Fuhl, A.F. Molisch, and E. Bonek. Unified Channel Model for Mobile Radio Systems with Smart Antennas. *IEEE Proceedings on Radar, Sonar and Navigation*, 145(1):32–41, Feb. 1998.

[47] O. Nørklit and J.B. Andersen. Diffuse Channel Model and Experimental Results for Array Antennas in Mobile Environments. *IEEE Transactions on Antennas and Propagation*, 46(6):834–840, June 1998.

[48] J.J. Blanz and P. Jung. A Flexibly Configurable Spatial Model for Mobile Radio Channels. *IEEE Transactions on Communications*, 46(3):367–371, Mar. 1998.

[49] J.C. Liberti and T.S. Rappaport. A Geometrically Based Model for Line-of-Sight Multipath Radio Channels. In *46th IEEE Vehicular Technology Conference 'Mobile Technology for the Human Race'*, volume 2, pages 844–848, Apr. 1996.

[50] P. Petrus, J.H. Reed, and T.S. Rappaport. Geometrical-based Statistical Macrocell Channel Model for Mobile Environments. *IEEE Transactions on Communications*, 50(3):495–502, Mar. 2002.

[51] E. Bonek, M. Herdin, H. Özcelik, and W. Weichselberger. Internal Report, MIMO for 4G Broadband Packet Access, Propagation Models. Technical report, Institut für Nachrichtentechnik und Hochfrequenztechnik, Technische Universität Wien, Aug. 2004.

[52] J.W. Wallace and M.A. Jensen. Statistical Characteristics of Measured MIMO Wireless Channel Data and Comparison to Conventional Models. In *IEEE 2002 Vehicular Technology Conference, VTC 2001 Fall*, volume 2, pages 1078–1082, Oct. 2001.

[53] A.G. Burr. Capacity Bounds and Estimates for the Finite Scatterers MIMO Wireless Channel. *IEEE Journal on Selected Areas in Communications*, 21(5):812–818, June 2003.

[54] A.M. Sayeed. Deconstructing Multiantenna Fading Channels. *IEEE Transactions on Signal Processing*, 50(10):2563–2579, Oct. 2002.

[55] Chen-Nee Chuah, J.M. Kahn, and D.N.C. Tse. Capacity of Mulit-Antenna Array Systems in Indoor Wireless Environment. In *IEEE Global Telecommunications Conference*, 1998.

[56] D. Chizhik, F. Rashid-Farrokhi, J. Ling, and A. Lozano. Effect of Antenna Separation on the Capacity of BLAST in Correlated Channels. *IEEE Communications Letters*, 4(11):337–339, Nov. 2000.

[57] Da-Shan, G.J. Foschini, M.J. Gans, and J.M. Kahn. Fading Correlation and Its Effect on the Capacity of Multielement Antenna Systems. *IEEE Transactions on Communications*, 48(3):502–513, Mar. 2000.

[58] J.P. Kermoal, L. Schumacher, K.I. Pedersen, P.E. Mogensen, and F. Frederiksen. A Stochastic MIMO Radio Channel Model with Experimental Validation. *IEEE Journal on Selected Areas in Communications*, 20(6):1211–1226, Aug. 2002.

[59] W. Weichselberger, M. Herdin, H. Özcelik, and E. Bonek. A Stochastic MIMO Channel Model with Joint Correlation of Both Link Ends. IEEE Transactions on Wireless Communications, in press.

[60] V. Erceg and et al. . TGn Channel Models. Technical report, IEEE P802.11 Wireless LANs, May 2004. grouper.ieee.org/groups/802/.

[61] http://www.lx.it.pt/cost273/.

[62] A. Papoulis. *Random Variables and Stochastic Processes.* New York: McGraw-Hill, 1991.

[63] T. Zwick, F. Demmerle, and W. Wiesbeck. Comparison of Channel Impulse Response Measurements and Calculations in Indoor Environments. In *Antennas and Propagation Society International Symposium*, volume 2, pages 1498–1501, Baltimore, MD, July 1996.

[64] D.P. McNamara, M.A. Beach, P.N. Fletcher, and P. Karlsson. Initial Investigation of Multiple-Input Multiple-Output Channels in Indoor Environments. In *IEEE Benelux Chapter Symposium on Communications and Vehicualar Technology*, pages 139–143, Leuven, Belgium, Oct. 2000.

[65] E. Bonek, H. Özcelik, M. Herdin, W. Weichselberger, and J. Wallace. Deficiencies of the 'Kronecker' MIMO Radio Channel Model. In *6th International Symposium Wireless Personal Multimedia Communications, WPMC 2003*, Yokosuka, Japan, Oct. 2003.

[66] H. Özcelik, M. Herdin, W. Weichselberger, J. Wallace, and E. Bonek. Deficiencies of the 'Kronecker MIMO Radio Channel Model. *Electronics Letters*, 39(16):1209–1210, 2003.

[67] D. Gesbert, H. Bölcskei, D.A. Gore, and A.J. Paulraj. MIMO Wireless Channels: Capacity and Performance Prediction. In *Global Telecommunications Conference, 2000. GLOBECOM '00*, volume 2, pages 1083–1088, San Francisco, CA, USA, Nov. 2000.

[68] D. Chizhik, G.J. Foschini, and R.A. Valenzuela. Capacities of Multi-Element Transmit and Receive Antennas: Correlations and Keyholes. *Electronics Letters*, 36:1099–1100, June 2000.

[69] V. Erceg, S.J. Fortune, J. Ling, A.J. Rustako, and R.A. Valenzuela. Comparisons of a Computer-based Propagation Prediction Tool with Experimental Data Collected in Urban Microcellular Environments. *IEEE Journal on Selected Areas in Communications*, 15(4):677–684, May 1997.

[70] J. Bach Andersen and I. Kovacs. Power Distributions Revisited. In *COST 273 TD (02) 004*, Guildford, UK, Januray 2002.

[71] D. Gesbert, H. Bölcskei, D.A. Gore, and A.J. Paulraj. Outdoor MIMO Wireless Channels: Models and Performance Prediction. *IEEE Transactions on Communications*, 50(12):1926–1934, Dec. 2002.

[72] P. Almers, F. Tufvesson, and A.F. Molisch. Measurement of Keyhole Effects in a Wireless Multiple-Input Multiple-Output (MIMO) Channel. *IEEE Communications Letters*, 7(8):373–375, Aug. 2003.

[73] A. Molisch, M. Toeltsch, E. Bonek, and R. Thomä. Measurement of the Capacity of MIMO Systems in Frequency-selective Channels. In *IEEE Vehicular Technology Conference*, volume 1, pages 204–208, Rhodes, Greece, May 2001.

[74] H. Steyskal and J.S. Herd. Mutual Coupling Compensation in Small Array Antennas. *IEEE Transactions on Antennas and Propagation*, 38:1971–1975, Dec. 1990.

[75] M. Debbah and R. Müller. Capacity Complying MIMO Channel Models. In *The Thrity-Seventh Asilomar Conference on Signals, Systems & Computers*, volume 2, pages 1815–1819, Nov. 2003.

[76] P. Soma, D.S. Baum, V. Erceg, R. Krishnamoorthy, and A.J. Paulraj. Analysis and Modeling of Multiple-Input Multiple-Output (MIMO) Radio Channel Based on Outdoor Measurements Conducted at 2.5 GHz for Fixed BWA Applications. In *IEEE International Conference on Communications, ICC 2002*, volume 1, pages 272–276, Apr./May 2002.

[77] K.I. Pedersen, J.B. Andersen, J.P. Kermoal, and P. Mogensen. A Stochastic Multiple-input-multiple-output Radio Channel Model for Evaluation of Space-time Coding Algorithms. In *IEEE Vehicular Technology Conference, VTC-Fall 2000*, volume 2, pages 24–28, Sept. 2000.

[78] M. Pätzold. *Mobilfunkkanäle — Modellierung, Analyse und Simulation.* Vieweg, Wiesbaden, Germany, 1999.

[79] J. Medbo and P. Schramm. Channel Models for HIPERLAN/2. ETSI/BRAN document no. 3ERI085B.

[80] J. Medbo and J.-E. Berg. Measured Radiowave Propagation Characterisics at 5GHz for Typical HIPERLAN/2 Scenarios. ETSI/BRAN document no. 3ERI084A.

[81] T. Svantesson and A. Ranheim. Mutual Coupling Effects on the Capacity of Multielement Antenna Systems. In *IEEE International Conference on Acoustics, Speech, and Signal Processing, ICASSP '01*, volume 4, pages 2485–2488, Salt Lake City, Utah, May 2001.

[82] J.W. Wallace and M.A. Jensen. The Capacity of MIMO Wireless Systems with Mutual Coupling. In *IEEE 2002 Vehicular Technology Conference, VTC 2002 Fall*, volume 2, pages 696–700, Sep. 2002.

[83] R. Janaswamy. Effect of Element Mutual Coupling on the Capacity of Fixed Length Linear Arrays. *IEEE Antennas Wireless Propagation Letters*, 1:157–160, 2002.

[84] C. Waldschmidt, C. Kuhnert, W. Sörgel, and W. Wiesbeck. MIMO-Antennas in Small Handheld Devices. *48. Internationales Wissenschafliches Kolloquium, TU Ilmenau*, pages 1–7, Sep. 2003.

[85] P. Kildal and K. Rosengren. Electromagnetic Characterization of MIMO Antennas Including Coupling Using Classical Embedded Element Pattern and Radiation Efficiency. In *IEEE Antennas and Propagation Society Symposium*, volume 2, pages 1259–1262, June 2004.

[86] R.S. Thomä, D. Hampicke, A. Richter, G. Sommerkorn, A. Schneider, U. Trautwein, and W. Wirnitzer. Identification of Time-variant Directional Mobile Radio Channels. *IEEE Transactions on Instrumentation and Measurement*, 49(2):357–364, Apr. 2000.

[87] http://www.channelsounder.de.

[88] M. Herdin, H. Özcelik, H. Hofstetter, and E. Bonek. Linking Reduction in Measured MIMO Capacity with Dominant-wave Propagation. In *10th International Conference on Telecommunications, ICT 2003*, volume 2, pages 1526–1530, Papeete, Tahiti, Feb./Mar. 2003.

[89] P.H. Lehne, F. Aanvik, J.-C. Bic, P. Pajusco, M. Grigat, I. Gaspard, and U. Martin. Calibration of Mobile Radio Channel Sounders. In *COST 259 TD (98) 088*, Duisburg, Germany, Sep. 1998.

[90] K. Pensel, H. Aroudaki, and J.A. Nossek. Calibration of Smart Antennas in a GSM Network. In *Signal Processing Advances in Wireless Communications, 1999. SPAWC '99*, pages 354–357, May 1999.

[91] B.H. Fleury. An Uncertainty Relation for WSS Processes and its Application to WSSUS Systems. *IEEE Transactions on Communications*, 44(12):1632–1634, Dec. 1996.

[92] M. Herdin. *Non-Stationary Indoor MIMO Radio Channels.* PhD thesis, Institut für Nachrichtentechnik und Hochfrequenztechnik, Vienna University of Technology, Aug. 2004. downloadable from http://www.nt.tuwien.ac.at/mobile.

[93] E. Bonek, M. Herdin, W. Weichselberger, and H. Özcelik. MIMO - Study Propagation First. In *Proceedings of IEEE International Symposium on Signal Processing and Information Thechnology*, pages 150–153, Darmstadt, Germany, Dec. 2003.

[94] N. Czink. Optimum Training for MIMO Wireless Channels. Master's thesis, Institut für Nachrichtentechnik und Hochfrequenztechnik, Vienna University of Technology, June 2004.

[95] M.T. Ivrlac and J.A. Nossek. Quantifying Diversity and Correlation of Rayleigh Fading MIMO Channels. In *IEEE International Symposium on Signal Processing and Information Technology, ISSPIT'03*, pages 158–161, Darmstadt, Germany, Dec. 2003.

[96] M. Herdin and E. Bonek. A MIMO Correlation Matrix Based Metric for Characterizing Non-Stationarity. In *IST Mobile and Wireless Communications Summit 2004*, Lyon, France, June 2004.

[97] J. Capon, R.J. Greenfield, and R.J. Kolker. Multidimensional Maximum-Likelihood Processing of a Large Aperture Seismic Array. *Proceedings of the IEEE*, 55:192–211, Februar 1967.

[98] J. Capon. High-Resolution Frequency-Wavenumber Spectrum Analysis. *Proceedings of the IEEE*, 57(8):1408–1418, Aug. 1969.

[99] J.C. Liberti and T.S. Rappaport. *Smart Antennas for Wireless Communications: Is-95 and Third Generation CDMA Applications.* Prentice Hall, 1999.

[100] A. Paulraj, R. Roy, and T. Kailath. Estimation of Signal Parameters via Rotational Invariance Techniques - Esprit. In *Nineteeth Asilomar Conference on Circuits, Systems and Computers, 1985*, pages 83–89, Nov. 1985.

[101] R. Roy and T. Kailath. ESPRIT-Estimation of Signal Parameters via Rotational Invariance Techniques. *IEEE Transactions on Acoustics, Speech, and Signal Processing*, 37(7):984–995, July 1989.

[102] M. Haardt and J.A. Nossek. Unitary ESPRIT: How to Obtain Increased Estimation Accuracy with a Reduced Computational Burden. *IEEE Transactions on Acoustics, Speech, and Signal Processing*, 43(5):1232–1242, May 1985.

[103] B.H. Fleury, D. Dahlhaus, R. Heddergott, and M. Tschudin. Wideband Angle of Arrival Estimation Using the SAGE Algorithm. In *IEEE 4th International Symposium on Spread Spectrum Techniques and Applications*, volume 1, pages 79–85, Sep. 1996.

[104] B.H. Fleury, M. Tschudin, R. Heddergott, D. Dahlhaus, and K. Ingeman Pedersen. Channel Parameter Estimation in Mobile Radio Environments Using the SAGE Algorithm. *IEEE Journal on Selected Areas in Communications*, 17(3):434–450, Mar. 1999.

[105] H. Özcelik, M. Herdin, R. Prestros, and E. Bonek. How MIMO Capacity is Linked with Single Element Fading Statistics. In *International Conference on Electromagnetics in Advanced Applications, ICEAA 2003*, pages 775–778, Torino, Italy, Sep. 2003.

[106] H. Özcelik, M. Herdin, H. Hofstetter, and E. Bonek. Capacity of Different MIMO Systems Based on Indoor Measurements at 5.2 GHz. In *5th European Personal Mobile Communications Conference, EPMCC 2003*, pages 463–466, Glasgow, Scotland, Apr. 2003.

[107] H. Özcelik, M. Herdin, H. Hofstetter, and E. Bonek. A Comparison of Measured 8x8 MIMO Systems with a Popular Stochastic Channel Model at 5.2 GHz. In *10th International Conference on Telecommunications, ICT 2003*, volume 2, pages 1542–1546, Papeete, Tahiti, Feb./Mar. 2003.

[108] D.P. McNamara, M.A. Beach, and P.N. Fletcher. Spatial Correlation in Indoor MIMO Channels. In *IEEE International Symposium on Personal, Indoor and Mobile Radio Communications, 2002*, volume 1, pages 290–294, Lisbon, Portugal, 2002.

[109] Kai Yu, M. Bengtsson, B. Ottersten, D. McNamara, P. Karlsson, and M. Beach. Second Order Statistics of NLOS Indoor MIMO Channels Based on 5.2 GHz Measurements. In *Global Telecommunications Conference, 2001. GLOBECOM '01*, volume 1, pages 156–160, San Antonio, TX, USA, Nov. 2001.

[110] C. Oestges, B. Clerckx, D. Vanhoenacker-Janvier, and A. Paulraj. Impact of diagonal correlations on MIMO capacity: application to geometrical scattering models. In *IEEE 58th Vehicular Technology Conference, VTC 2003-Fall*, volume 1, pages 394–398, Oct. 2003.

[111] C. Oestges and A.J. Paulraj. Beneficial Impact of Channel Correlations on MIMO Capacity. *Electronics Letters*, 40(10):606–608, May 2004.

[112] H. Özcelik. Diagonal-Correlation Channels: Better than i.i.d.? In *COST 273 TD (04) 133*, Gothenburg, Sweden, June 2004.

[113] H. Özcelik and C. Oestges. Capacity of Diagonally Correlated MIMO Channels. IEEE Vehicular Technology Conference, Spring 2005, May-June 2005, accepted for publication.

[114] M. Abramowitz and I.A. Stegun (Eds.). *Exponential Integral and Related Functions.* New York: Dover, 1972. Chapter 5 in Handbook of Mathematical Functions with Formulas, Graphs, and Mathematical Tables.